UNIVERSIDAD NACIONAL DE COLOMBIA

Payload analysis and control of manipulators for human interactive environments

Jaime Enrique Arango Castro

Universidad Nacional de Colombia
Faculty of Engineering and Architecture, Department of Electrical, Electronic and Computer Engineering
Manizales, Colombia
2014

UNIVERSIDAD NACIONAL DE COLOMBIA

Análisis de la capacidad de carga y control de manipuladores en ambientes de interacción con humanos

Jaime Enrique Arango Castro

Universidad Nacional de Colombia
Facultad de Ingeniería y Arquitectura, Departamento de Ingenirías Eléctrica, Electrónica y Computación
Manizales, Colombia
2014

Payload analysis and control of manipulators for human interactive environments

Jaime Enrique Arango Castro

A Thesis presented for the degree of::
Ph. D. in Engineering - Automatic

Advisor:
Ph. D. Gustavo Adolfo Osorio Londoño

Research Areas:
Automation and Control
Research group:
Perception and Intelligent Control

Universidad Nacional de Colombia
Faculty of Engineering and Architecture, Department of Electrical, Electronic and Computer Engineering
Manizales, Colombia
2014

To my parents and beloved wife for their support and patience in the difficult moments. You are the main inspiration and motivation in my life.

Acknowledgements

I would like to thank to PhD. Fabiola Angulo for its support during my Masters studies and some control analysis in this work; to my advisor and friend PhD. Gustavo Osorio for the continued feedback and enthusiastic support; to the Automatic Control Department (ESAII) at Technical University of Catalonia (UPC), the Institut de Robòtica i Informàtica Industrial (CSIC-UPC) and its brilliant professionals; to the Department of Electrical, Electronic and Computer Engineering and the Postgraduate Program at the National University of Colombia in Manizales, to the Faculty of Engineering and Architecture and its Direction of Research and Extension for the financial support to my research, studies and mobility and the Direction of Research at Manizales (DIMA). Finally, I would like to thank to the Perception and Intelligent Control (PCI) and Soft and Hard Applied Computing (SHAC) research groups members at the National University of Colombia for the helpful support.

Abstract

This doctoral thesis presents the results of numerical simulations and some experimental analysis of three main topics: the dynamical modeling of multiple degree of freedom (MDoF) manipulators ($n > 2$ DoF), dynamic load carrying capacity computation (DLCC) for the payload handling issue and nonlinear control analysis and design including Unfalsified Adaptive Control (UAC). We performed analysis of two (2) cases of study: the 5 DoF SCORBOT ER V PLUS manufactured by Intelitech Corp. and the 7 DoF redundant Whole Arm Manipulator (WAM) manufactured by Barrett Technology Inc. with intrinsic safety, backdrivable and compliant characteristics and suitable for human-robot interaction (HRI).

Initially, we computed and validated the dynamical model of the cases of study. The inverse and direct dynamical models of the SCORBOT ER V PLUS were numerically validated. Then, an experimental validation of inverse dynamical model of the WAM presents a comparison between numerical and experimental data, identifying the need for better friction models. After that, we proposed and evaluated a methodology for DLCC computation in the entire workspace of manipulators for different types of controllers. Then, for the analysis of the data-driven UAC with fading memory for multiple DoF manipulators, we performed a comparison with a traditional model-based Adaptive Controller and applied to the SCORBOT ER V PLUS manipulator. Finally, the Unfalsified Control technique was successfully applied to the WAM model for a similar simulation setup.

In conclusion, this work may contribute to the use of advanced nonlinear control and payload handling techniques for redundant backdrivable multiple DoF manipulators, suitable for human interactive environments.

Keywords: Robotic manipulator, nonlinear switching control, Dynamic Load Carrying Capacity, DLCC, Unfalsified Adaptive Control, UAC, WAM, Human-Robot Interaction, HRI.

Resumen

Esta tesis doctoral presenta los resultados de simulaciones numéricas y algunos análisis experimentales de tres aspectos principales: el modelamiento dinámico de manipuladores de múltiples grados de libertad (GdL) ($n > 2$ GdL), el cálculo de la capacidad dinámica de carga asociada al manejo de dicha carga, y el análisis y diseño de controladores nolineales incluyendo el Control Adaptitivo por Desfalsificación (CAD). Se desarrollaron análisis de dos (2) casos de estudio: el SCORBOT ER V PLUS fabricado por Intelitech Corp. de 5 grados de libertad y el manipulador redundante de 7 grados de libertad conocido como el Whole Arm Manipulator (WAM) fabricado por Barrett Technology Inc. y que cuenta con características de seguridad intrínseca, manipulación inversa y docilidad, y es aplicable en la interación humano-robot (IHR).

Inicialmente, se calculó y validó el modelado dinámico de los casos de estudio. Los modelos dinámicos inverso y directo del SCORBOT ER V PLUS fueron validados numericamente. Luego, una validación experimental para el WAM presenta una comparación entre los datos numéricos y experimentales, identificando la necesidad de un mejor modelo de la fricción seca. Después, se propuso y evaluó una metodología para el cálculo de la capacidad dinámica de carga en el espacio de trabajo completo de manipuladores para diferentes tipos de controladores. Luego, para el análisis del Control Adaptitivo por Desfalsificación con factor de olvido para manipuladores de múltiples grados de libertad, se realizó una comparación con un controlador adaptativo tradicional basado en el modelo y se aplicó al modelo del manipulador SCORBOR ER V PLUS. Finalmente, la técnica de Control por Desfalsificación fue exitosamente aplicada al modelo del WAM.

En conclusión, este trabajo puede contribuir al uso de técnicas de control nolineal avanzado y manejo de carga para manipuladores redundantes con manipulación inversa, aplicables en ambientes de interacción con humanos.

Palabras clave: Manipuldor robótico, control nolineal no suave, Capacidad Dinámica de Carga, CDC, Control Adaptitivo por Desfalsificación, CAD, WAM, Interacción Humano-Robot..

Contents

List of Figures

List of Tables

List of symbols and abbreviations

Symbol/Abbreviation	Meaning
HRI	Human-robot interaction
$UASC$	Unfalsified adaptive switching control
UAC	Unfalsified adaptive control
UC	Unfalsified control
DoF	Degree of Freedom
WAM	Whole Arm Manipulator
$DLCC$	Dynamic load carrying capacity
$pHRI$	Physical Human-Robot interaction
IAD	Intelligent assist devices
DEA	Differential elastic actuators
$PARs$	Power assist robots
HRC	Human-robot collaboration
$AMMs$	Assistive mobile manipulators
OFC	Optimal feedback controller
$RULA$	Rapid Upper Limb Assessment
$RLfD$	Robot Learning from Demonstration
LWR	Lightweight robot
DPC	Distributed power control
$SCLI$	Stably causally left invertible
$MIMO$	Multiple-input multiple-output
$ASSC$	Adaptive switching supervisory control
VR	Virtual (fictitious) reference
$CSTR$	Continuous stirred-tank reactor
PID	Proportional-Integral-Derivative
DDC	Data-driven control
MBC	Model-based control
ILP	Iterative linear programming
$TPBVP$	Two-point boundary value problem
FEM	Finite element method
WMM	Wheeled mobile manipulators
PKM	Parallel kinematic manipulators

Symbol/Abbreviation	Meaning
q_i, $\dot{q}_i$, $\ddot{q}_i$	Angular positions, velocities and accelerations of manipulator's joint i.
m_i	Mass of the manipulator's link i
$\mathbf{H}(\mathbf{q})$	Inertia matrix of the compact dynamical model of a manipulator.
$\mathbf{C}(\mathbf{q},\dot{\mathbf{q}})$	Coriolis and centripetal terms of the manipulator's dynamical model.
$\mathbf{g}(\mathbf{q})$	Gravitational terms of the compact dynamical model of a manipulator.
τ	Torques applied to the joints of the manipulator.
$D-H$	Denavit-Hartenberg method for kinematic modeling.
s	"Steepness" of the sigmoidal model of friction.
b_c	Kinetic Coulomb friction.
B	Viscous friction coefficient.
MSE	Mean-squared error
MRAC	Model Reference Adaptive Control
MSE	Mean-squared error
FLC	Feedback linearization controller
ADPGS	Adaptive controller with gain scheduling
PIDAW	PID controller with antiwindup

1. Introduction

The following sections present a chronological revision of three main current research topics: Human-Robot Interaction (HRI), the Unfalsified Adaptive Control (UAC) as an adaptive switching control strategy, and finally, the payload computation for robot manipulators. The purpose of this chapter is to provide a general framework for the problem statement of this doctoral thesis, related with the payload analysis of robot manipulators for human interactive environments.

1.1. Robots for human interactive environments

Human-Robot Interaction (HRI) is a field dedicated to study, design and evaluate robotic systems used by humans in a variety of challenging environments. For HRI, one of the basic topics is the communication between robots and humans. This interaction may take several forms depending, among others, to each other proximity (remote or proximate interaction). Proximate interaction may be represented by mobile assistant robots or required physical interaction. Safety is an important issue to consider as well. It would also require social interaction, including social, emotive and cognitive aspects.

In [32], Goodrich *et al.* present multiple developments in the last decades for cognitive capabilities in Human-Robot Interaction (HRI). They state that in the near future, there will be robots with social capabilities to interact with final end-users in multiple scenarios. Hence, HRI would emerge as a field of science study that requires strong interdisciplinary works with various scientific and engineering fields. Besides, this field includes many challenging problems and has the potential to produce solutions with positive social impact.

In [81], Shibata *et al.* present the concept of "virtual nonholonomic constraints" applied to the end-effector of a redundant robotic manipulator. This concept relates to common activities like riding a bicycle, driving a car or handling a wheel barrow, that involve geometrically nonholonomic constraints and require to get used to do. For a robotic manipulator, the operator may use the ability of the robot to sustain the load, forced by the environment or the operator by holding the end-effector and moving it as using a shopping cart or a barrow. Users like elderly people and children, may use robots without any specific knowledge on the robotic system. The system should be easy to understand and predict how it will move next.

Robots used to execute tasks in cooperation with humans should include control systems that adapt to human characteristics in order to successfully accomplish the proposed tasks. A basic example may be pushing a cart down on a frictionless plane in cooperation with a human, as proposed in [14]. Controlling the motion of the object down a frictionless plane requires pushing in one direction and supporting in the opposite direction. Besides, the compliance control method measures forces and moments exerted by the environment for robotic interaction with the environment, to avoid saturation of actuator related to increase of contact force or damage of the part in contact.

Rehabilitation robots are widely used for individuals with limited use of their hands and arms. Hence, it is necessary to consider functionality of the user as a priority. As evaluated in [86], the devices must be able to accommodate to a wide range of object manipulation tasks in a variety of unstructured environments. Some common examples are picking things up from the floor or off a shelf as the most prioritized tasks, opening doors and drawers and personal help in tasks as eating or personal hygiene. The reaching tasks are generally well-performed by robotic arms mounted in a wheelchair, depending on the weight and size of the objects to be grasped.

The transfer of objects between humans and robots is a fundamental way to coordinate activities and cooperatively perform useful work. Some issues have to be considered, like physical contact, reach direction, and grasp shape, in order to facilitate object transfer [24]. During collaborative tasks a robot requires understanding intentions and desires of a person, in order to behave as a partner rather than just a tool [13]. But reaching gestures may be enough for inexperienced subjects in robotics to hand to or take an object from a robot [24].

Results in [96] shown how a robot should approach a human in a fetch and carry task. The authors propose that seated subjects do not like to be approached by a robot directly from the front even when seated behind a table. They prefer a frontal approach when standing in an open area. Besides, humans do not usually like the robot to move or approach directly from behind or out of sight, even if this means the robot taking a non-optimum path. Domestic and office robots will have to move physically around in the same space as humans, but robots should not simply move around and avoid people in the same way as an inanimate object, they should respect social spaces and shared workspace preferences of the people.

In [21], the perspective of physical Human-Robot Interaction (pHRI) counts with multiple issues to address in order to approximate to a safe and dependable interaction. Safety is related to mechanical and control issues, and dependability relates to attention mainly by sensors, control architectures and fault handling. Hence, metrics for safety and dependability were developed in order to introduce the robots in daily environments. This metrics represent an evaluation criterion for mechanical design, actuation and control strategies. Robots like the lightweight DLR-III, capable of operating a payload equal to its own weight, and the Whole Arm Manipulator (WAM) with cable-actuated and backdrivable joints, are examples of intrinsic safety robots for low inertia compliant

collision situations and variable gain actuation.

Wearable robots for assistive human upper extremities require interfacing the human and robot, as analyzed in [61]. These are designed to be a human force increasing systems to allow humans to use the forces generated by the robot. This systems may operate in multiple environments such as medical services and military equipments to reduce the load on the back of the users. Also, it may be applied in industrial settings helping to manage heavy materials. The wearable robots are categorized according to bio-information sensor types as: biomedical signals, force signals and hybrids. They may react before or after human motion depending on the signal used by the feedback system.

In [60], Kruger *et al.* evaluated robotic systems as important components in fully automated assembly processes and highly efficient production. Due to the rising demands for augmented flexibility and adaptability to variable assembly tasks, robot assisted but human guided assembly shows significant advantages to full automation. Flexibility and changeability as cooperative tasks improves assembly processes, particularly when the robot provides power assistance to the user. An essential consideration is the safety of the user delivered by sensor systems available in the market for surveillance of the interaction with the robot. Hence, research in the field of Intelligent Assist Devices (IAD) is being developed. The next generation of robots should interact with humans for cooperative manipulation, where the robot is responsible for the management of the load and precision and the human may help with sensing, intelligence and skills.

Direct physical interaction is used by humans to move objects and guide people in a variety of settings, from industrial to natural environments, and the same would be expected of robotic systems. However, most of current mobile robots use non-backdrivable motors for locomotion, making them potentially dangerous in case of collision. In [28], the robot named AZIMUT-3 shows steerable wheels using backdrivable and torque controlled Differential Elastic Actuators (DEA), capable of being force-guided. The robot may move efficiently in response to physical commands by a human pushing in a desired direction.

A nursing-care assistant robot known as RIBA, presented in [67], deals with direct physical contact with patients, specially elderly people. The robot interacts with its environment and humans through multiple and distributed contact regions on its arms and body. Tasks including the transfer of patients, such as lifting and moving a patient from a bed to a wheelchair and back, are among the most physically challenging tasks in nursing care. RIBA has tactile sensors on a wide area of its arms to obtain information of that whole-body contact. When controlling position and orientation of a person, the relative position and orientation of contacting surfaces should be preserved as long as possible. Stable forces and pressure patterns of each contact region require the use of tactile feedback to avoid skin grazing.

Kalakrishnan *et al.* analyze in [39] how the development of fine manipulation skills with compliant actuation and control are very important to behave safely in human interactive environments. Manipulation requires complex contact interaction with the external world and involves control of the forces and torques to be applied. This often results impractical in contact conditions due to computational complexity and lack of precise dynamical models of the environment. There are suggested solutions focused on learning the manipulation skills through teaching position trajectories and learning forces and torques to be controlled at the end-effector by haptic systems.

In industry, handling heavy objects is a common tasks, as evaluated in [75]. It may be difficult due to the probability of causing work disabilities or diseases as back pain. In some cases, handling objects by autonomous devices may not be flexible. Power Assist Robots (PARs) may be a solution for handling heavy objects, but they are not currently available in practice. At this moment, the PARs were mainly developed for the elderly, disabled people and for rehabilitation. Although, there are other applications like assistance for agricultural or manufacturing workers, hydraulic power-assist for automobiles, assist for sports, baby carriage lifting, etc. Conventional PARs are not enough safely and friendly interactive for humans. Issues like the need of touch of the object causes attenuation of perceived heaviness, that may cause excessive load force and sudden increase of object acceleration, fearfulness of the human, lack of maneuverability and stability, etc. Studies on lifting and lowering heavy loads for PARs are open fields and may consider the differences in control for both tasks.

Robots safety functions should become an important part of the robot systems. Safety on manufacturing robots uses mechanical equipment or electronic control devices such as safety fences, light curtains and laser scanners. But these devices use unnecessary space and are not easy to implement and relative high priced. Strict robot safety functions are necessary for Human-Robot Collaboration (HRC) as an effective way to accomplish tasks with high complexity and variance. Hence, the definition and development of robot speed and area restrictions are necessary. Besides, HRC should integrate safety monitoring systems related to identified risks or levels of danger. Some international safety standards are applicable to industrial fields, like $ISO13849-1$ and $IEC61508$. In [7], the "Safe Space" systems and algorithms show the hardware and software necessary to ensure safety for the users and equipment and is applied to the robot safety function of Hyundai Heavy Industries Co. Ltd. (HHI).

Chen *et al.* present in [16] the *Robot for Humanity* project for people with severe motor impairments to interact with their own bodies and manipulate their environment. The project evaluates the use of Assistive Mobile Manipulators (AMMs) like the PR2 (Personal Robot 2, developed by Willow Garage). The mobile manipulators may operate away from the user and have a large dexterous workspace and not directly burden the user. The project uses an interactive design process with a quadriplegic to improve the designs and develop the next set of capabilities. Two areas are covered: understanding how individuals with severe impairments may use these robots for self-

care tasks and house hold activities, and the exploration of how mobile manipulators may assist the user in an unstructured domestic environment. Videos an code associated with the project may be found at http://www.willowgarage.com/robotsforhumanity.

In [76], a power assist robot for lifting objects presents two force control methods. Hence, the authors evaluate force control methods for a 1 DoF power assist robot with weight perception like the humans. The performance of the individual controllers is evaluated using perceived heaviness, force and motion features, safety and stability. The authors present the development of these control methods for robots in industry and domestic applications to improve productivity. The manipulation of heavy objects is applicable in tasks like loading and unloading heavy bags or luggage from different public transportation systems or in industries such as automobile, agriculture, military, ship building, forestry, mining, etc.

1.1.1. Manipulation

Programming-by-demonstration is often used for a multi-fingered multi-joined robotic hand to move synchronously and cooperatively to execute a task. In [63], Matsuo *et al.* propose a segmentation method of human manipulation tasks based on measurement of contact force of a human hand on a grasped object. They define an index measure for segmenting a human manipulation task into primitives. The indexes are computed from the set of contact forces measured at different contact points during a manipulation task. Then, they applied an expectation-maximization algorithm to the set of indexes in order to segment the manipulation task into primitives. These primitives map in the robotic hand to control adequate contact forces on a grasped object. Experimental results show successful segmentation of manipulation tasks performed in daily human life.

Mitrovic *et al.* present in [64] an Optimal Feedback Controller (OFC) of movement in large redundant Degree of Freedom (DoF) manipulators (like the WAM), with emphasis on the reaching task. It is challenging due to redundancy, because the controller has to make a choice between many different possible trajectories and applicable motor commands for a particular task. The friction model usually consists of static and kinetic Coulomb component as well as of a viscous friction. The authors propose to approximate the frictional joint torques as a combination of only kinetic Coulomb and viscous friction components, using a smooth and continuous sigmoidal function. Then, they estimated the kinetic Coulomb friction coefficients and the viscous friction coefficients for the WAM using a least-square estimation method, based on experimental measurements.

Robots are developed to resemble the size an physical abilities of a human in human interactive environments and to operate autonomously with no physical threat to humans. Paik *et al.* evaluate in [68] the construction of a humanoid-applicable anthropomorphic 7-DoF arm with an 8-DoF hand. The design claims to be compact, compliant, powerful and functionally flexible, with dexterous hand movements. The arm and hand are capable of sensing and interpreting external force using

measures of current signals in each motor joint, and without torque sensors. The arm includes obstacle avoidance algorithm and the hand is capable of object grasping.

In [30], Gan *et al.* propose a human-like manipulation planning method for articulated robots. The method uses the evaluation and optimization concepts managed by humans. This constrained optimization problem in robot configuration space is divided into different subregions using the applied ergonomics strategy of Rapid Upper Limb Assessment (RULA). The proposed method integrates model based and model free approaches for manipulation planning. The optimization problem uses task compatibility measurements of the robot velocity transmission ratio along a specified direction.

In HRI, robot designers need to consider human-oriented constraints to perform various tasks for humans. Hence, it is not sufficient that the robot selects grasp and placement of the object considering only the stability. In [69], Pandey *et al.* propose a set of key configurations for planning basic interactive manipulation tasks. The authors based on the human behavioral psychology of the mutually dependent nature of grasp and placement selection. Grasp and placement are constrained by the task, the environment and the perspective of the subject. As results, they presented a generic planner to synthesize the configuration, orientation and position for trajectory planning, inspired in the human behavioral psychology.

In [22], Dumora *et al.* present a method that allows humans to perform complex large object manipulation tasks with a robot. This is achieved by the use of a set of assistances for *a-priori* unknown collaborative tasks. It uses haptic cues to naturally transmit the intention of the user in a collaborative motion and the robot chose on-line from a set the corresponding assistance. Hence, under the assumption that the task was known and repetitive, a common approach would be to design a robot able to anticipate to human actions and participate in the effort sharing. It is common to use programming by demonstration in this kind of tasks.

Robot Learning from Demonstration (RLfD) is a key technique for making robots useful in daily use. Previous works use learning to obtain a kinematic model related to the task and then the task is developed with a position controller. But some times that is not enough to achieve the goal, for example, those task requiring contact or needing specific responses to physical perturbations. Hence, the adjustment of compliance for different needs is an open field in RLfD. Robots like the WAM manufactured by Barrett Technology Inc. and the Lightweight Robot (LWR) made by KUKA, are manipulators with inherent compliance associated to their designs. In [59], the authors propose teaching interfaces that allow to change the stiffness of the robot by physically interacting with it.

Quintero *et al.* in [73] present an interactive semi-autonomous teleoperation control for robot manipulators. The method focuses in two interactions: a human can control a robot arm by a visually

tracked human skeleton for rough motion and precise positioning is performed using an autonomous image-based visual servoing routine, launched by a gesture interface. Results show the gesture interface switching between two modes: in mode 1 the user teleoperates a WAM robot arm directly from the user arm movements with gesture control commands like opening and closing; in mode 2 the user selects and object of interest, initiate a tracking algorithm and start a visual servoing routine with gesture commands. Rough motion is successfully obtained. In cases when teleoperated motions is fast, the movement is not very smooth and precise, hence, visual servoing shows to be a good complement.

In a human tasks requiring contact, an approach is to describe those contacts by contact states. These are kinematic configurations where one or more vertices, edges, or planes of an object contacts another. The states and transitions between them are organized into a graph. Hence, for a robot to perform control strategies based in contact like humans requires the identification of complete sequences of intermediate contact states connecting arbitrary states in the contact graph, and developing hybrid force-position controllers for the transition between those states. Klingbeil *et al.* present in [41] an approach to characterize human contact control strategies for complex contact manipulation tasks, during rigid body manipulation. Results show than while humans visit many states, they reliably visit only a small subset of the states (approx. 2 %), indicating that their control strategy is invariant to most contact states.

1.2. Data-driven adaptive switching supervisory control: Unfalsified adaptive control (UAC)

Safonov and Tsao in [79] define Unfalsified Adaptive Control (UAC or UC). A theory for the identification of adaptive switching control laws, without the use of the plant model. The control laws are related to performance objectives and past experimental data, proving these control laws on-line to decide about its insertion in the feedback loop. This theory may characterize a set of possible controllers to unstabilize with new experimental data related with prior assumptions or earlier data. The authors claim as the main feature of UAC theory, its flexibility and simplicity of implementation to nonlinear time-varying and to linear time-invariant plants.

In [80], Safonov presents an examination of UAC theory using the behavioral perspective of Willems [100]. This paper presents a min-max optimization problem formulation that unifies direct adaptive control, learning theory and system identification problems in a common behavioral setting based on the controller unfalsification perspective. Theoretical results show the conceptual link between adaptive control technique and system identification strategy, related to UAC from the behavioral view point.

Paul *et al.* present in [70] a successful application of UAC for transmitted power in wireless net-

works. The transmitted power in these networks is critical for maintaining the quality of service, maximize channel utilization and minimize near-far effect for suboptimal receivers. The proposed data driven algorithm uses multiple candidate PID controller gains for controlling transmitted power. It adapts to different number of users in a cell, selecting and placing one controller from the set in the feedback loop depending on stability and performance. Simulation results show that the proposed scheme performs better than several candidate controllers, including a Distributed Power Control (DPC) algorithm for higher number of users in the cell.

In [18, 105], the authors present two advanced PI controller tuning methods: unfalsified control and fussy control. They applied the controllers to an industrial weigh belt feeder that has significant nonlinearities. Neither method requires an explicit plant model. One advantage of the unfalsified PI control design method is that is able to directly incorporate multiple performance criteria. The fuzzy logic allows to incorporate human reasoning in the design process. A detailed comparison of the two approaches is given in the areas of design specifications, process knowledge requirements, computational requirements, controller development effort, transient performance, and the ability to handle motor saturation. Experimental results show effectiveness of both control methods.

Wang *et al.* present in [99] the stability analysis of Unfalsified Adaptive Control, based in the Morse-Mayne-Goodwin hysteresis algorithm [66], using multiple controllers. The UAC uses cost functions with cost detectability properties, as presented in [87]. Simulation results proved that the stability can be guaranteed whenever the adaptive stabilization problem is feasible, *i.e.* whenever there is a stabilizing controller in the set of candidate controllers. The hysteresis algorithm performs safe adaptive control without plant model assumptions. Simulations demonstrated that the proposed controllers are not only safe, but also quick.

In [98], the authors prove that using $\mathfrak{L}_{2e}$-gain-related cost detectable functions together with Stably Causally Left Invertible (SCLI) candidate controllers is sufficient to ensure that the Morse-Mayne-Goodwin hysteresis algorithm [66] correctly detects destabilizing candidate controllers without assumptions on the plant, eliminating plant model-mismatch instability problems. The conditions ensure that the cost function correctly selects controllers, so that the hysteresis algorithm performs a safe adaptive control that is guaranteed to be stable if the feasibility requirement is fulfilled, that is, there exists at least one stabilizing controller in the set of candidate controllers.

In [33], VanHelvoort *et al.* present a data-driven multivariable controller design using ellipsoidal UC. It does not require a plant model, only measured input/output data. It uses the concept of controller unfalsification, where it is recursively checked which of the controllers in a set would have met the predefined performance requirements without the need to actually implement them. For ellipsoidal UC, the region of unfalsified controllers is updated each sample, and the continuous region is described by an ellipsoid. The proof of stability for Multiple-Input Multiple-Output (MIMO) systems is deduced from the theory of Simple-Input Simple-Output (SISO) ellipsoidal UC.

The Annual Reviews in Control in 2008 [4] present a review of challenges in adaptive control. In the model-free adaptive control section, the analysis of the UAC states that it is not yet mature and that it has a number of question that are currently unanswered, like: related to the possible misleading notions of "model-free" and "no prior assumption on the plant", how much information about the plant is required to guarantee a practical and safe model-free adaptive control?. It states that this control approach gives no guarantee of protection against inserting a destabilizing in the loop, or that controller can remain in the closed loop for a long period of time resulting in very large control signals. Besides, it proposes that the closed-loop system can actually turn unstable but the instability need not be revealed by a value of the cost function tending to infinity with time.

In [88], Stefanovic *et al.* address the theoretical explanation of the model-mismatch instability problem related to certain adaptive control design schemes and propose a solution. A class of data-driven cost-detectable functions is introduced, intended to detect evidence of instability without reference to prior plant models or plant assumptions. The solution is proposed as a setting of standard optimization problem. The result is called "safe adaptive control", because it robustly achieves adaptive stabilization goal when it is feasible, without the risk of model-mismatch instability, improving results of previous hysteresis switching control approaches.

Battistelli *et al.* propose in [9] a different switching logic, combined with appropriate test functions for Adaptive Switching Supervisory Control (ASSC). This proposed change makes it possible to extend UAC, restricted to time-invariant systems, to the case of nonlinear systems with dynamics that are subject to infrequent but possibly large variations, like payload changing manipulators. Furthermore, this different switching logic can also be used with model-based test or cost functions, making it possible to improve the closed loop behavior in case a set of nominal plant models are available.

In [8], Baldi *et al.* present differences between the main current approaches to Adaptive Switching Supervisory Control (ASSC). The analysis focuses on how to on-line determine stability of a feedback control loop with a candidate controller that only uses inputs and outputs from the plant, while the plant is driven by a different controller. Hence, it is used the concept of Virtual Reference (VR), related to the unfalsified adaptive switching control. It proposes a supervised switching mechanism to determine the chance that destabilizing controllers be switched-on and reduce both magnitude and time durations of starting estimation transients. The asymptotic stability is guaranteed under the assumption that a stabilizing candidate controller exist, also known as feasibility requirement.

In [10], Battistelli *et al.* presented the input-output stability analysis of an Unfalsified Adaptive Switching Control (UASC) in a noisy environment. It is discussed the issue of equivalence among different input-output definitions. Hence, the authors show than in some cases robustness against disturbances is more complex to achieve than in a classical time-invariant feedback loop. Besides,

there is no guarantee of finite-time convergence for switching due to the assurance that test functional (cost detectable functions) remain bounded for indexes related to candidate controllers.

In [38], Jin *et al.* constructed a new cost-detectable function based on fading memory data to reduce the influence of older data. A new controller switching algorithm is designed to guarantee stops and that the closed-loop system is stable. Simulation results show that when the plant changes slowly, the algorithm can detect instability and switch to stabilizing controller, once the currently active controller becomes destabilizing for the new plant dynamics. Hence, the controller is able to avoid large magnitudes of the output signal due to instability.

Felicio *et al.* applied an UAC in [25] to an experimental inverted pendulum. Using a set of six candidate controllers, of which two are destabilizing, a supervisory program is built. Experimental results show that the best controllers are selected most of the time. When a destabilizing controller is put in the loop, it is quickly removed and the performance does not degrade significantly. Hence, unfalsified control may be useful for control adaption to parameter changes, even though it may select destabilizing controllers for a short time period. Candidate controllers may be designed using the plant model, but it is not used by the supervisory system.

In [101], an algorithm for the automatic adaption of linear controllers, based in the idea of the UC, proposes the adaption of the set of controllers after a change of the operating point of the plant. Due to problems related to the proposed cost detectable function, based on the so-called fictitious reference, the authors proposed a different cost function and a new method for online evaluation of off-line controllers. The new cost function allows the adaptation of the set of controllers based on an evolution strategy and a diversity operator. The method, demonstrated on a Continuous Stirred-Tank Reactor (CSTR) model with van der Vusse reaction and PID controllers, shows better and faster performance compared to a fixed non-adaptive PID controller.

In [17], Cheong *et al.* proposed a switching algorithm for UAC, developed to use a pair of cost functions, called primary and secondary cost functions. The primary cost function satisfies certain conditions to accomplish the stability of the UAC system. The secondary cost function may be designed based on a performance measure of interest without any condition to satisfy. Hence, the secondary cost function may use prediction-based and data-based cost functions. Besides, the secondary cost function may help to find the best stabilizing controller in the controller set. Then, the authors presented successful simulation results for theoretical models.

Hou *et al.* presented in [35] a survey about definitions, classifications, relevant topics and state of the art of the data-driven control methods, including Unfalsified Adaptive Control. It also proposes a discussion about differences and relationships between the Model-Based Control (MBC) and the Data-Driven Control (DDC) methods. Conclusions on the comparisons provide a perspective on those theories and potential future research topics.

1.3. Payload analysis in the robot load-space and Dynamic Load Carrying Capacity (DLCC) computation

The maximum allowable load of a fixed base manipulator is often defined as the maximum payload that the manipulator can repeatedly lift in its fully extended configuration [54]. But some other factors like the inertia effect of the load for different control tasks and the manipulator dynamics should be considered to compute the maximum allowable load of a manipulator. In [92], the authors used the load capacity as a criterion for sizing the actuators of a robotic manipulator at the design stage, considering the maximum load in the neighborhood of the robot configuration.

In [97], Wang *et al.* proposed that the maximum allowable load of a fixed base manipulator on a given trajectory is primarily constrained by the joint actuators torque and its velocity characteristics. In [103, 51], the rigid body assumption is removed for links and joints. For flexible manipulators, the authors present additional constraints related to end-effector deflection and a method to determine maximum allowable load of flexible manipulators subject to both actuator and end-effector deflection constraints. Then, they applied this methods to two degree of freedom manipulators.

In [54], Korayem *et al.* present a computational technique for determining the maximum allowable load of wheeled mobile manipulators for a predefined trajectory, using the augmented Jacobian technique. The authors state that some applications and motion planning algorithms of mobile manipulators consider cases of carrying a full load, *i.e.* in construction, military or hazardous working sites such as nuclear power plants or chemical production plants. Besides, factors like the dynamic properties of mobile base and mounted manipulator limit the maximum allowable load manageable by a mobile manipulator during a tracking task. Hence, the authors propose additional constraints functions in the task space. Simulation results obtained from a 2 DoF manipulator, mounted on a differentially drive mobile base, show that the value of maximum allowable load on a given trajectory directly depends on the additional constraint function.

In [45], Korayem *et al.* presented the load carrying capacity of mobile base manipulators operated by limited force or torque actuators. The authors propose that the maximum allowable load on a given trajectory is a function of the base position, considering that the load workspace defines the set of places where the base may be located carrying a load on a desired trajectory. The workspace is divided into a grid of possible positions of the base, allowing to move it to each grid point. Actuators torque constraints applied to each base location define the load carrying capacity of the mobile manipulator. The optimum base location is a global maximum of the load carrying capacity of the manipulator for the desired trajectory. Results show that in cases where there is no freedom to change the load path, the base relocation may maximize the Dynamic Load Carrying Capacity (DLCC) of the manipulator.

Korayem *et al.* in [56] formulate and numerically solve the problem of finding the maximum dynamic load of mobile manipulators for a given two-end-point task. The authors considered three main constraints for computing maximum DLCC of mobile manipulators: actuator capacity of the manipulator, the kinematic redundancy related to base mobility and nonholonomic constraints. For the redundancy issue and nonholonomic constraints, the authors used the extended Jacobian matrix concept. This trajectory constrained nonlinear optimization problem used the Iterative Linear Programming (ILP) method for solution. Simulation results show that while the mobile manipulator moves along an optimal trajectory, the coupling inertia of the manipulator and load are minimized preserving the constraints. In [55], Korayem *et al.* presented a computational technique for obtaining optimal trajectory of mobile manipulators with flexible links and joints to maximize their DLCC for a given point-to-point task.

In [26], a control scheme for single-link flexible very lightweight robots consists of two nested loops: an internal loop (PD regulator) that controls the motor dynamics and an external loop (feedback of torques at the base of the link, measured by a strain gauge) that allows the tip to be positioned in space. Simulation show that the control scheme is robust to payload variations due to the use of strain gauges to measure link deflection and errors in parameter estimation or motor parameter change. Then, simulations focus on comparison of the controller with classical controller. After that, Feliu *et al.* presented in [27] a robust scheme for trajectory tracking of the same kind of manipulators. The controller achieves stability during motion for different values of tip mass, while accurately tracks the desired trajectory. The controller also guarantees stability of small uncertainties in parameters such as stiffness or motor friction. Analytical development and numerical simulation with variations in the robot parameters are compared with some of the most efficient robust control strategies as: Integral resonant control, Wave-based Control, H-Infinity and LQR Control, showing that the proposed method exhibits the best tip trajectory tracking. Besides, experimental results show that the controller is very effective in canceling the first vibration mode, while leaving higher modes unaltered, which is suitable for a very lightweight arm, where vibration modes higher than the first one may be considered negligible.

In [52, 53], the authors presented a method to compute the DLLC of manipulators with joint elasticity, subject to accuracy and actuators constraints, using feedback linearization technique to minimize end-effector deflection. Feedback control law obtained a full state linearization that gives input-output decoupling. Simulation results drawn for different sets of tracking trajectories show different load carrying capacities in each case, as expected.

Korayem et.al presented in [47] the maximum dynamic load carrying capacity of flexible joint manipulators in point-to-point motion as an optimal control problem, using the indirect solution method. This proposes a Two-Point Boundary Value Problem (TPBVP) solved numerically. The authors propose two different perspectives: The first one may be used to plan the optimal path for

a given payload, and the second may be applied to find the maximum payload and corresponding optimal path. Simulation results show various optimal trajectories with different characteristics and maximum payloads. A comparison of effects of flexibility with rigid robots shows that the more stiffness leads to maximum payload and high stiffness values converge to the rigid joint results.

In [46], kinematic and dynamic equations using Finite Element Method (FEM) enables to consider the full nonlinear dynamics of mobile manipulators with flexible links. Results show that the actuator torque capacity is the dominant constraint for determining the DLCC of the motion. Besides, there are other alternatives for carrying more loads in comparison with fixed base robots, due to the fact that the base trajectory may be changed without changing the end-effector trajectory.

Then, [48] analyzes the DLCC and the joint optimal path for kinematically redundant manipulators to track a given end-effector path, subject to actuator torque limits. It uses the indirect solution of open-loop optimal control problem to solve the path-planing problem and take advantage of redundancy to increase the load-carrying capacity. Decomposing joint coordinates in redundant and nonredundant parts allows the derivation of dynamic equations. Then, a Two-Point Boundary Value Problem (TPBVP) uses numerical methods to solve the optimization problem. Simulation results, applied to a 3 DoF mobile manipulator with one extra DoF, computed the DLCC for redundant manipulators and the payload increased using the extra DoF.

In [43], Korayem *et al.* proposed a method based on stability for determining the maximum DLCC of a coordinated mobile manipulator in an environment with the presence of obstacles. It considers the tip over stability on zero moment point criterion for a predefined end-effector path but free position of the mobile platform. The obstacle avoidance scheme uses potential functions. An iterative method based on the stability criterion and motor restriction (torque and jerk) computes the maximum DLCC. Simulation and experimental results on a nonholonomic Wheeled Mobile Manipulators (WMM: differential drive mobile base and a robotic arm) show that in the presence of one obstacle and a specified path of the end-effector, in some cases, the accuracy of tracking the desired path is satisfied. Obstacles causes a difference in path, as expected. The stability constraint may become a dominant constraint. Comparison of simulation and experimental results showed a difference of 7 % between the maximum allowable loads.

In [31], Ghariblu *et al.* presented a computational technique for determining the maximum DLCC of cooperative manipulators for a desired trajectory of the load. The configuration of this manipulators considers as most important constraints the dynamic properties related to redundancies, actuator torque limitations and trajectory accuracy. The proposed methodology first develops the kinematic and dynamic equations, then computes the maximum torques on each joints and finally the maximum DLCC. Simulation results of two cooperative three-link manipulators show the validity of the algorithm for determining the maximum DLCC and that the allowable load is variable along the desired trajectory.

In [44], Korayem *et al.* proposed a DLCC computation method for a cable-suspended parallel manipulator. The manipulator is assumed to be a rigid manipulator. The joint actuator torque and cable tension force capacities are the major limiting factors in determining the payload. These constraints are a common framework for dynamic characterization of the cable-suspended parallel robot. Two cable robots of 3 and 6 DoFs permits the computation by simulation of the maximum DLCC. Then, the authors present in [58] a control system based on feedback linearization for both rigid and flexible joints in cable robots, showing satisfactory simulation results. Again, Korayem *et al.* presented in [57] a method for trajectory planning (find the manipulator DLCC in a Point-to-Point task) for cable robots using optimal control approach by solving the corresponding nonlinear two point boundary value problem. Finally, the authors presented in [50] an approach for trajectory planning of cable-suspended parallel robots using optimal control, applied to an experimental prototype. Experimental results show an slightly difference with the simulation results related to the maximum DLCC computation.

Chen *et al.* proposed in [15] a methodology to determine the maximum DLCC for reconfigurable motor-driven Parallel Kinematic Manipulators (PKM). The methodology uses the identification of the optimal configuration for the maximum DLCC for the desired trajectory, limited to the constraints determined by the kinematics and dynamics of the manipulator structure. The proposed method uses a two loop optimization process. The Particle Swarm Optimization (POS) algorithm is used for the outer-loop optimization, and the Linear Programming (LP) algorithm is used for the inner-loop optimization. Relocating the base points along linear guideways achieves the reconfiguration. Simulation results presented the effect of base mobility on maximizing the DLCC along a prescribed trajectory and shown that optimally changing the base position has a high increase in the maximum DLCC, due to the use of torque bounds on more actuators.

1.4. Problem statement

The history of robotics is related with the idea of replacing human workers from monotonous, unpleasant or dangerous tasks. Hence, powerful, large and hazardous robots requires of perimeter-protected working spaces. This was not a problem in the industry, but excluded environments where humans were present. Therefore, houses, hospitals, offices and other spaces were not an option for robotic interventions and new concepts for robots were needed for safely interact with humans.

Multiple applications in HRI involve manipulation: rehabilitation for individuals with limited use of their hands, transfer of objects between robots and humans for collaborative work, physical HRI with patients, wearable Power Assistive Robots (PARs) for human extremities in industry or other applications for handling heavy objects, the use of Assistive Mobile Manipulators (AMMs) like the PR2, etc.

Considering the wide research spectrum in robotic manipulation, this work will focus on two issues: payload handling analysis and control systems related to manipulators suitable for HRI.

1. The maximum payload issue in manipulation is commonly treated as the maximum payload that the manipulator can repeatedly lift in its fully extended configuration, but other factors like the inertia effect of the load for different control tasks and the manipulator dynamics should be considered to compute the maximum allowable load of a manipulator. In HRI the payload is an important issue related with tasks which require lifting or manipulation of payloads. Hence, it should be proposed a research about a methodology for the computation of the maximum payload in the entire workspace. We suggest the use of cell to cell mapping, as an intensive computational strategy, to analyze the DLCC for MDoF manipulators and its ability to map different paths, with potential use in path planning in various environments, like in HRI settings.

2. The data-driven Unfalsified Adaptive Control (UAD) has been successfully used in some applications, motivating us to propose a research of its application in Multiple Degree of Freedom (MDoF) manipulators ($n > 2$ DoF). Comparisons with traditional control techniques for robotic arms would serve to identify the usability of this currently developing control strategy. It should be evaluated the application of UAD with fading memory for two cases of study, including the compliant Whole Arm Manipulator (WAM).

1.5. Participations and diffusion of results

1. Two (2) international congresses:
   - "Dynamic Load Carrying Capacity computation Using Nonlinear Analysis" in the $26th$ International Conference on CADCAM, Robotics and Factories of the Future (CARs and FOF), Kuala Lumpur (Malaysia), July 2011.
   - "Dynamic Load Carrying Capacity computation of manipulators using cell to cell mapping concept" in the $5th$ International Congress of Mechanical Engineering and $3th$ of Mechatronic Engineering, Bogotá (Colombia), August 2011.

2. One (1) research stage: "Whole Arm Manipulator (WAM) kinematic and dynamical modeling with experimental validation", Institut de Robòtica i Informàtica Industrial - IRI, Universitat Politècnica de Catalunya - Barcelona Tech., Sept - Nov 2012. Continued collaboration.

3. One (1) paper under review: "Unfalsified control for multiple DOF manipulators under load disturbances and parameter uncertainties" in the International Journal of Advanced Manufacturing Technologies, Springer (IF:1.205 in 2012). Submitted in March 2014.

4. One (1) paper in elaboration: DLCC in the entire workspace for multiple DoF manipulators.

1.6. Document organization

The remaining of this document presents in chapter 2 the theoretical and simulation of the dynamical models of two Multiple Degree of Freedom (MDoF for $n > 2$ DoF) cases of study, used for the rest of this work: the 5 DoF SCORBOT ER V PLUS manipulator and the 7 DoF redundant Whole Arm Manipulator (WAM). The chapter 3 presents different approaches to manipulator control techniques, from model-based to data-driven control methods. The chapter 4 proposes a computational methodology to find the maximum Dynamic Load Carrying Capacity (DLCC) in the entire workspace, applicable to any kind of manipulator including the lightweight and low inertia used in HRI applications. Finally, conclusions and future perspectives are presented in chapter 5.

2. Modeling of multiple degree of freedom (MDoF) manipulators

There are basically two approaches to obtain the dynamical model of manipulators: Dynamics of Lagrange, based on the balance of energy of conservative systems, and the Newton-Euler dynamics which considers balance of forces and moments [20, 29, 62].

The dynamical model of Newton-Euler consists of a recursive set of equations of motion developed by Luh *et al.* [62], with regard to all the velocities, accelerations, inertia matrices, location of centers of mass, forces and moments related to the coordinates system of each link of the manipulator. The procedure consists on the application of a recursive algorithm that computes each articulation force from the base to the end effector and returns from the end effector to the base computing individual moments.

For convenience, Eq. (2-1) presents the algorithm to compute the Newton-Euler inverse dynamical model, repeatedly used in this work for numerical simulation and validation results.

$$
\begin{aligned}
&{}^{i}\omega_i = {}^{i-1}\mathbf{R}_i^T\,{}^{i-1}\omega_{i-1} + \hat{\mathbf{e}}_z\dot{q}_i \\
&{}^{i}\dot{\omega}_i = {}^{i-1}\mathbf{R}_i^T\,{}^{i-1}\dot{\omega}_{i-1} + \hat{\mathbf{e}}_z\ddot{q}_i + ({}^{i-1}\mathbf{R}_i^T\,{}^{i-1}\omega_{i-1}) \times \hat{\mathbf{e}}_z\dot{q}_i \\
&{}^{i}\ddot{\mathbf{P}}_i = {}^{i-1}\mathbf{R}_i^T \left({}^{i-1}\ddot{\mathbf{P}}_{i-1} + {}^{i-1}\omega_{i-1} \times {}^{i-1}\mathbf{P}_i + {}^{i-1}\omega_{i-1} \left({}^{i-1}\omega_{i-1} \times {}^{i-1}\mathbf{P}_i\right)\right) \\
&{}^{i}\ddot{\mathbf{s}}_i = {}^{i}\ddot{\mathbf{P}}_i + {}^{i}\dot{\omega}_i \times {}^{i}\hat{\mathbf{s}}_i + {}^{i}\omega_i \times \left({}^{i}\omega_i \times {}^{i}\hat{\mathbf{s}}_i\right) \\
&{}^{i}\hat{f}_i = m_i\,{}^{i}\ddot{\mathbf{s}}_i \\
&{}^{i}\hat{n}_i = {}^{i}\mathbf{I}_i\,{}^{i}\dot{\omega}_i + {}^{i}\omega_i \times \left({}^{i}\mathbf{I}_i\,{}^{i}\omega_i\right) \\
&{}^{i}f_i = {}^{i}\mathbf{R}_{i+1}\,{}^{i+1}f_{i+1} + {}^{i}\hat{f}_i \\
&{}^{i}n_i = {}^{i}\mathbf{R}_{i+1}\,{}^{i+1}n_{i+1} + {}^{i}\hat{n}_i + {}^{i}\hat{\mathbf{s}}_i \times {}^{i}\hat{f}_i + {}^{i}\mathbf{P}_{i+1} \times \left({}^{i}\mathbf{R}_{i+1}\,{}^{i+1}f_{i+1}\right) \\
&\tau_i = \hat{\mathbf{e}}_z^T\,{}^{i}n_i,
\end{aligned}
\tag{2-1}
$$

where ${}^{i}\omega_i$ and ${}^{i}\dot{\omega}_i$ are the angular velocity and acceleration of the reference frame of the link i; q_i, $\dot{q}_i$ and $\ddot{q}_i$ are the angular positions, velocities and accelerations of the joint i; ${}^{i-1}\mathbf{R}_i^T$ is the transposed rotation matrix of the reference frame of the link i from the reference frame of the previous link; $\hat{\mathbf{e}}_z = \begin{bmatrix} 0 & 0 & 1 \end{bmatrix}^T$; ${}^{i-1}\mathbf{P}_i$, ${}^{i-1}\dot{\mathbf{P}}_i$ and ${}^{i-1}\ddot{\mathbf{P}}_i$ are the translational positions, velocities and accelerations of the reference frame of the link i with respect to the reference frame of the previous link; ${}^{i}\ddot{\mathbf{s}}_i$ is the linear acceleration of the center of mass of the link i, ${}^{i}\hat{\mathbf{s}}_i$ is the distance from the reference frame of the link i to the center of mass of the same link; m_i is the mass of the link i and ${}^{i}\mathbf{I}_i$ is the inertia tensor associated with the link i; ${}^{i}\hat{f}_i$ and ${}^{i}\hat{n}_i$ are the forces and moments applied at the center

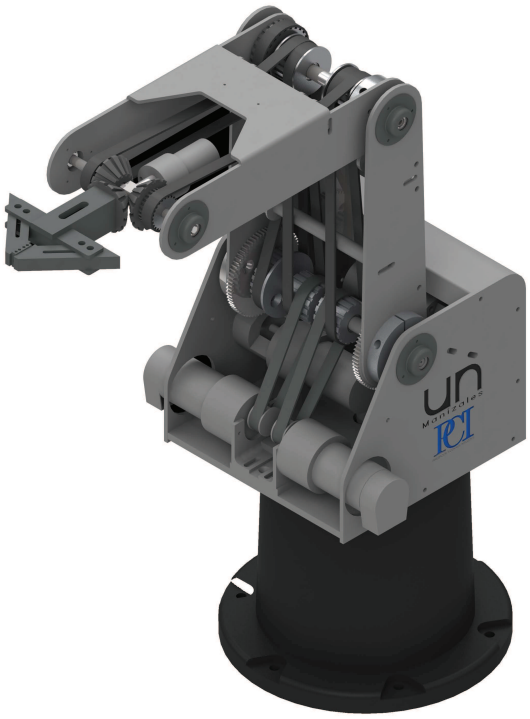

Figure 2-1.: SCORBOT ER V PLUS [37]

of mass of the link i; ${}^{i}f_i$ and ${}^{i}n_i$ are the forces and moments required for the joints in motion and τ_i are the torques applied to the joint i to generate that motion.

The remaining of this chapter shows the process of modeling and validating of those models for two cases of study, using the Newton-Euler recursion for numerical and experimental validation.

2.1. Modeling a 5 DoF manipulator like the SCORBOT ER V PLUS

Fig. **2-1** shows a CAD (Computed Aided Design) model of the 5 Degree of Freedom (DoF) manipulator known as the SCORBOT ER V PLUS, manufactured by Intelitek Corp. This case of study is used in the present section to show the procedures to obtain and numerically validate the dynamical model of multiple degree of freedom (MDoF) manipulators.

The dynamical model of a 5 degrees of freedom manipulator is the mathematical representation of a Multi-Input Multi-Output (MIMO) system, with specific kinematic and dynamical parameters. Durango *et al.* in [23] develop the kinematic and dynamical model of the SCORBOT ER V PLUS, using the Newton-Euler recursive methodology.

Using Matlab® symbolic toobox, Durango *et al.* obtain an analytical expression of the dynamical model of the SCORBOT ER V PLUS manipulator using the recursive Newton-Euler algorithm presented in Eq. (2-1). This model allows the analysis, simulation and control design of the robotic system as presented in [5]. The application of this algorithm results on a "non-compact" form of the model [20]. Later in this section, a compact form is obtained to compute the state variable representation for simulation and design of nonlinear control strategies.

The analytical dynamical model of a 5 DoF manipulator has hundreds of nonlinear terms. The size of the model significantly grows with the increase on the number of degrees of freedom and becomes difficult to be operated and transformed. The state equation for the 5 DoF SCORBOT ER V PLUS manipulator counts with ten highly nonlinear first order differential equations.

2.1.1. Compact representation and end-effector transformation matrix

The compact representation of the analytical dynamical model of the manipulator is used to perform analysis of the system and fast simulation. The recursive algorithm developed by Luh *et al.* [62] allows to systematically and recursively compute the inverse dynamics of the manipulator, based on kinematic and dynamical parameters.

The compact form of the dynamical model of a generic manipulator is presented in Eq. (2-2).

$$\mathbf{H}(\mathbf{q})\ddot{\mathbf{q}} + \mathbf{C}(\mathbf{q},\dot{\mathbf{q}})\dot{\mathbf{q}} + \mathbf{g}(\mathbf{q}) + \mathbf{F}(\dot{\mathbf{q}}) = \tau, \tag{2-2}$$

where, for $n = 5$ DoF manipulator, $\mathbf{q}$, $\dot{\mathbf{q}}$ and $\ddot{\mathbf{q}}$ in $\mathbf{R}^5$ are joint position, velocity and acceleration vectors, respectively; $\mathbf{H}(\mathbf{q})$ is the 5×5 inertia matrix, $\mathbf{C}(\mathbf{q},\dot{\mathbf{q}})$ contains the 5×1 Coriolis and centripetal terms, $\mathbf{g}(\mathbf{q})$ are the 5×1 gravitational terms, $\mathbf{F}(\dot{\mathbf{q}})$ are the 5×1 friction terms and τ is the 5×1 vector of torques applied to each joint of the manipulator.

Durango *et al.* applied in [23] the algorithm proposed by Luh in [62]. To this end, they used the Matlab® symbolic toolbox to obtain the inverse dynamical model. They assumed the inertial parameters, due to the difficulty to measure or estimate them, and the lack of information provided by the manufacturer. In [5], reorganization of to the inverse dynamical model in [23] allowed the computation of a compact representation of the model. Additionally, a complete rotation matrix including the effects of external forces allowed the representation of the payload as a punctual mass at the center of gravity of the end-effector.

The Fig. **2-2** states the reference position of the SCORBOT ER V PLUS proposed in [23], and used in this work.

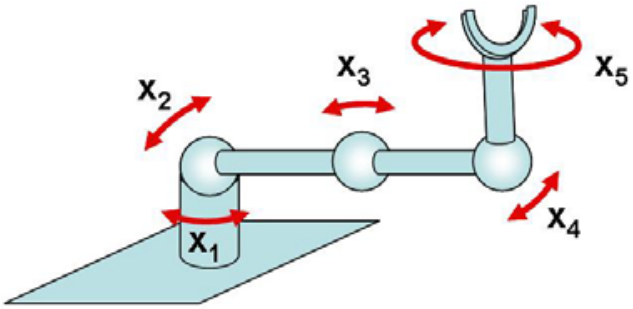

Figure 2-2.: Reference position of the SCORBOT ER V PLUS.

The rotation matrix of the end-effector with respect to the base results from the sequential multiplication of the rotation matrices of each element of the manipulator relative to the previous, from the base to the last element. Hence, the rotation matrix corresponds to the expression presented in Eq. (2-3).

$$^{0}\mathbf{R}_{T} = {}^{R}\mathbf{R}_{0}{}^{0}\mathbf{R}_{1}{}^{1}\mathbf{R}_{2}{}^{2}\mathbf{R}_{3}{}^{3}\mathbf{R}_{4}{}^{4}\mathbf{R}_{5}{}^{5}\mathbf{R}_{T}, \tag{2-3}$$

where $^{i-1}\mathbf{R}_{i}$ is the rotation matrix of the element i with respect to the elements $i-1$, and the superscript R and subscript T correspond to the frames of reference and the end effector (or tool), respectively. This rotation matrix is computed in [5], since this calculation is not included in the model presented by Durango *et al.* in [23]. It shows that Durango *et al.* did not consider the ability of the system to interact with a payload or any external force applied to the end-effector.

To obtain the compact representation, the analytic Newton-Euler recursion computation result is organized using Matlab® to isolate the independent symbolic terms of the inertia matrix $\mathbf{H}(\mathbf{q})$, the matrix of Coriolis and centrifugal terms $\mathbf{C}(\mathbf{q},\dot{\mathbf{q}})$ and the terms of the gravitational matrix $\mathbf{g}(\mathbf{q})$. The friction $\mathbf{F}(\dot{\mathbf{q}})$ only includes the viscous friction for dynamical analysis purposes. These symbolic matrices have hundreds of nonlinear terms.

2.1.2. State variable representation

The state variable representation for the 5 DoF manipulator uses the symbolic terms of the compact representation, together with the state vector shown in Eq. (2-4).

$$\mathbf{x} = [q_1, q_2, q_3, q_4, q_5, \dot{q}_1, \dot{q}_2, \dot{q}_3, \dot{q}_4, \dot{q}_5], \tag{2-4}$$

where $\mathbf{q}$ and $\dot{\mathbf{q}}$ in $\mathbf{R}^5$ are joint position and velocity vectors, respectively.
Thus, for a n DoF manipulator, with $k = 1...n$, the inverse inertia matrix may be defined as $\mathbf{H}(\mathbf{x_k})^{-1} = \left[h(\mathbf{x_k})_{ij}\right]_{n\times n} = (\mathbf{H}(\mathbf{x_k})^{-1})_{ij}$, with i as the rows and j as the columns of the matrix.

For a manipulator with $n = 5$ DoF and $k = 1 \ldots 5$, the corresponding transformation results in the state equation Eq. (2-5).

$$\begin{aligned}
\dot{x}_1 &= x_6 \\
\dot{x}_2 &= x_7 \\
\dot{x}_3 &= x_8 \\
\dot{x}_4 &= x_9 \\
\dot{x}_5 &= x_{10} \\
\dot{x}_6 &= (\mathbf{H}(\mathbf{x_k})^{-1})_{1j}(\tau - \mathbf{C}(\mathbf{x}) - \mathbf{g}(\mathbf{x_k}) - \mathbf{F}(\mathbf{x_{k+5}})) \\
\dot{x}_7 &= (\mathbf{H}(\mathbf{x_k})^{-1})_{2j}(\tau - \mathbf{C}(\mathbf{x}) - \mathbf{g}(\mathbf{x_k}) - \mathbf{F}(\mathbf{x_{k+5}})) \\
\dot{x}_8 &= (\mathbf{H}(\mathbf{x_k})^{-1})_{3j}(\tau - \mathbf{C}(\mathbf{x}) - \mathbf{g}(\mathbf{x_k}) - \mathbf{F}(\mathbf{x_{k+5}})) \\
\dot{x}_9 &= (\mathbf{H}(\mathbf{x_k})^{-1})_{4j}(\tau - \mathbf{C}(\mathbf{x}) - \mathbf{g}(\mathbf{x_k}) - \mathbf{F}(\mathbf{x_{k+5}})) \\
\dot{x}_{10} &= (\mathbf{H}(\mathbf{x_k})^{-1})_{5j}(\tau - \mathbf{C}(\mathbf{x}) - \mathbf{g}(\mathbf{x_k}) - \mathbf{F}(\mathbf{x_{k+5}})).
\end{aligned} \tag{2-5}$$

In a more compact form, it may be expressed as: $\dot{\mathbf{x}} = \mathbf{f}(\mathbf{x}, \tau)$, with $\mathbf{x} \in R^p$, $\tau \in R^q$ with $p = 10$ and $q = 5$. For convenience of notation, the size of the matrices for analytical operations related to the above state equation will not be included.

As a reminder, a quality derived from the geometrical and physical conditions of the manipulator makes $\mathbf{H}(\mathbf{x_k})$ a positive definite and invertible matrix in all cases [83].

2.1.3. Numerical validation of the compact inverse dynamical model

The representation in state variables enables the validation of the direct and inverse dynamical model. A Matlab® numerical toolbox for robotics used in [23], named *Hemero* and developed by Ollero *et al.* in [11], is also used here for the validation. This toolbox has similar functionalities than the popular toolbox developed by Corke in [19]. The validation lies in the comparison of the computed compact dynamical model against the corresponding functions of the recognized toolboxes. Durango *et al.* perform in [23] a similar validation by comparison of their models.
The numerical validation requires the solution of the inverse dynamical problem stated in Eq. (2-6). This solution computes the torques required in each actuator of the manipulator to achieve a set of desired joint trajectories.

$$\tau = \mathbf{H}(\mathbf{q})\ddot{\mathbf{q}} + \mathbf{C}(\mathbf{q}, \dot{\mathbf{q}})\dot{\mathbf{q}} + \mathbf{g}(\mathbf{q}) + \mathbf{F}(\dot{\mathbf{q}}). \tag{2-6}$$

A Matlab® function implemented to this end, uses the inputs: positions, velocities, accelerations and inertial and friction parameters, to compute the torques. This function is recurrently used in this work and in the stability analysis presented in [5].

The developed function is used for the validation of the inverse dynamical model for predefined joint trajectories, and compared to the output torques of the *rne* (recursive Newton-Euler) function

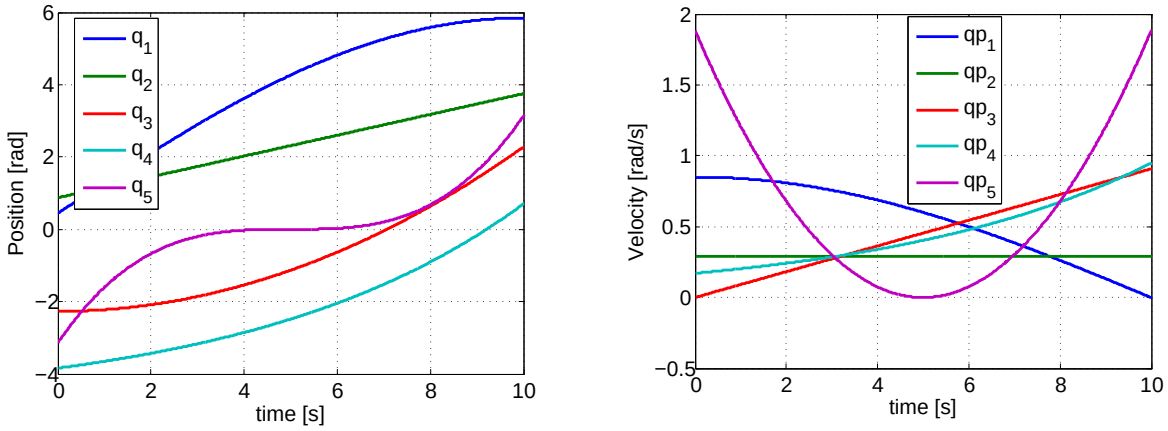

Figure 2-3.: Validation trajectories, proposed in [23]

of the *Hemero* toolbox. The comparison computes the related errors, looking for confirmation of the correct operation of the functions and appropriate modifications to the model. The same trajectories proposed in [23] are used in [5], but applying the compact function to compute the inverse dynamics.

Thus, the desired trajectories used in the numerical validation process are presented in Table **2-1**.

Table 2-1.: Trajectories for validation, proposed in [23].

POSITIONS	VELOCITIES	ACCELERATIONS
$x_1 = 5,4106\sin(0,1571t) + 0,4363$	$\dot{x}_1 = 0,85\cos(0,1571t)$	$\dot{x}_6 = -0,1335\sin(0,1571t)$
$x_2 = 0,2879t + 0,8727$	$\dot{x}_2 = 0,2879$	$\dot{x}_7 = 0$
$x_3 = 0,04538t^2 - 2,2689$	$\dot{x}_3 = 0,09076t$	$\dot{x}_8 = 0,09076$
$x_4 = e^{0,17116t} - 4,8397$	$\dot{x}_4 = 0,17116e^{0,17116t}$	$\dot{x}_9 = 0,02929575e^{0,17116t}$
$x_5 = 0,02513(t-5)^3$	$\dot{x}_5 = 0,07539(t-5)^2$	$\dot{x}_{10} = 0,15078(t-5)$

The Fig. **2-3** shows the desired validation trajectories presented in Table **2-1**.
The Fig. **2-4** presents the results after the application of the desired trajectories to the compact inverse dynamical function. The error corresponds to the comparison between torques of the compact model and the *rne* (recursive Newton-Euler) function of the *Hemero* toolbox. It is worth to note that the error percentages are about 10^{-10} Nm, showing the accuracy of the model.

Similarities with the validation performed by Durango *et al.* in [23] demonstrates the adequate implementation of the corresponding function.

The Fig. **2-5** shows a final test, with the fully outstretched position of the manipulator, where $\mathbf{x} = \mathbf{q}$. In this situation, the desired trajectories are defined in Table **2-2**.

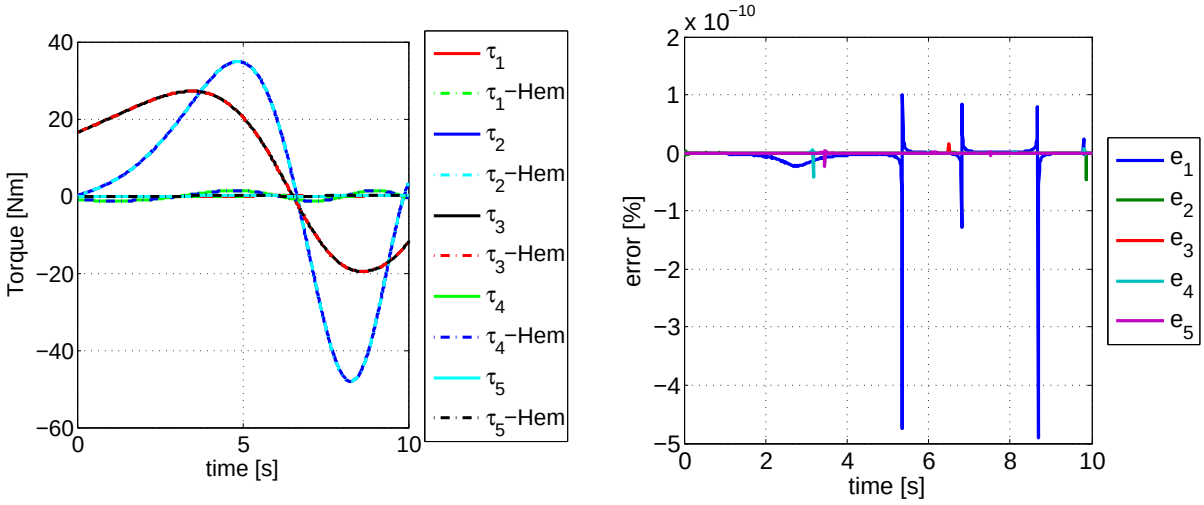

Figure 2-4.: Torques and error (percentage) of the compact form of the inverse dynamics compared to *Hemero* [11].

Table 2-2.: Trajectories for validation, from the most effort demanding position.

Positions	Velocities	Accelerations
$x_1 = 0$	$\dot{x}_1 = 0$	$\dot{x}_6 = 0$
$x_2 = 0{,}2879t + 0{,}8727$	$\dot{x}_2 = 0{,}2879$	$\dot{x}_7 = 0$
$x_3 = 0$	$\dot{x}_3 = 0$	$\dot{x}_8 = 0$
$x_4 = -\frac{\pi}{2}$	$\dot{x}_4 = 0$	$\dot{x}_9 = 0$
$x_5 = 0$	$\dot{x}_5 = 0$	$\dot{x}_{10} = 0$

The desired trajectory is a linear displacement for the second joint (the shoulder), with initial condition defined as the outstretched arm with an inclination given by $x_2 = 0{,}87$ rad. The motion results in a planar displacement, maintaining a constant position of the base ($x_1 = 0$ rad) and remaining extended over the entire trajectory, up to the end position ($x_2 = 3{,}74$ rad). The velocity remains constant for the entire trajectory, as shown in Table **2-2**.

Fig. **2-6** presents the torques applied to the joints to achieve the proposed motion. This results are obtained using the inverse dynamical computation function in the compact form. In the case of the joint x_2, it may be verified the peak torque at startup ($\tau_2 = 9{,}11$ Nm), the zero crossing point at which the arm is vertical ($x_2 = \pi/2$ rad) and the maximum absolute value (negative minimum) in which $\tau_2 = -14{,}32$ Nm, which occurs when the position of the manipulator is fully horizontal ($x_2 = \pi$ rad). This torque would represent the maximum torque required for the joint q_2, in this particular configuration without payload.

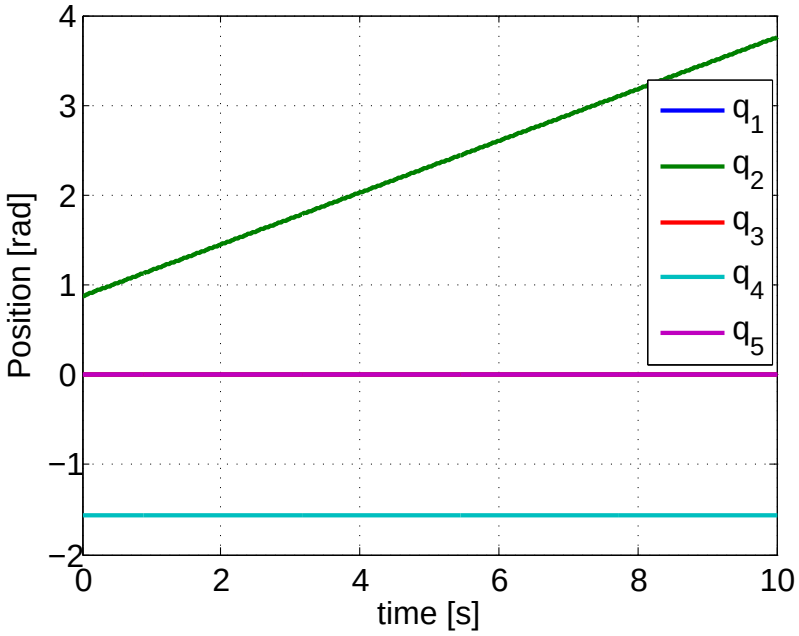

Figure 2-5.: Trajectories for validation from the most effort demanding position.

Fig. **2-7** shows the graph of comparative errors between the torques of the compact inverse dynamical model and the computed torques with the *rne* (recursive Newton - Euler) function of *Hemero* toolbox. It may be noticed that the errors are about 10^{-15} Nm, demonstrating again the validity of the compact function.

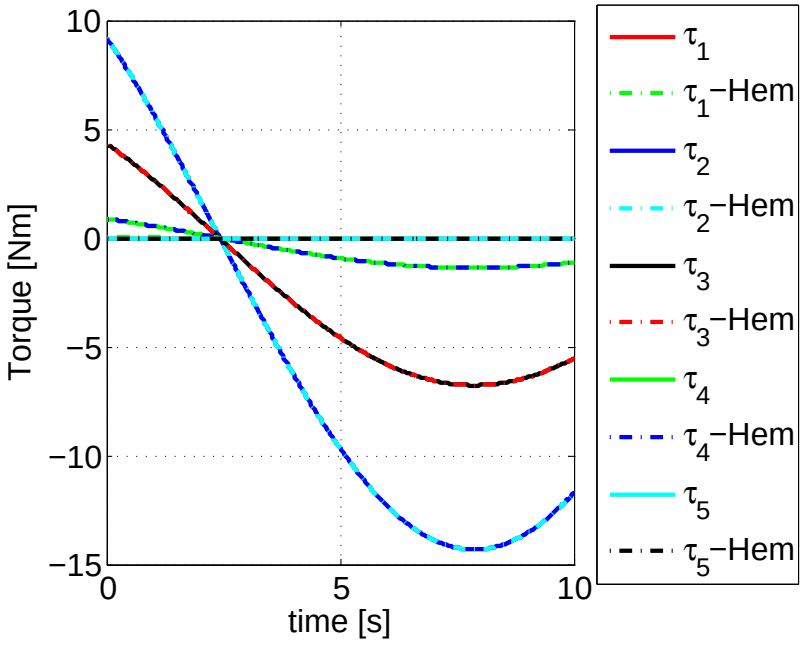

Figure 2-6.: Computed torques overlaid with *Hemero* torques.

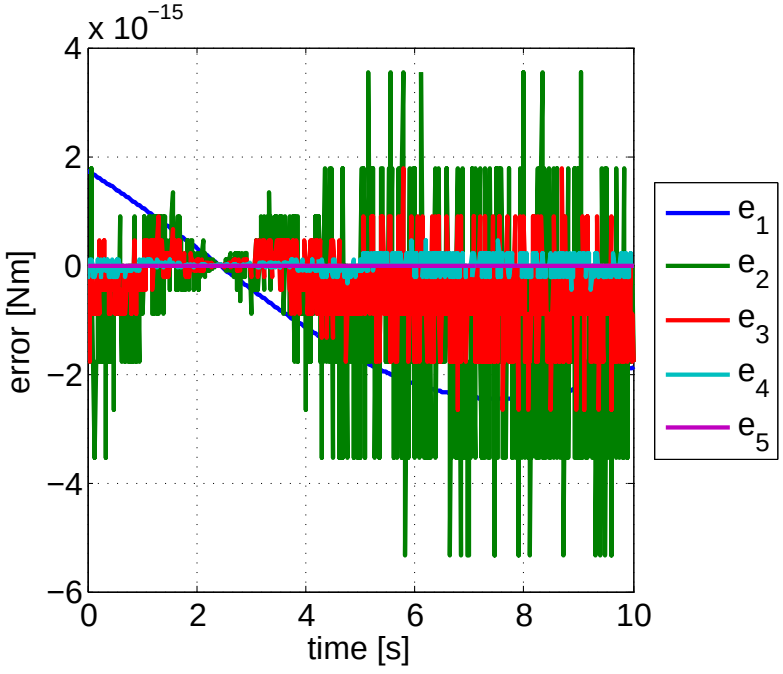

Figure 2-7.: Torque errors (percentage) compared with *Hemero* torques.

2.1.4. Validation of direct dynamical model

The direct dynamical problem requires the computation of current positions, velocities and accelerations, based on the knowledge of actual torques applied by the actuators to the joints of the manipulator. This results a more complex task, since there are several solutions for each set of torques [20, 23, 29]. In general, the solution of this issue consists of solving the state equation in Eq. (2-5), using a classic integration algorithms (*i.e.* Runge-Kutta). A set of integration algorithms, known as ODEs, are available in Matlab®. The ODE45 and ODE15, allow the configuration of automatic or manual integration step, specific time interval and initial condition. These functions provide a tool for the complete integration of trajectories for smooth and continuous systems.

Thus, from a general view point, the solution to the direct dynamical problem consists in solving Eq. (2-7):

$$\ddot{\mathbf{q}} = \mathbf{H}(\mathbf{q})^{-1}(\tau - \mathbf{C}(\mathbf{q},\dot{\mathbf{q}})\dot{\mathbf{q}} - \mathbf{g}(\mathbf{q}) - \mathbf{F}(\dot{\mathbf{q}})). \tag{2-7}$$

As presented above, a condition derived from the physical characteristics of the inertia matrix $\mathbf{H}(\mathbf{q})$ ensures that, in all cases, it is a positive definite matrix and always invertible [83].

The effect of the transient response of the open loop system increases the tracking error during this period and may even destabilize the system. The validation of this model takes into account the transient response period of the open loop system for analysis purposes. It is desirable to present the response after that period for comparison with the desired trajectory. In this case, the response depends on the time constant of the second order coupled systems, related to each DoF. Thus, the validation involves the analysis of the behavior of the system after a sufficient transient time. Several numerical simulations for the open loop system, including the first 7 s of simulation showed a divergent unstable behavior. This could happen due to accumulative errors of the double numerical integration related with this computation. Hence, final simulations were performed in a smaller time range, with initial time as 7 s and after the transient response of the open loop system. This considerations improved the validation results presented by Durango *et al.* in [23], due to the reduction of the error in the tracking task.

The same validation procedure proposed in [23] applied to compute tracking errors, corresponding to predefined torque trajectories, allows the current comparison. To this end, the procedure uses the same torque trajectories obtained in the inverse dynamical model validation, presented previously in section 2.1.3. The Fig. **2-8** shows the simulated trajectories, isolating and capturing the response after 7 s. Fig. **2-9** shows the comparison between reference trajectories presented in Table **2-1** and the computed positions resulting of the double integration of Eq. (2-7), after a transient time of 7 s.

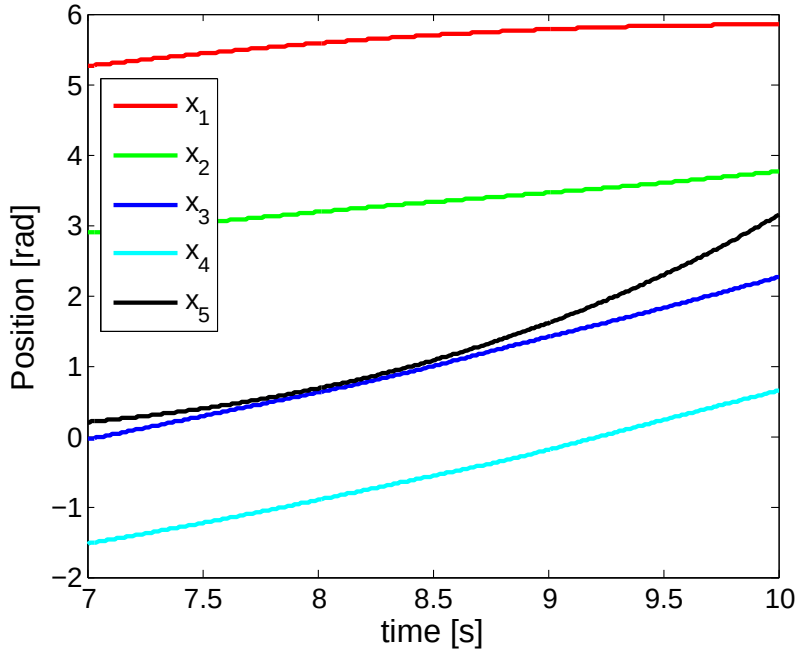

Figure 2-8.: Computed position for the direct dynamical model, after 7 s.

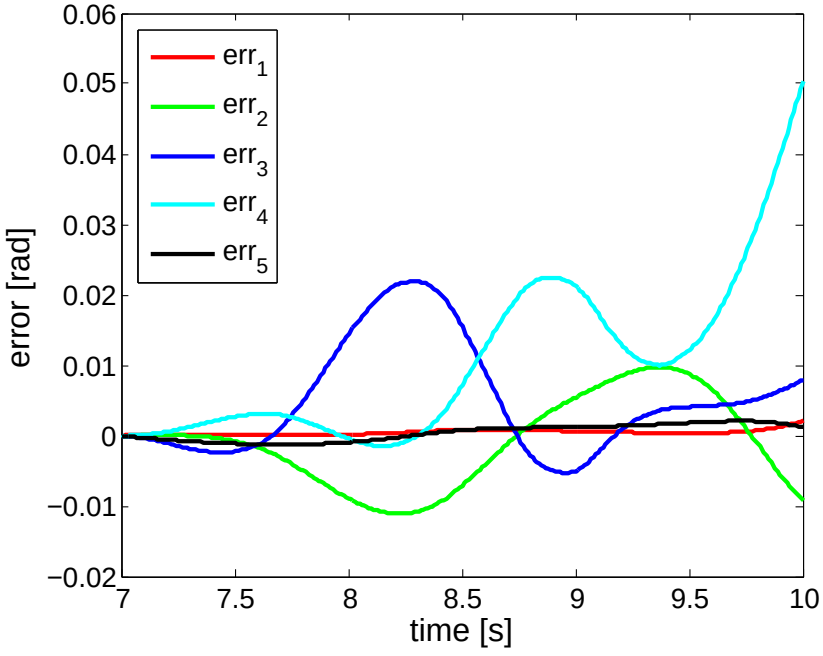

Figure 2-9.: Position error for direct dynamical model, after 7 s.

2.2. Modeling a 7 DoF manipulator with redundant joints, like the Whole Arm Manipulator (WAM)

From the Barret Technology Inc. web page [1]: "*The WAM® Arm is a highly dexterous, naturally backdrivable manipulator. The only arm sold in the world with direct-drive capability supported by Transparent Dynamics® between the motors and joints, so its control of contact forces is robust-independent of mechanical force or torque sensors. It is built to outperform conventional robots with unmatched human-like grace and dexterity*".

The Whole Arm Manipulator (WAM), presented in Fig. **2-10**, is the result of a project developed by researchers at MIT, who produced a design methodology for robots with intrinsically safety for interaction with humans and its environment. It has been continuously developed and commercialized by Barrett Technology at USA. The design methodology for the WAM is worried about the forces over the whole arm and the end effector while the robot interacts with the environment, that would be the reason for its name.

It is a modular manipulator which has two main configurations: 4 degree of freedom (DoF) and 7 DoF with a three axis attachable wrist, both with kinematics comparable to the human arm. The 4 DoF configuration has a rotary base, a 2 DoF shoulder and an elbow between the upper arm and forearm.

Besides, it has especial characteristics as [1, 77]:

- The joint moving ranges are wider than those for conventional robotic and human arms.
- Higher performance than conventional manipulators: smooth motion due to its custom designed electronics with inherently backdrivable cable drives, high performance and most power-efficient light weight servo-electronics and a light servo-drives (43 grams) included in the arm structure.
- Servo-motors are rare-earth brushless, high torque-inertia ratio [93].

The open-loop backdrivability is one of the most significant characteristics of the WAM. Defined as the accurate reproduction in the inputs of the manipulator (the motors) of the forces applied at the output end-effector. Hence, any person may manipulate the arm by applying a force at the end effector with smooth and safety motion. The WAM senses forces over the hole arm by measurement of the currents in the drive motors, allowing the ability to control forces over the whole arm for safer operation with humans.

Traditional transmissions using gears have problems with the inverse relation between friction and backlash. The drives using cables and cylinders are low friction and does not have the problem

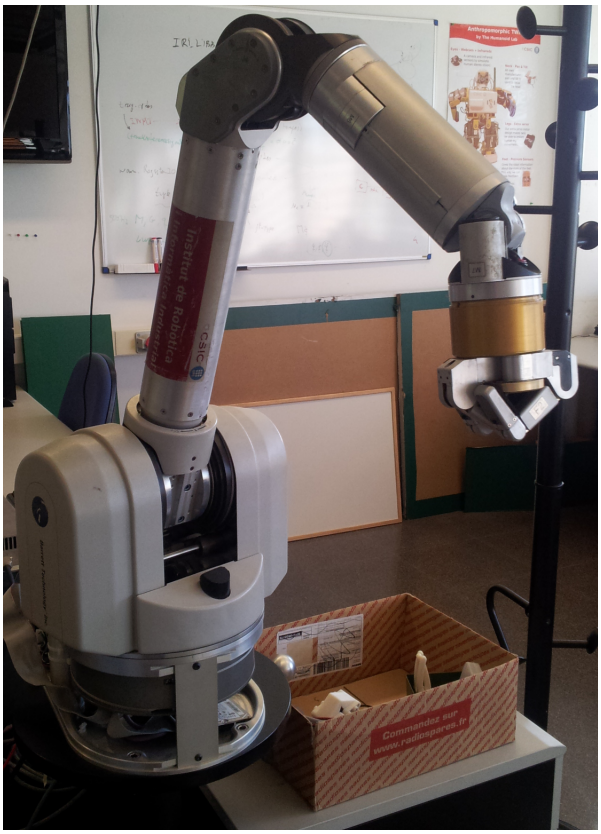

Figure 2-10.: Redundant, seven (7) DoF, Whole Arm Manipulator (WAM).

with backlash. That is the main reason why the WAM uses this kind of transmissions [77].

The 4 DoF WAM was designed to provide kinematic redundancy and control of each joint. The redundancy enables the arm to be driven to a variety of poses for any end position. This enables the user to teach both the end position and the elbow pose to safely achieve tasks even without direct "line of sight" and using the compliant contact characteristic for safety interaction with objects or people in the environment. The 7 DoF configuration adds the 3 DoF wrist to the 4 DoF redundant configuration, taking advantage of this condition.

2.2.1. WAM Kinematics

The variant form of the Denavit-Hartenberg (D-H) method is used to establish the coordinate frames in the zero position (or Home). Appendix A presents the configurations for the 4 and 7 DoF settings.

The D-H parameters obtained from those configurations, and used for numerical simulations in this work, are shown in Table **2-3** for 4 DoF system and Table **2-4** for 7 DoF system.

Table 2-3.: D-H parameters for the 4 DoF configuration of the WAM.

Joint i	a_i	α_i	d_i	θ_i
1	0	$-\pi/2$	0	θ_1
2	0	$\pi/2$	0	θ_2
3	0.045	$-\pi/2$	0.55	θ_3
4	-0.045	$\pi/2$	0	θ_4
T	0	0	0.35	

Table 2-4.: D-H parameters for the 7 DoF configuration of the WAM.

Joint i	a_i	α_i	d_i	θ_i
1	0	$-\pi/2$	0	θ_1
2	0	$\pi/2$	0	θ_2
3	0.045	$-\pi/2$	0.55	θ_3
4	-0.045	$\pi/2$	0	θ_4
5	0	$-\pi/2$	0.3	θ_5
6	0	$\pi/2$	0	θ_6
7	0	0	0.06	θ_7
T	0	0	0	

Each of the joints has a mechanical stop that limits the motion. Table **2-5** shows a complete listing of the joint limits for each axis.

Table 2-5.: Joint limits of the WAM

Joint	**Positive Joint Limit. Rad(deg)**	**Negative Joint Limit. Rad(deg)**
1	2.6 (150)	-2.6 (-150)
2	2.0 (113)	-2.0 (-113)
3	2.8 (157)	-2.8 (-157)
4	3.1 (180)	-0.9 (-50)
5	1.24 (71)	-4.76 (-273)
6	1.6 (90)	-1.6 (-90)
7	3.0 (172)	-3.0 (-172)

The relation between adjacent coordinate frames is defined by Eq. (2-8), where *c* and *s* stand for *cos* and *sin* trigonometric functions respectively and the parameter stated in Table **2-3** for 4 DoF system and Table **2-4** for 7 DoF system.

$$ {}^{i-1}T_i = \begin{Bmatrix} c\theta_i & -s\theta_i c\alpha_i & s\theta_i s\alpha_i & a_i c\theta_i \\ s\theta_i & c\theta_i c\alpha_i & -c\theta_i s\alpha_i & a_i s\theta_i \\ 0 & s\alpha_i & c\alpha_i & d_i \\ 0 & 0 & 0 & 1 \end{Bmatrix}. \tag{2-8} $$

The forward kinematics are determined for any frame on the robot by sequential multiplication of all the transform matrices up to and including the final frame. To determine the end-effector location and orientation for the 4 DoF configuration, it has to be used the expression presented in Eq. (2-9):

$$ {}^{0}T_{Tool} = {}^{0}\ T_1^1 T_2^2 T_3^3 T_4^4 T_{Tool}. \tag{2-9} $$

And for the 7 DoF configuration the related expression in Eq. (2-10) is:

$$ {}^{0}T_{Tool} = {}^{0}\ T_1^1 T_2^2 T_3^3 T_4^4 T_5^5 T_6^6 T_7^7 T_{Tool}. \tag{2-10} $$

2.2.2. WAM Dynamics

It is necessary to define the basic dynamical parameters to perform the inverse dynamical model computation using the Newton-Euler recursion. Generally, 13 values are important and summarized in Tables **2-6** and **2-7** (All units are in kilograms and meters unless otherwise indicated): Table **2-6** presents mass and X, Y, Z location of the center of mass and Table **2-7** presents I_{xx} through I_{zz} (9 inertia-tensor values).

This work initially uses the kinematic and dynamic characterization of the friction model estimated by Mitrovic *et al.* in 2010 [64]. The authors proposed to approximate the frictional joint torques,

Table 2-6.: Mass and Center of mass position of the WAM [3]

		Center of mass		
Link	**Mass**	**X**	**Y**	**Z**
1	10,7677	-0,00443	0,12189	-0,00066
2	3,8749	-0,00237	0,03106	0,01542
3	1,8023	-0,03826	0,20751	0,00003
4	2,17266212	0,00553408	0,00006822	0,11927695
5	0,35655692	0,00005483	0,02886286	0,00148493
6	0,40915886	-0,00005923	-0,01686123	0,02419052
7	0,0754827	0,00014836	0,00007252	-0,00335185

Table 2-7.: Inertia tensor of the WAM [3]

Link	I_{xx}	I_{xy}	I_{xz}	I_{yx}	I_{yy}	I_{yz}	I_{zx}	I_{zy}	I_{zz}
1	0,13488033	-0,00213041	-0,00012485	-0,00213041	0,11328369	0,00068555	-0,00012485	0,00068555	0,0904633
2	0,02140958	0,00027172	0,00002461	0,00027172	0,01377875	-0,0018192	0,00002461	-0,0018192	0,01558906
3	0,05911077	-0,00249612	0,00000738	-0,00249612	0,0032455	-0,00001767	0,00000738	-0,00001767	0,05927043
4	0,01067491	0,00004503	-0,00135557	0,00004503	0,01058659	-0,00011002	-0,00135557	-0,00011002	0,00282036
5	0,00037112	-0,00000008	-0,00000003	-0,00000008	0,00019434	-0,00001613	-0,00000003	-0,00001613	0,00038209
6	0,00054889	0,00000019	-0,0000001	0,00000019	0,00023846	-0,0000443	-0,0000001	-0,0000443	0,00045133
7	0,00003911	0,00000019	0	0,00000019	0,00003877	0	0	0	0,00007614

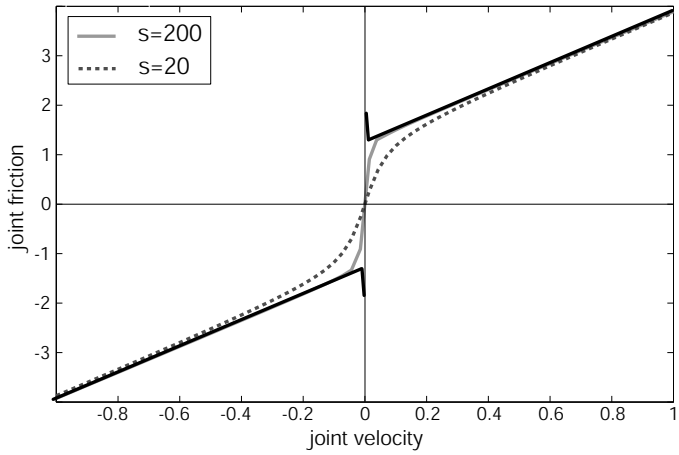

Figure 2-11.: Approximate continuous friction model for two values of *s*. [64]

usually modeled to consist of static and kinetic Coulomb component as well as of a viscous friction component, as a combination of only kinetic Coulomb and viscous friction components using a smooth and continuous sigmoidal function, of the form:

$$\mathrm{b}(\dot{\mathrm{q}}) = \mathrm{b_c} \mathit{arctan}(\mathrm{s}\dot{\mathrm{q}})\frac{2}{\pi} + \mathrm{B}\dot{\mathrm{q}}, \tag{2-11}$$

where *s* indicates the "steepness" of the fitted *arctan* function presented in Fig. **2-11**, b_c is the kinetic Coulomb friction, and *B* is the viscous friction coefficient.

Using experimental results and a least-square estimation method, the kinetic Coulomb friction coefficients and the viscous friction coefficients are estimated as presented in Table **2-8**.

Table 2-8.: Estimated joint friction parameters of the WAM [64]

Joint	q_1	q_2	q_3	q_4	q_5	q_6	q_7
B	1,142	0,946	0,309	0,255	0,025	0,039	0,004
b_c	2,516	2,581	2,038	0,956	0,323	0,315	0,066

2.2.3. Numerical Validation of the dynamical model of the WAM

The initial objective was to obtain the dynamical model using the recursive Newton-Euler formulation implemented in Matlab® symbolic toolbox and using Mapple® engine, but due to the dimensionality of the problem it was an unproductive intent. The fast growth in the amount of nonlinear terms, related mainly to the inertia matrix, makes the compact dynamical model of the 7 DoF manipulator an unpractical tool for numerical simulation and control design.

Using the Robotics Toolbox Matlab® developed by Corke *et al.* in [19], we performed validations of the inverse dynamical model. This toolbox allows the definition of parameters of the manipulator and computation of the torques on each joint for a specific trajectory.

The 7th version of the mentioned toolbox, includes a matrix to define all the parameters of a robot with either rotational or prismatic joints. It uses the matrix named *DYN* to represent the manipulator kinematics and dynamics, based on the parameters of the n-axis robot, and defining the $n \times 20$ matrix presented in Table **2-9**.

The first 5 columns of the *DYN* matrix contain the kinematic parameters and may be used anywhere that a D-H kinematic matrix as required, the rest of columns are dynamical information.

The experimental validation of the dynamical model of the WAM implemented a simple process with the actual manipulator, intended to compare the numerical model with measured data. For specific trajectories, the process is as follows: the trajectory teaching to the manipulator consists of defining the initial, intermediate and final positions of the trajectory and taking advantage of the backdrivability and gravity compensation features of the manipulator; then, data acquisition using the controller and open-source software provided by the manufacturer and finally an error comparison of torques measured and computed using the toolbox developed by Corke. After several tests and with a trial an error process, it was possible to identify problems with the friction compensation, related to torque errors.

Fig. **2-12** shows a comparison of torques between experimental data and the numerical model using the mentioned Matlab® toolbox. It is a difference between numerical and experimental trajectories mainly at the transient period, due to the friction model used for simulation. This may be concluded after some trial and error adjustments of Coulomb friction constants of the numerical model,

Table 2-9.: Robot DYN matrix definition in the toolbox by Corke [19]

COLUMN	PARAMETER	DESCRIPTION
1	α	link twist angle
2	A	link length
3	θ	link rotation angle
4	D	link offset distance
5	σ	joint type, 0 for revolute, non-zero for prismatic
6	Mass	mass of the link
7	r_x	Link Center of Gravity (COG) with respect to the link coordinate frame
8	r_y	
9	r_z	
10	$I_x x$	Elements of link inertia tensor about the link COG
11	$I_y y$	
12	$I_z z$	
13	$I_x y$	
14	$I_y z$	
15	$I_x z$	
16	J_m	Motor Armature inertia
17	G	Reduction gear ratio. joint speed/link speed
18	B	Viscous friction constants, motor refered
19	Tc+	Coulomb friction (positive rotation), motor refered
20	Tc-	Coulomb friction (negative rotation), motor refered

showing the lack of accuracy of the Mitrovic *et al.* [64] estimation of this parameters, and proposes future experimental work in this specific issue.

For the trajectory presented in Fig. **2-12** it is computed the mean squared error (MSE), and mean, minimum, and maximum errors. Table **2-10** shows the computed values for each joint of the manipulator.

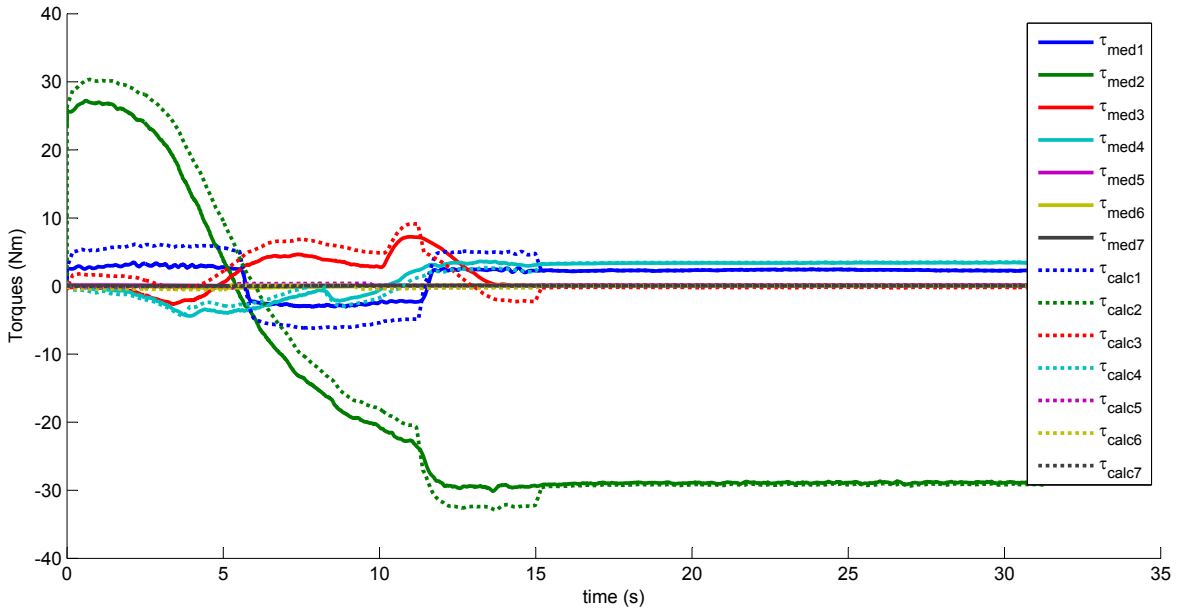

Figure 2-12.: Comparison of experimental and numerical torques of the WAM.

Then, a trial and error correction of the Coulomb friction constant in joint q_3 (changing from $b_c = 2{,}036$ to $b_c = 0{,}5$) was applied to verify performance improvement by simulation of the dynamical model. Tables **2-10** and **2-11** show error comparison before and after correction, respectively. The mean-squared error (MSE) indicator for the joint q_3 shows the reduction associated to that change in the parameter, stating the need for a better estimation process of the friction constants for the manipulator dynamical model. In Fig. **2-13** it is shown the error reduction after that correction.

The global tendency of trajectories and decreased error with an improvement in the dynamical model shows a promising option for simulation and control design of the modeling tool and numerical model.

Table 2-10.: Mean squared, mean, minimum and maximum errors between experimental and computed torques.

	τ_1	τ_2	τ_3	τ_4	τ_5	τ_6	τ_7
MSE	3,106	7,691	**1,714**	0,32	0,039	0,055	0,002
MEAN	-0,215	-0,754	-0,245	0,035	0,044	0,112	0,001
MIN	-3,274	-5,905	-2,374	-1,346	-0,301	-0,375	-0,068
MAX	3,342	23,203	2,376	1,343	0,388	0,428	0,067

Table 2-11.: Errors: Joint q_3 with improved friction model.

	τ_1	τ_2	τ_3	τ_4	τ_5	τ_6	τ_7
MSE	3,106	7,691	**0,157**	0,32	0,039	0,055	0
MEAN	-0,215	-0,754	0,072	0,035	0,044	0,112	0,001
MIN	-3,274	-5,905	-0,836	-1,346	-0,301	-0,375	-0,068
MAX	3,342	23,203	0,838	1,343	0,388	0,428	0,067

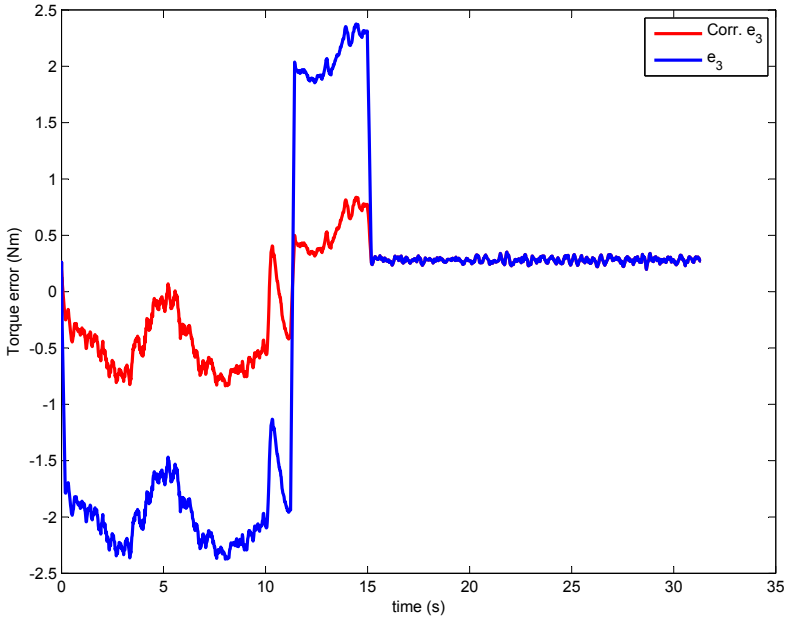

Figure 2-13.: Torque error reduction for q_3, due to Coulomb's friction correction.

3. Nonlinear control for MDoF manipulators: From model-based to data-driven control

Traditional and new control strategies should be tested for different configurations, in order to prepare robotic manipulators to coexist with humans. New challenges emerge from tasks involving contact, cooperation and any physical interaction. The highly changing and unstructured characteristic of human environments requires flexible, adaptable and robust control systems to support interactive tasks.

The following sections briefly present three nonlinear control strategies applied to robot manipulation, and used along this work. The first two are traditional model-based control strategies used in robotic manipulators, the third one is a current developing data-driven control strategy which, to the knowledge of the author, has not been applied for multiple DoF manipulators ($n > 2$ DoF), and requires evaluation and analysis for lightweight and low inertia manipulators like the WAM, suitable for HRI.

3.1. Feedback linearization control: Computed torque

In systems with multiple inputs and multiple outputs (MIMO), as in the case of a manipulator of more than one degree of freedom, the design of this control strategy consists of: first, to generate a linear relationship between input and output, and then formulate a control law based on linear control strategies [83].

A MIMO system, may be defined as in (3-1):

$$\begin{aligned} \dot{\mathbf{x}} &= \mathbf{f}(\mathbf{x}) + \mathbf{G}(\mathbf{x})\mathbf{u} \\ \mathbf{y} &= \mathbf{h}(\mathbf{x}). \end{aligned} \tag{3-1}$$

Just as for a SISO systems, if it is necessary to differentiate the system output r_i times to obtain an explicit relationship between the output y_i and input u_i, then it may be said that the system has partial relative degree r_i. In this case, the total relative degree is the sum of the system partial relative degrees.

For the MIMO case, the relation between input and output expressed in terms of the Lie derivative, can be presented in the form of (3-2) [83]:

$$y_i^{(r_i)} = L_f^{r_i} h_i + \sum_{j=1}^{m} L_{g_j} L_f^{r_i - 1} h_i u_j, \tag{3-2}$$

which is equivalent to:

$$\begin{bmatrix} y_1^{(r_1)} \\ \cdots \\ \cdots \\ y_m^{(r_m)} \end{bmatrix} = \begin{bmatrix} L_f^{r_1} h_1(\mathbf{x}) \\ \cdots \\ \cdots \\ L_f^{r_m} h_m(\mathbf{x}) \end{bmatrix} + \mathbf{E}(\mathbf{x})\mathbf{u}, \tag{3-3}$$

where, $\mathbf{E}(\mathbf{x})$ is known as decoupling matrix and is invertible.

Thus, the control law, also known as the decoupling control law can be expressed in the form of (3-4):

$$\mathbf{u} = \mathbf{E}(\mathbf{x})^{-1} \begin{bmatrix} \nu_1 - L_f^{r_1} h_1(\mathbf{x}) \\ \cdots \\ \cdots \\ \nu_m - L_f^{r_m} h_m(\mathbf{x}) \end{bmatrix}, \tag{3-4}$$

Leading to m equations of the form:

$$y_i^{(r_i)} = \nu_i. \tag{3-5}$$

In the case where the total relative degree is equal to the system order no internal dynamic exists and input-state linearization is obtained. Hence, it may be designed a desired condition in the same way as is done for the SISO case for regulation and tracking tasks, without worrying about the stability of the internal dynamics. This is the case of a n DoF manipulator, in which it can be demonstrated that the total relative degree is equal to the system order, with no internal dynamics.

Later in this work, it is presented and applied the procedure for designing this nonlinear controller for robotic manipulators.

3.2. Adaptive control: traditional model-based control strategy

For a system with slow varying parameters is desirable to use control laws and adaptive mechanisms capable of adjusting to those changes. For this end, some fundamental approaches are: Model Reference Adaptive Control (MRAC), Adaptive Control of Auto-tuning and adaptive versions

of other control strategies such as the control by feedback linearization and Robust Control.

In general, an adaptive controller is a system that has two feedback loops, the first includes the outputs of the plant and the controller, and the second contains the elements of adjustment based on the parameters. The Fig. **3-1** shows a generalized block diagram of this technique, presented by Åström *et al.* in [6].

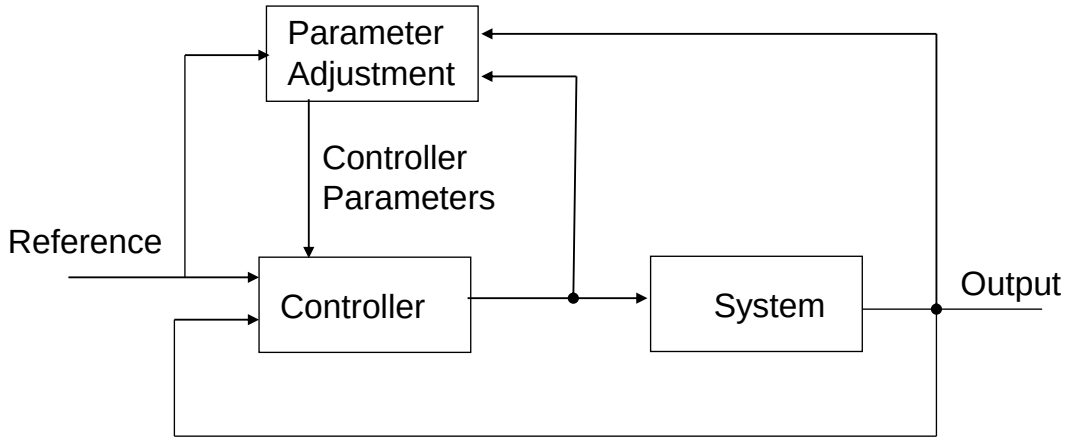

Figure 3-1.: Adaptive Control General Scheme [6]

For cases in which reaching a position (regulation) is not enough, and it is necessary to follow a specified trajectory (tracking), such as avoiding obstacles or the completion of a task on a predefined time, it must be defined the precision in tracking the trajectory. If in addition, it is required the variation of the payload handled by the manipulator, it is necessary to use some control laws that adapt to these changing conditions. In this case, the payload is considered as part of the end-effector of the manipulator, directly affecting its inertial characteristics.

To find control and adaptation laws for the variable parameter, given a desired trajectory $q_d(t)$, $\tilde{a} = \hat{a} - a$ is defined as the error parameter estimation, being a the real and $\hat{a}$ the estimated parameters. It uses the possibility to represent the dynamics of the manipulator as a linear function of the variable parameter. To this end, Slotine *et al.* in [83] presented a relationship as follows:

$$\mathbf{H}(\mathbf{q})\ddot{\mathbf{q}}_\mathbf{r} + \mathbf{C}(\mathbf{q},\dot{\mathbf{q}})\dot{\mathbf{q}}_\mathbf{r} + \mathbf{g}(\mathbf{q}) = \mathbf{Y}(\mathbf{q},\dot{\mathbf{q}},\dot{\mathbf{q}}_\mathbf{r},\ddot{\mathbf{q}}_\mathbf{r})\mathbf{a}, \tag{3-6}$$

where $\mathbf{H}(\mathbf{q})$, $\mathbf{C}(\mathbf{q},\dot{\mathbf{q}})$ and $\mathbf{g}(\mathbf{q})$ are linearly dependent of a_i, and $\dot{\mathbf{q}}_\mathbf{r}$ is a notational manipulation called "reference rate" vector in [83], which is the "error rate" $\mathbf{s}$, related to the first order sliding surface presented in (3-7):

$$\mathbf{s} = \dot{\tilde{\mathbf{q}}} + \Lambda\tilde{\mathbf{q}} = \dot{\mathbf{q}} - \dot{\mathbf{q}}_\mathbf{r}, \tag{3-7}$$

where $\dot{\mathbf{q}}_\mathbf{r} = \dot{\mathbf{q}}_\mathbf{d} - \Lambda\tilde{\mathbf{q}}$ is the difference between the desired velocity $\dot{\mathbf{q}}_\mathbf{d}$ and the position error $\tilde{\mathbf{q}}$, and Λ is a positive definite symmetric matrix.

For the adaptive control tracking task, Slotine *et al.* proposed in [83] an adaptive control law of the form presented in (3-8), as follows:

$$\begin{aligned} \tau &= \mathbf{Y}\hat{\mathbf{a}} - \mathbf{K_D}\mathbf{s} \\ \dot{\hat{\mathbf{a}}} &= -\Gamma\mathbf{Y^T}\mathbf{s}, \end{aligned} \tag{3-8}$$

where $\mathbf{Y}\hat{\mathbf{a}}$ is the feedforward term, $\mathbf{K_D}\mathbf{s}$ is a proportional derivative term and Γ is a positive definite symmetric matrix.

In order to determine the stability of the controlled system, the authors used the Lyapunov candidate function:

$$V(t) = \frac{1}{2}\left[\mathbf{s}^T\mathbf{H}\mathbf{s} + \tilde{\mathbf{a}}^T\Gamma^{-1}\tilde{\mathbf{a}}\right]. \tag{3-9}$$

Differentiating the previous function, it results:

$$\dot{V}(t) = \mathbf{s}^T\mathbf{Y}\tilde{\mathbf{a}} - \mathbf{s}^T\mathbf{K_D}\mathbf{s} + \dot{\hat{\mathbf{a}}}^T\Gamma^{-1}\tilde{\mathbf{a}}. \tag{3-10}$$

By using the adaptation law presented in (3-8), it may be concluded that:

$$\dot{V}(t) = -\mathbf{s}^T\mathbf{K_D}\mathbf{s} \leq 0. \tag{3-11}$$

As evidenced by Slotine *et al.* in [83], using the Barbalat's lemma it may be verified that $\tilde{\mathbf{q}}$ and $\dot{\tilde{\mathbf{q}}}$ tend to zero as t tends to infinity. Thus, it can be assured overall system stability and the convergence of the tracking error.

This alternative does not necessarily allows to accurately estimate the value of parameters, simply generates values that let the task to be adequately fulfilled [83].

3.3. Unfalsified Adaptive Control (UAC or UC) with fading memory: data-driven switching control

Over the last decades, a considerable number of model-based control strategies for manipulators has been proposed. Among them, two commonly used techniques are feedback linearization and adaptive control [36, 83, 84, 82]. However, as the complexity of manipulators increases, the application of model-based control techniques becomes cumbersome and prone to modeling errors. In these applications, the control strategies have to deal with highly nonlinear and coupled dynamics. To fulfill a proper regulation, model-based controllers require accurate measurements or estimations of inertial and friction parameters.

In practice, the measurement or estimation of these parameters is far from trivial and there are multiple methods to deal with this, like the traditional inverse dynamic identification model and least squares techniques [90, 102, 91, 34]. Modeling errors, associated with imprecise parameters measurement or estimation, could lead to undesirable behavior of the controlled plant [90]. Another problematic issue in the control of manipulators is related to the payload and the ability to carry a load along the entire workspace. Steady and sudden changes in the load carried by the manipulator are common and the maximum load that can be carried in a tracking task (Dynamic Load Carrying Capacity or DLCC) should be taken into account as an operational constraint [53, 42, 57].

The UC theory is a recent approach in the field of adaptive control [79, 78, 89]. The main difference with respect to previous paradigms is that no prior hypothesis on the plant is used besides the observed data, without depending on the system model. An UC controller consists of a set of controllers, a performance criterion and a switching algorithm. The last one evaluates the performance of each controller within the set by using measures of the input and output of the plant without actually being inserted in the loop. If one of the controllers not inserted into the loop achieves better performance, the switching algorithm replaces the current controller by the best one. The UC approach has been used in several applications, among these, the control of robotic manipulators [94, 71]. In these works, UC is used as a supervisor, which selects the most suitable controller for the current operating conditions.

Stefanovic and Safonov published in [89] a compilation of results applied to the Unfalsified Adaptive Control and defined by them as *Safe Adaptive Control*. They state the framework for this control theory including preliminary definitions and stability lemmas and theorem, some of which are presented in Appendix B for convenience.

3.3.1. Robot modeling and base controller definition

The classic dynamical model of an n-link rigid manipulator is based on traditional mechanic concepts resulting in a highly nonlinear differential equations of the form

$$\mathbf{H}(\theta,\mathbf{q})\ddot{\mathbf{q}}+\mathbf{C}(\theta,\mathbf{q},\dot{\mathbf{q}})+\mathbf{G}(\theta,\mathbf{q})+\mathbf{F}(\dot{\mathbf{q}})=\tau, \tag{3-12}$$

where $\theta\in\mathbb{R}^p$ is a parameter vector, function of the inertial terms; $\mathbf{q},\tau\in\mathbb{R}^n$ are the joint positions and torques; $\dot{\mathbf{q}}$, $\ddot{\mathbf{q}}\in\mathbb{R}^n$ are the joints velocity and acceleration. $\mathbf{H}(\theta,\mathbf{q})$ is the inertia matrix, $\mathbf{C}(\theta,\mathbf{q},\dot{\mathbf{q}})$ includes the Coriolis and centripetal terms, $\mathbf{G}(\theta,\mathbf{q})$ encloses the gravitational terms and $\mathbf{F}(\dot{\mathbf{q}})=\gamma\dot{\mathbf{q}}$, is the damping friction with γ as the damping friction constant [82].

The dynamical model for rigid manipulators may be presented as linear to inertial terms which would be useful for traditional control strategies, as adaptive control [83, 84, 82]. It is also worth

to notice that saturations of the actuators may be taken into account for the present analysis.

As a linear function of the parameter vector θ, the dynamical model may be presented in the form [83]

$$\mathbf{Y}(\mathbf{q},\dot{\mathbf{q}},\ddot{\mathbf{q}})\theta+\mathbf{F}(\dot{\mathbf{q}})=\tau, \tag{3-13}$$

where $\mathbf{Y}:\mathbb{R}^{3n}\rightarrow\mathbb{R}^{n\times p}$ is a matrix function of the joint positions, velocities and accelerations. Therefore, the dynamical model is linear on the parameter vector θ for a n degrees of freedom manipulator.

Feedback linearization control (or computed torque control) is a well known control strategy for robot manipulators and it is used in this section as the UC base controller. For the system (3-12), the control law using feedback linearization is given by

$$\tau=\mathbf{H}(\theta,\mathbf{q})\nu+\mathbf{H}(\theta,\mathbf{q})\ddot{\mathbf{q}}+\mathbf{C}(\dot{\mathbf{q}},\mathbf{q})\dot{\mathbf{q}}+\mathbf{G}(\theta,\mathbf{q})+\mathbf{F}(\dot{\mathbf{q}}), \tag{3-14}$$

where

$$\nu=(\ddot{\mathbf{q}}_{\mathbf{d}}-\ddot{\mathbf{q}})+k_1(\dot{\mathbf{q}}_{\mathbf{d}}-\dot{\mathbf{q}})+k_o(\mathbf{q}_{\mathbf{d}}-\mathbf{q}), \tag{3-15}$$

and $\mathbf{q_d}$ is the desired joint position. The above control law achieves the cancellation of nonlinearities and looks for a pole placement for the input-output system.

Without loss of generality, it may be defined $k_1=2\lambda$ and $k_o=\lambda^2$, where λ determines the convergence rate for the controller [83].

When used as main control strategy, the control law (3-14) assumes a precise knowledge of inertial and geometrical parameters of the robot, including inertia tensor, friction, flexibility, etc. This assumptions may result strong in practice because the lack of precision in determining the robot parameters, leading to errors that may affect the performance of the manipulator [83, 82].

3.3.2. Application of UC to MDoF manipulators

The main ideas regarding the UC are based on the discussions proposed by Popper and his thoughts in Epistemology [72]. Learning (*i.e.* controller identification) is achieved by using experimental data to falsify hypothesis.

Let define the following sets:

- $\mathbf{P}$, the set of signals $(\mathbf{r},\mathbf{u},\mathbf{y})$ consistent with past measurements of input $\mathbf{u}$ and output $\mathbf{y}$, with $\mathbf{r}$ being the reference.

- **M**, the set of signals $(\mathbf{r},\mathbf{u},\mathbf{y})$ satisfying the behavioral equations of a controller K.
- **T**, the set of signals $(\mathbf{r},\mathbf{u},\mathbf{y})$ that fulfills the performance specifications.

Then, the controller K is not falsified by the available information set **P** if

$$\mathbf{P}\cap\mathbf{M}\subset\mathbf{T}. \tag{3-16}$$

Otherwise, the controller K is said to be falsified by the available information.

The condition (3-16) formalizes the idea behind controller falsification, which consists basically in evaluating if a given controller K satisfies the specifications expressed in the form of a subset of the data **P**. UC theory claims as its main advantage that a model of the plant is not necessary. The controller can be falsified or not just with the information given by the data $\mathbf{z}=(\mathbf{u},\mathbf{y})$. In addition, the controller can be falsified without actually being inserted in the closed loop. To this end, the controllers should be causally left invertible, *i.e.*, it should be possible to compute a *fictitious* reference signal $\tilde{\mathbf{r}}$ from the inversion of the controller expression and the data **z**.

The criterion to decide whether or not a controller satisfies (3-16) is based on a cost functional $V(K,\mathbf{z},t)$, which must be cost-detectable, *i.e.*, the function must be capable of detecting from the data **z** if the controller is not stabilizing. A common example, used in this work, of cost-detectable function is

$$V(K,\mathbf{z},t)=\frac{F_\eta(e(t),t)+F_\eta(u(t),t)}{F_\eta(\tilde{r}(t),t)+\alpha}, \tag{3-17}$$

where $e_i(t)=\tilde{r}_i(t)-y(t)$, $\alpha>0$ prevents division by zero and

$$F_\eta(y(t),t)=\sum_{\tau=0}^{t}y^T(\tau)y(\tau)\eta^{t-\tau}, \tag{3-18}$$

where $\eta<1$ is a fading factor used to reduce the importance of the oldest samples. This kind of norm with fading memory provides a better adaptability in case of nonlinear systems since it allows the UC algorithm to decide which controller is better based on the current operating conditions [38].

With the cost function in Eq. (3-17), it is possible to state an adaptive control strategy. The UC scheme consists of a set of controllers $\mathbf{K}=\{K_i,\,i=1,\ldots,N\}$, designed with any control theory, and the switching algorithm that, at each time t_k, verifies

$$\min_i(V(K_i,\mathbf{u},\mathbf{y},t_k))<V(\hat{K},\mathbf{u},\mathbf{y},t_{k-1})+\varepsilon, \tag{3-19}$$

where $\hat{K}$ is the controller acting in the closed-loop at t_{k-1} and ε is a small constant. If the condition in Eq. (3-19) holds, the current controller $\hat{K}$ is replaced by $K_i\in\mathbf{K}$ [65].

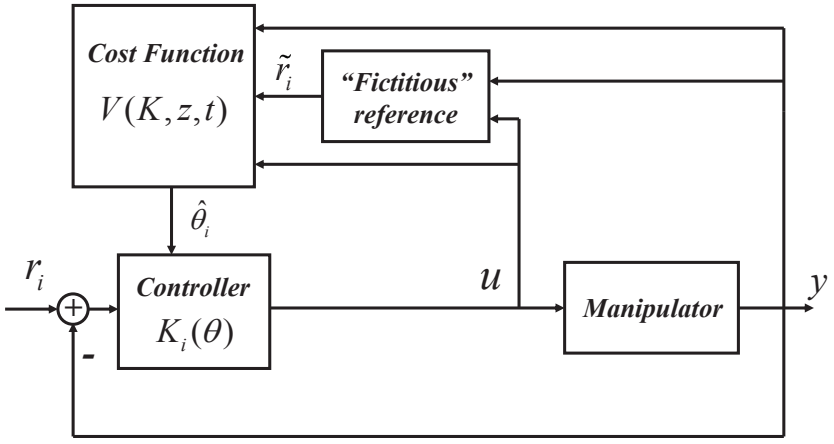

Figure 3-2.: Unfalsified Control scheme for MDoF manipulators

The UC scheme for MDoF manipulators is shown in Fig. **3-2**. The fictitious reference generator computes the set of $\tilde{\mathbf{r}}$ from the data $(\mathbf{u},\mathbf{y})$ for each controller $K_i \in \mathbf{K}$. In this case, the control signal $\mathbf{u}$ corresponds to the torques τ applied to the manipulator joints. With the fictitious references and the measured data, the falsifier checks the condition in Eq. (3-19) and decides whether or not the controller should be replaced. This procedure is repeated at each sampling time T_s.

The reference $\mathbf{r}$, input $\mathbf{u}$ and output $\mathbf{y}$ are defined as

$$\begin{aligned}
&\mathbf{r} = \begin{bmatrix}\mathbf{q_d}^T & \dot{\mathbf{q}}_\mathbf{d}^T & \ddot{\mathbf{q}}_\mathbf{d}^T\end{bmatrix}^T \in \mathbb{R}^{3n\times 1},\\
&\mathbf{u} = \tau \in \mathbb{R}^n,\\
&\mathbf{y} = \begin{bmatrix}\mathbf{q}^T & \dot{\mathbf{q}}^T & \ddot{\mathbf{q}}^T\end{bmatrix}^T \in \mathbb{R}^{3n\times 1}.
\end{aligned} \tag{3-20}$$

The *fictitious* reference

$$\tilde{\mathbf{r}}_\mathbf{i} = \begin{bmatrix}\hat{\mathbf{q}}_\mathbf{d}^T & \dot{\hat{\mathbf{q}}}_\mathbf{d}{}^T & \ddot{\hat{\mathbf{q}}}_\mathbf{d}{}^T\end{bmatrix}^T \in \mathbb{R}^{3n\times 1} \tag{3-21}$$

can be computed from the inversion of the controlled dynamic equation in Eq. (3-14) as

$$\begin{aligned}
&\ddot{\hat{\mathbf{q}}}_\mathbf{d} + 2\lambda\dot{\hat{\mathbf{q}}}_\mathbf{d} + \lambda^2\hat{\mathbf{q}}_\mathbf{d} = \mathbf{H}^{-1}\left(\tau + \mathbf{H}(\ddot{\mathbf{q}} + 2\lambda\dot{\mathbf{q}} + \lambda^2\mathbf{q})\right.\\
&\left.-\mathbf{H}\ddot{\mathbf{q}} - \mathbf{C}\dot{\mathbf{q}} - \mathbf{g} - \mathbf{F}\right)
\end{aligned} \tag{3-22}$$

and using the measured data $\mathbf{z}$.

4. Payload analysis and control of MDoF manipulators

Human Robot Interaction (HRI) has been developed and applied during last decades on situations like personal support, power assistance, medical care, industrial activities, among others, with the common issue of handling and controlling unstructured and variable payloads. This chapter presents a computational methodology to determine the maximum Dynamic Load Carrying Capacity (DLCC) in the entire workspace of manipulators, including the lightweight and low inertia arms used in HRI applications. Besides, the Unfalsified Adaptive Controller (UAC) applied on two cases of study is numerically analyzed and evaluated. The UAC performance is compared with a traditional Adaptive Controller for the SCORBOT ER V PLUS, and then applied to the Whole Arm Manipulator (WAM).

4.1. Dynamic Load Carrying Capacity (DLCC) computation for MDoF manipulators using cell to cell mapping

The Dynamic Load Carrying Capacity (DLCC) for manipulators has been studied the last decades by researchers in the field. Some suggested methods for computing the Dynamic Load Carrying Capacity (DLCC) for multiple degree of freedom (DoF) robotic arms are applied to rigid, flexible and redundant manipulators. Previous works on DLCC computation are commonly focused on the trajectory analysis for the tracking control task, based on two constraints: saturation of torques in the actuators and the accuracy to follow the desired trajectory [49, 104, 97]. On those works, the saturation constraint considers this nonlinear behavior of motors as a function of its velocity, using it as upper and lower bounds for DLCC computation. The trajectory accuracy limitation is a function of the maximum allowed deflection at each trajectory point.

The International Standard $ISO9946-99$ defines the characteristic presentation for industrial robot manipulators. In this standard, the maximum allowable load of an industrial fixed base manipulator is defined as the maximum payload that the manipulator can repeatedly lift in its fully extended configuration. However, to determine the maximum allowable load of a manipulator, the inertia effect of the load along a desired trajectory as well as the manipulator dynamics must be taken

into account, even more if it is a lightweight and low inertia manipulator, like the used in HRI applications.

This section proposes a methodology to compute the DLCC based on nonlinear numerical analysis and inspired in cell to cell mapping for the regulation task. The idea with the cell to cell mapping is to divide the workspace in cells, used in an iterative algorithm to compute the DLCC for the regulation task between each possible combination of these cells . The DLCC computation considers the torque saturation of actuators as a common behavior in paths that accomplish the regulation objective. The maximum DLCC computation uses the control task achievement consideration (regulation error) and local joint mechanical constraints (mobility ranges). The maximum DLCC for the entire workspace would be the minimum of the maximum payloads associated to each accomplished regulation task in the proposed procedure. Three controllers are used for performance comparison: feedback linearization (or computed torque), traditional adaptive control and PID with antiwindup. This approach is intended to be a practical alternative for DLCC computation in manipulator applications, like in HRI and industry.

4.1.1. Robot dynamical modeling and the regulation control task

The classic dynamical model of a manipulator is based on traditional mechanics laws of Newton-Euler or Lagrange. The general dynamical equation of a n-link rigid manipulator is highly nonlinear, and might be formulated as:

$$\mathbf{H}(\mathbf{q})\ddot{\mathbf{q}} + \mathbf{C}(\mathbf{q},\dot{\mathbf{q}})\dot{\mathbf{q}} + \mathbf{g}(\mathbf{q}) = \tau, \tag{4-1}$$

where $\mathbf{q}$, $\dot{\mathbf{q}}$ and $\ddot{\mathbf{q}}$ in $\mathbf{R}^n$ are position, velocity and acceleration joint vectors, respectively, $\mathbf{H}(\mathbf{q})$ is the $n \times n$ inertia matrix, $\mathbf{C}(\mathbf{q},\dot{\mathbf{q}})$ contains the $n \times 1$ vector of Coriolis and centripetal terms, $\mathbf{g}(\mathbf{q})$ is the $n \times 1$ vector of gravitational terms and τ is the vector of torques applied to the joints of the manipulator. In general, for the case of a serial kinematic chain configuration with n rotational joints, there are n degrees of freedom (DoF).

The torque of the actuators in a manipulator is one example of a control input with saturation and should be considered in the closed loop regulation task as shown in Fig. **4-1**.

The control input may be modeled as a piecewise linear (nonsmooth) signal of the form:

$$\tau = \begin{cases} \tau_{sat} & \tau \geq \tau_{sat}, \\ \tau_c & -\tau_{sat} < \tau < \tau_{sat}, \\ -\tau_{sat} & \tau \leq -\tau_{sat}, \end{cases} \tag{4-2}$$

with τ_c the control torque and τ_{sat} the saturation torque for each actuator. It has to be mentioned that τ_{sat} is a function of the motor angular velocity, but in this work it is considered as a constant.

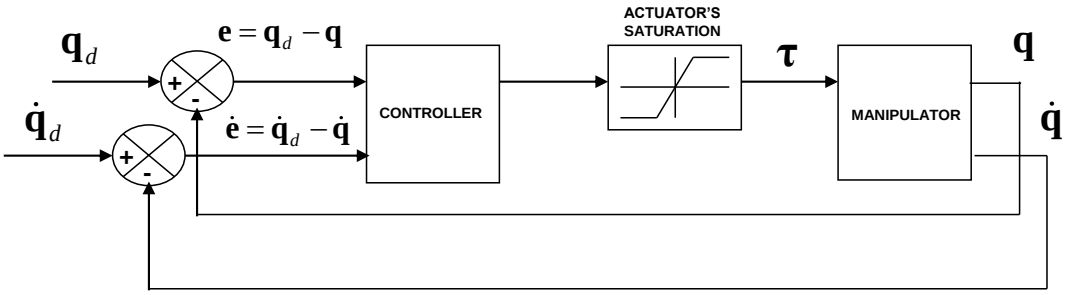

Figure 4-1.: Closed loop control systems with nonsmooth saturation.

Three control strategies are used to compare performance on the DLCC computation process. The desing process for those strategies is summarized here for convenience as follows:

1. Feedback linearization control design

   The Feedback Linearization control, for MIMO systems, is used as a control alternative for the last decades, and is commonly known as the computed torque control. Consider a region Ω_x which contains the state vector $\mathbf{x}$. Consider a system with the same number m of inputs and outputs (square system), in the following companion form [83]:

   $$\begin{aligned} \dot{\mathbf{x}} &= \mathbf{f}(\mathbf{x}) + \mathbf{G}(\mathbf{x})\mathbf{u}, \\ \mathbf{y} &= \mathbf{h}(\mathbf{x}), \end{aligned} \tag{4-3}$$

   where $\mathbf{x}$ is the $n \times 1$ state vector, $\mathbf{u}$ is the $n \times 1$ control input vector, $\mathbf{y}$ is the $m \times 1$ vector of system outputs, $\mathbf{f}$ and $\mathbf{h}$ are smooth vector field, and $\mathbf{G_i}$ is a $n \times m$ matrix whose columns are smooth vector fields $\mathbf{g_i}$. The standard procedure for the MIMO case is to differentiate the outputs y_i until the inputs u_i appears. The control law based on input output linearization for the manipulator is then developed. For the robot manipulator, the following version of the companion form for the Eq. (4-1) may be used:

   $$\mathbf{x}^n = \mathbf{f}(\mathbf{x}) + \mathbf{b}(\mathbf{x})\mathbf{u}. \tag{4-4}$$

   Then, Eq. (4-1) may be reformulated in the form:

   $$\ddot{\mathbf{q}} = \mathbf{H}(\mathbf{q})^{-1}(\tau - \mathbf{C}(\mathbf{q}, \dot{\mathbf{q}})\dot{\mathbf{q}} - \mathbf{g}(\mathbf{q})). \tag{4-5}$$

   In order to perform regulation tasks, the following control input may be used:

   $$\tau_c = \mathbf{H}(\mathbf{q})\nu + \mathbf{C}(\mathbf{q}, \dot{\mathbf{q}})\dot{\mathbf{q}} + \mathbf{g}(\mathbf{q}), \tag{4-6}$$

   where

   $$\nu = \ddot{\mathbf{q}}_d - k_o(\mathbf{q} - \mathbf{q}_d) - k_1(\dot{\mathbf{q}} - \dot{\mathbf{q}}_d). \tag{4-7}$$

Where $\mathbf{q_d}$ is the desired joint position. The above control law achieves cancelation of non-linearities and looks for a pole placement for the input output system. Besides, it assumes perfect knowledge of the model [83]. The following linear relation between the output $\mathbf{y}$ and the new input ν is as follows:

$$\ddot{\mathbf{q}} = \nu \ . \tag{4-8}$$

By combination of Eq. (4-5), Eq. (4-6) and Eq. (4-7) the closed loop error dynamics are found as:

$$\ddot{\mathbf{e}} + k_1\dot{\mathbf{e}} + k_o\mathbf{e} = 0 \ , \tag{4-9}$$

where $\mathbf{e} = \mathbf{q}_d - \mathbf{q}$. The constants k_0 and k_1 must be chosen so that the closed loop polynomial Eq. (4-9) has all its roots with negative real part:

$$K(p) = p^2 + k_1 p + k_o \ . \tag{4-10}$$

Without loss of generality, it can be defined: $k_1 = 2\lambda$ and $k_o = \lambda^2$, where λ is a design parameter for the controller [83].

2. Adaptive control with gain scheduling

The uncertain time variation of the system mass properties motivates the use of adaptive control systems, which can be obtained based on a robust proportional derivative (PD) controller. Given the desired trajectory of position $\mathbf{q_d}$ and considering that some manipulator parameters are unknown, the adaptive controller design problem is to obtain a control law for the actuator torque, and an estimation law for the unknown parameters, such that the manipulator output $\mathbf{q}$ closely tracks the desired trajectory or accomplish the regulation task [83].

Let us define $\tilde{\mathbf{a}} = \hat{\mathbf{a}} - \mathbf{a}$ as the parameter estimation error, with $\mathbf{a}$ being a constant vector of unknown parameters describing the manipulator mass properties, and $\hat{\mathbf{a}}$ its estimate. Since the terms $\mathbf{H}(\mathbf{q})$, $\mathbf{C}(\mathbf{q},\dot{\mathbf{q}})$ and $\mathbf{g}(\mathbf{q})$ depend linearly on a, the system dynamics can be linearly parametrized as follows:

$$\mathbf{H}(\mathbf{q})\ddot{\mathbf{q}}_r + \mathbf{C}(\mathbf{q},\dot{\mathbf{q}})\dot{\mathbf{q}}_r + \mathbf{g}(\mathbf{q}) = \mathbf{Y}(\mathbf{q},\dot{\mathbf{q}},\dot{\mathbf{q}}_r,\ddot{\mathbf{q}}_r)\mathbf{a}, \tag{4-11}$$

from the above equation, the matrix $\mathbf{Y} = \mathbf{Y}(\mathbf{q},\dot{\mathbf{q}},\dot{\mathbf{q}}_r,\ddot{\mathbf{q}}_r)$ and $\mathbf{a}$ are known. Then, the control law is:

$$\tau = \mathbf{Y}\hat{\mathbf{a}} - \mathbf{K}_D\mathbf{s}, \tag{4-12}$$

and the parameter estimation law is:

$$\dot{\hat{\mathbf{a}}} = -\Gamma\mathbf{Y}^T\mathbf{s}. \tag{4-13}$$

The term **s** is defined as follows:

$$\mathbf{s} = -\dot{\mathbf{e}} - \Lambda \mathbf{e} \ , \tag{4-14}$$

where $\mathbf{e} = \mathbf{q_d} - \mathbf{q}$. With the above control system, the output error converges to the surface $s = 0$, **e** and $\dot{\mathbf{e}}$ tend to 0 as $t \to \infty$ [83]. So, the above controller guarantees the following:

- The global stability of the system: boundedness of the vectors **q**, $\dot{\mathbf{q}}$ and $\hat{\mathbf{a}}$.
- The convergence of the tracking or positioning error.

3. PID with Antiwindup

   The PID Controller is one of the most used controllers in applications involving manipulators. The antiwindup technique is used to improve the response of the controller when nonlinearity saturation is present in the system, as occurs in the motors of a manipulator. There is a variety of antiwindup models [12, 95]. Then, it is used the model presented in the Fig. **4-2**.

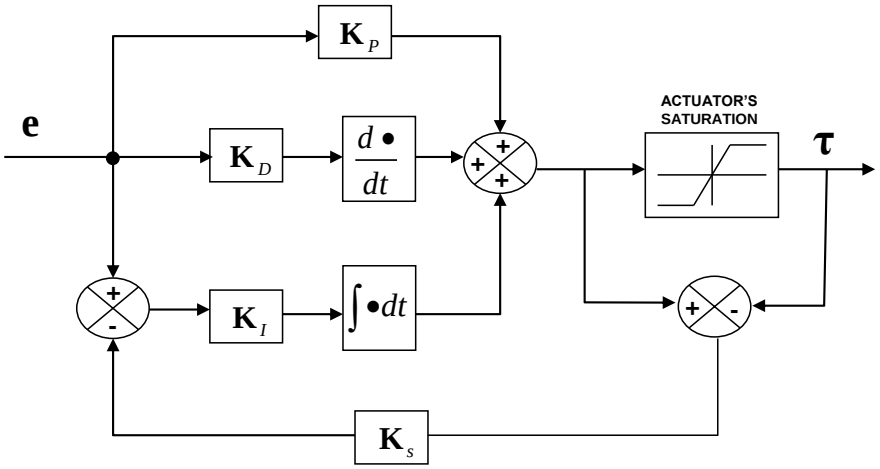

Figure 4-2.: PID Controller with Antiwindup.

4.1.2. Previous works on DLCC computation

Two main constraints related to DLCC computation on flexible and redundant manipulators are: maximum allowable torques on each actuator and accuracy on the tracking control task [53, 103]. These constraints may be calculated in a trajectory discretized into $j = 1...m$ points and summarized as follows:

- The actuators constraint is computed as a function of an upper and lower torque bounds depending on joint velocities, to calculate a load coefficient as:

$$(c_a)_j = \text{mín} \left\{ \ \frac{(\tau_a)_i}{\text{máx}\{\tau_e\} - \text{máx}\{\tau_n\}} \quad ; i = 1...n \ \right\}, \tag{4-15}$$

with $(\tau_a)_i$ the maximum allowable torque at joint i, τ_e the torque at the end-effector with added mass and τ_n the no-load end-effector torque.

- The end-effector accuracy constraint is calculated as a function of the no-load deflection $(\Delta_n)_j$, deflection with loaded end-effector $(\Delta_e)_j$ and the maximum allowable deflection for the loaded end-effector (Δ_p) at each trajectory point. The load coefficient is defined as:

$$(c_p)_j = \frac{\Delta_p - (\Delta_e)_j}{\text{máx}\{\Delta_e\} - \text{máx}\{\Delta_n\}}. \tag{4-16}$$

Hence, the trajectory load coefficient is computed as

$$c = \text{mín}\left\{(c_p)_j, (c_a)_j\right\}, \tag{4-17}$$

and the maximum load m_{load} for the trajectory would be

$$m_{load} = cm_e, \tag{4-18}$$

with m_e the mass at the end-effector.

4.1.3. DLCC computation based on cell to cell mapping on the entire workspace for the regulation task

In the regulation task, there is a maximum payload associated to some predefined accuracy related to the task. The accuracy is a measure of the error of the final position for a specific regulation task. On the other hand, the trajectory accomplished by the controller may have mechanical constraints related to each joint or to the workspace it self. The numerical analysis of the solutions based on the cell to cell mapping strategy allows to compute the maximum DLCC related to the workspace of the manipulator and potentially serve as a path planing strategy.

The proposed methodology, presented in the block diagram Fig. **4-3a**, may be enumerated as follows:

1. Divide the workspace into cells. The center of each cell will be used as a candidate position.
2. Examine the workspace, based on the mechanical constraints of the manipulator (applying the inverse kinematic model), to select possible candidate positions.
3. Compute the DLCC between each pair of candidate positions, building a cell to cell mapping, based on position error of the regulation task. The maximum DLCC m_{rt} for each cell combination may be defined as the maximum load capable of being carried by the manipulator between two points in the workspace, as shown in Eq. (4-19). This procedure is presented in the flow diagram of Fig. **4-3b**. Hence,

$$m_{rt} = \text{máx}\left\{\ (m_{rt})_i\ \right\}. \tag{4-19}$$

4. The evaluation of the entire workspace would result to be the minimum of those maximum DLCCs or the maximum load capable of being carried by the manipulator between all the candidate positions. Hence, the maximum DLCC m_{load} would be the minimum of the $(m_{rt})_i$ for $i = 1...q$ regulation tasks as stated in Eq. (4-20):

$$m_{load} = \min\left\{ \ (m_{rt})_i \quad , i = 1...q \ \right\}. \tag{4-20}$$

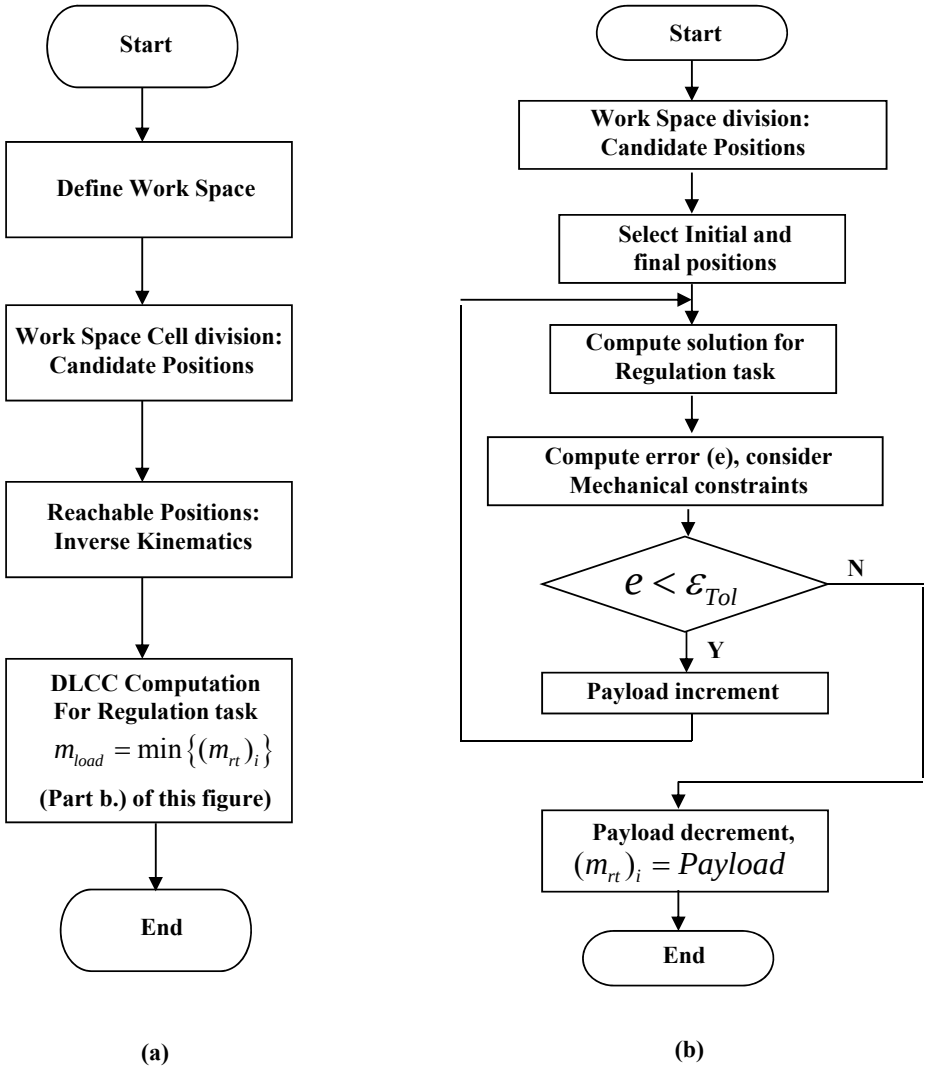

Figure 4-3.: Methodology algorithm: a) Main procedure. b) DLCC computation algorithm.

4.1.4. Numerical analysis of maximum DLCC computation and controller performance comparison

For a 5 DoF ($n = 5$) rotational joint manipulator ($\mathbf{q} = \theta$), with state vector $\mathbf{x} = [\mathbf{q_k}, \dot{\mathbf{q}}_\mathbf{k}]$, for $k = 1 \ldots 5$. Let us define:

$$\mathbf{H}(\mathbf{x_k})^{-1} = [h(x_k)_{ij}^{-1}]_{(n\times n)} = (\mathbf{H}(\mathbf{x_k})^{-1})_{ij}. \tag{4-21}$$

Hence, the state variable representation:

$$\begin{aligned} \dot{x}_k &= x_{k+5}, \\ \dot{x}_{k+5} &= (\mathbf{H}(\mathbf{x_k})^{-1})_{kj}(\tau - \mathbf{C}(\mathbf{x}) - \mathbf{g}(\mathbf{x_k})). \end{aligned} \tag{4-22}$$

In a compact form, it can be presented as: $\dot{\mathbf{x}} = \mathbf{f}(\mathbf{x}, \tau)$, with $\mathbf{x} \in \mathbf{R^p}$, $\tau \in \mathbf{R^q}$, for $p = 10$ and $q = 5$.

The considerations used for numerical analysis and simulation for a 5 DoF manipulator are:

1. The controllers are implemented using the following criteria:
   - The feedback linearization controller is designed to obtain the critically damped transient response.
   - The adaptive controller with gain scheduling proved its best setting by minimizing the convergence time of the adapted parameter (payload). To this end, a trial and error procedure was applied.
   - The PID with antiwindup was configured to have a damped solution.
2. The saturation torque related to the actuators is chosen to be $\tau_{sat} = 18{,}2$ Nm.
3. The reference error was defined as $\varepsilon_{Tol} = 10^{-3}$ rad, for the accuracy constraint in the regulation task.
4. The workspace is a $\mathbf{R^3}$ space of the following span: $X = (-400, 400)$ mm, $Y = (-400, 400)$ mm and $Z = (-0, 800)$ mm.

Fig. **4-4** shows the center of each cell in the workspace division for 1000 candidate positions, resulting from a $10 \times 10 \times 10$ separation and a cell size of $80 \times 80 \times 80$ mm. Then, Fig. **4-5** shows an exemplifying subset of 6 reachable positions, extracted from a random group of 10 candidate positions using the inverse kinematic model of the manipulator, as applied in the second step of the proposed methodology. This is obtained by the use of a MatLab® function *plotbot* included in [11].

The regulation task is computed for each pair of candidate positions using different controllers. As shown in Fig. **4-6** for one of the tasks (with the initial and final positions presented below) and using feedback linearization control, the regulation task is accomplished for a payload of $m_{rt} = 2{,}26$ kg.

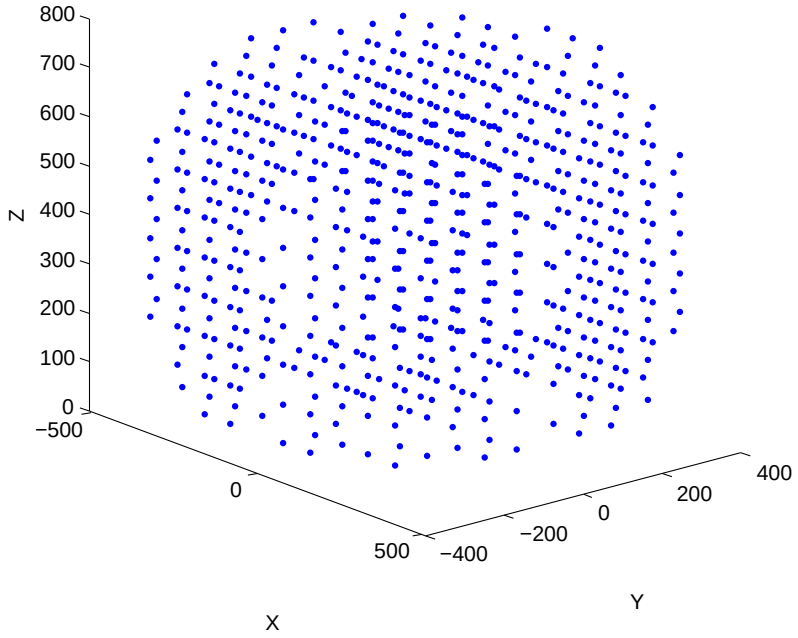

Figure 4-4.: Workspace division in 1000 cells ($10 \times 10 \times 10$).

Notice in Fig. **4-7** the saturation in the control torque τ_2 (the most demanding joint) for a simulation time between 1,5 s and 10 s approximately, but the task is fulfilled with the expected accuracy.

The testing condition may be defined as:

- The initial position:
  1. Workspace: $X = -400$ mm, $Y = -29$ mm and $Z = 371$ mm.
  2. Joint space: $\theta_1 = -3{,}07$ rad, $\theta_2 = -1{,}11$ rad, $\theta_3 = -2{,}03$ rad, $\theta_4 = -0{,}65$ rad and $\theta_5 = 0$ rad.
- The final position:
  1. Workspace: $X = -29$ mm, $Y = 342$ mm and $Z = 742$ mm.
  2. Joint space: $\theta_1 = 1{,}65$ rad, $\theta_2 = 0{,}93$ rad, $\theta_3 = 0{,}46$ rad, $\theta_4 = -2{,}95$ rad and $\theta_5 = 0$ rad.

The maximum DLCC for the entire workspace, using feedback linearization control on this particular manipulator configuration resulted to be $m_{load} = 0{,}82$ kg, for the adaptive controller the $m_{load} = 0{,}33$ kg and for the PID with antiwindup $m_{load} = 0{,}15$ kg.

The Fig. **4-8** presents a comparison histogram between the three proposed controllers. It shows the frequency of control task achievement for each controller as a function of the payload (with

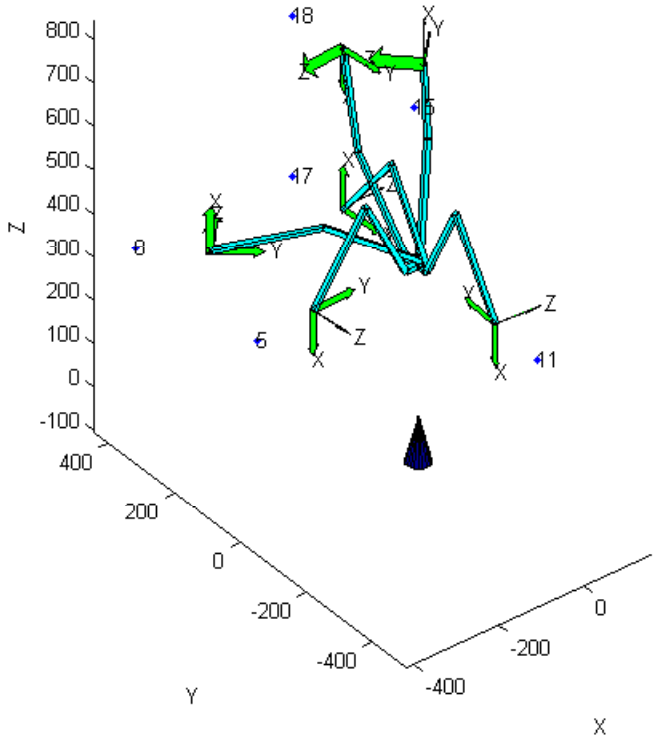

Figure 4-5.: Exemplifying reachable configurations for 10 candidate positions.

increments of 1 kg). The exemplifying random group of 10 candidate positions is used to compare the performance of the controllers for all the possible combinations of the reachable positions on that subset. It shows that the most of the tasks are grouped in the lower payload scale ($\leq$ 3 kg). For the Feedback Linearization Controller (FLC) some of the tasks (with close initial and final positions) can carry payloads above 3 kg, the Adaptive Controller with Gain Scheduling (ADPGS) has a decreasing performance when the payload increases. The PID controller with Anti-Windup (PIDAW) shows a relatively consistent behavior in the lower payload range ($\leq$ 3 kg).

Other important issues to be considered are:

- As the inverse kinematics is evaluated as part of the methodology, there may be multiple solutions for some specific candidate position and one of them have to be chosen.

- There are mechanical constraints related to possible obstacles in the workspace and the joints. They may be used as constraints for the regulation task trajectories.

- There could be some other controller parameter settings that may contribute to fulfill the regulation task in cases where it is not accomplished.

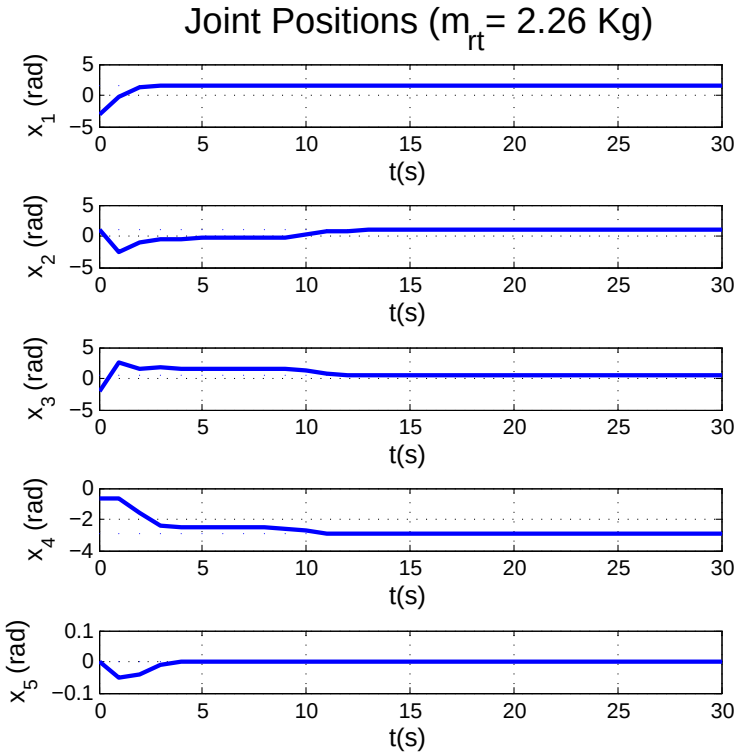

Figure 4-6.: Joint trajectories of the SCORBOT's joints.

- The control effort may be computed as an indicator in order to find the most demanding trajectories.
- There are multiple trajectories to go from one cell to another. The control effort or any other performance criterion may be used to optimize the task. Hence, this procedure may be used for path planning.

4.1.5. Results

The maximum DLCC for the entire workspace using nonlinear numerical analysis is a different approach, which may be used for application setting, manipulators design and potentially for path planning. It would be realistic to consider the saturation as part of the normal performance of the control tasks, because the behavior of the motors. The comparison between different controllers shows the best performance of the feedback linearization controller, counting with the fact that it is based in the perfect knowledge of the manipulator model. The adaptive controller would be more practical because of the uncertain nature of some manipulator applications. The PID is justified because of the common use of this controller in industrial applications. The cell to cell mapping used for DLCC computation in manipulators may help to improve performance based on its structured nature.

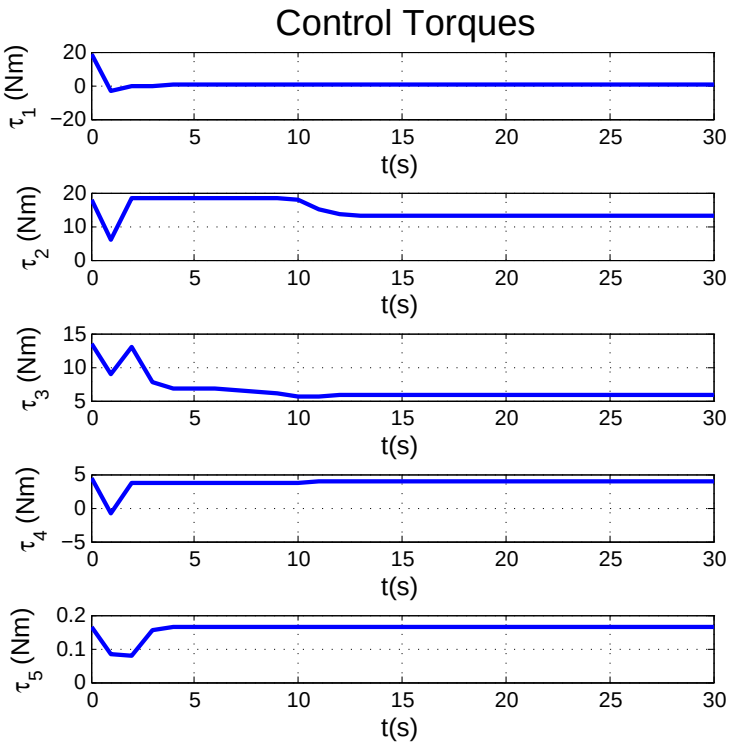

Figure 4-7.: Control Torques for $m_{rt} = 2{,}26$ kg.

Besides, it is recommended the inclusion of the proposed methodology in manipulators design that would help to improve characterization and application performance. The saturation in manipulator control may be considered as part of the natural behavior of the tasks, allowing controllers design and setting that accomplish its objectives based on performance. The cell to cell mapping concept may be used for trajectory planning based on control effort or other optimization criterion.

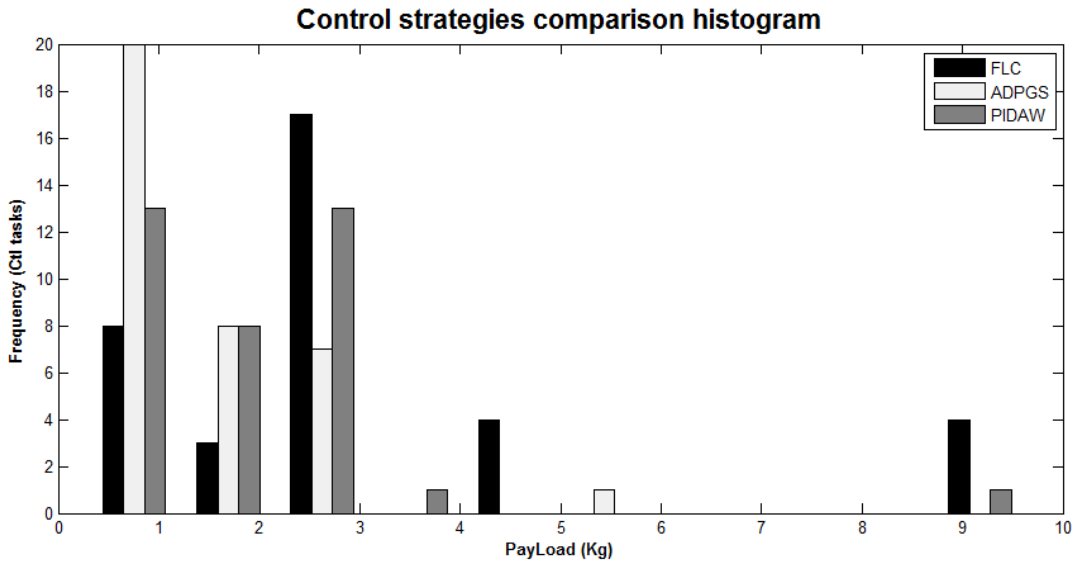

Figure 4-8.: Comparison among control strategies for the proposed methodology.

4.2. Data-driven Unfalsified Control (UC) compared with the traditional model-based Adaptive control: Effect of controllers in the maximum DLCC.

The aim of this section is to evaluate in simulation both performance and robustness of the UC strategy for MDoF manipulators, extending the results in [94, 71] and considering the effect in the DLCC. The proposed UC scheme includes fading memory to improve the adaptability of the controller to recent operating conditions. UC with fading memory has been introduced in [38] to reduce the importance of the oldest information in the switching algorithm. This is more suitable in nonlinear or time-varying plants as MDoF manipulators and also improves the capability of the UC algorithm to detect destabilizing controllers. Traditional feedback linearization is used as base controller for the UC controller set.

This section shows results related to the DLCC computation for the tracking task, with a comparison between UC and a traditional model-based adaptive control and then an evaluation of its relation to the precise estimation of the manipulators model. Three scenarios were considered: performance of controllers for two fixed loads at the end of the manipulator, performance of controllers with periodic non-smooth load changes between two fixed values and performance of controllers by the application of worst-case disturbances to the model inertial parameters. The proposed control is compared in simulation with a well-known adaptive control strategy, showing that the independence of the robot model may result in better performance and higher DLCC. The UC is capable of a better behavior in a larger operating range. Also, the UC is more robust as can

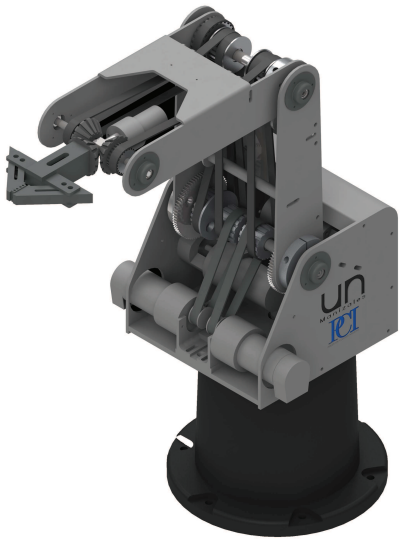

Figure 4-9.: CAD model of the SCORBOT ER V PLUS [37]

be concluded when the system parameters are perturbed.

4.2.1. Analysis of controller performance and robustness

The case of study considered in this section is a 5-DoF manipulator like the SCORBOT ER V Plus CAD model shown in Fig. **4-9**, with the parameters proposed in [23] as:

$$
\begin{aligned}
&m_i = 1 \text{ kg}, i = 1,\ldots,5,\\
&l_1 = 0{,}35 \text{ m}, \; l_2 = l_3 = 0{,}22 \text{ m}, \; l_4 = l_5 = 0{,}14 \text{ m},\\
&\mathbf{I_{xy}} = \begin{cases} 0{,}1, & \text{if } x = 1,\ldots,5 \text{ and } y = 1,2,3,\\ 0, & \text{if } x = 1,\ldots,5 \text{ and } y = 4,5. \end{cases}
\end{aligned}
$$

Based on previous simulations and analysis presented in [5], the maximum DLCC of the manipulator for the tracking task is assumed to be 2 kg. The load at the end of the manipulator is assumed attached to the end-effector of mass m_5 and unknown for the controller implementation.

For analysis purposes, the following desired trajectories were used:

$$
q_{d_i} = \begin{cases} \dfrac{2\pi}{3}\left(1-\cos\left(\dfrac{2\pi}{5}t\right)\right), & \text{if } i = 1,3,5,\\ \pi\left(1-\cos\left(\dfrac{2\pi}{5}t\right)\right), & \text{if } i = 2,4. \end{cases}
$$

The initial conditions for all simulations were $q_{d_i}(0) = 0$ and $\dot{q}_{d_i}(0) = 0$ ($i = 1, \ldots, 5$). Note that trajectories are periodic, with period $T = 5$ s. The damping friction constant for all joints was defined as $\gamma = 0{,}1$. The parameter related to the controller Eq. (3-15) was set at $\lambda = 20$ as a result of several simulations, for the smaller tracking error and fastest response [5]. Although the actuator saturation torques are a function of the velocity, the upper and lower bounds of the control signal were assumed to be constant for simplicity, as ± 30 Nm.

The controller set $\mathbf{K}$ for the UC is defined by Eq. (3-14), where the parameter θ (load applied at the end of the manipulator, including the mass of the end effector) takes values $\hat{\theta}$ in a set Θ, for an interval from the no-load condition to the maximum DLCC of the case of study, *i.e.*

$$\Theta = \{1, 2, 3\}. \tag{4-23}$$

In terms of the payload, and considering that $m_5 = 1$ kg (actual mass of the end effector without load), this means that the corresponding interval for the controller parameter (payload) is $[0, 2]$ kg.

The used cost function is defined in Eq. (3-17), with $\alpha = 0{,}001$ and $\eta = 0{,}9$ as the fading constant. The cost function is evaluated periodically with $T_s = 0{,}01$ s, based on the cost minimization hysteresis switching algorithm with fading memory presented in Section 3.3.2. The initial controller parameter used by the UC for the simulation was $\hat{\theta}(0) = 1$. All simulations were performed for a 15 s time interval, which includes three complete periods of the desired trajectories.

Three scenarios were considered: *i*) performance of controllers for two fixed loads at the end of the manipulator; *ii*) performance of controllers with periodic non-smooth load changes between two fixed values; and *iii*) performance of controllers applying the worst-case disturbances to the model inertial parameters.

The control effort (CE) and the integral squared tracking error (ISE) are used as performance evaluation criterion. They are related to the performance specifications stated by the cost function Eq. (3-17), since the errors and inputs (torques) are considered. Besides, the influence of both controllers in the maximum DLCC is analyzed.

Considering the periodic feature of trajectories, and counting with the defined integral quality of the CE and ISE, it is used a moving window computation of those integrals for the entire period of the desired trajectory ($T = 5$ s in this case), defining the integration interval between $t - T$ and t.

The ISE is computed as

$$ISE_{q_i}(t) = \int_{t-T}^{t} e_i^2(t)dt, \tag{4-24}$$

where $e_i(t)$ $(i = 1 \dots 5)$ are the tracking errors.

The CE is computed as

$$CE_{q_i}(t) = \int_{t-T}^{t} \tau_i^2(t)dt, \tag{4-25}$$

where $\tau_i(t)$ $(i = 1 \dots 5)$ are the control torques. Note that although these calculations are presented in continuous time, in practice they are computed in discrete time, with relatively small sampling time compared with the evaluation of the cost functions in Eq. (3-19).

The UC scheme was compared with the model-based adaptive controller proposed in [83], which uses the linear model presented in Eq. (3-13) and was designed to adapt to load changes, with proven Lyapunov stable control and converging adaption laws as

$$\begin{aligned} \mathbf{u} &= \mathbf{Y}\hat{\mathbf{a}} - \mathbf{K_D}\mathbf{s}, \\ \dot{\hat{\mathbf{a}}} &= -\Gamma \mathbf{Y}^T \mathbf{s}, \end{aligned} \tag{4-26}$$

where the first-order sliding surface $\mathbf{s} = \dot{\tilde{\mathbf{q}}} + \Lambda\tilde{\mathbf{q}}$, with $\tilde{\mathbf{q}} = \mathbf{q_d} - \mathbf{q}$; $\mathbf{Y}\hat{\mathbf{a}}$ is a feedforward term, $\hat{\mathbf{a}}$ is the load adaption parameter, Γ, Λ are symmetric, positive definite matrices and $\mathbf{K_D}\mathbf{s}$ is the proportional derivative term. The adaptive controller tuning for the smaller tracking error and fastest adaption convergence are given in [5] as a result of several simulations. For the current simulation, $\mathbf{K_D} = 100\mathbf{I}_5$, $\Lambda = 150\mathbf{I}_5$ and $\Gamma = \text{diag}(0{,}3, 0{,}5)$, where $\mathbf{I}_5$ is a 5×5 identity matrix.

4.2.2. Controller performance analysis for two fixed loads at the end-effector

Initially, it is analyzed the performance of both controllers for the most effort demanding joints (joints q_2 and q_3). As the performance of both controllers is tested to be well behaved for light loads, simulations are performed for fixed loads of 1,5 kg and 1,7 kg (load remains constant along the entire trajectory), supposing the precise knowledge of the model inertial parameters, meaning that no disturbances are applied to the model.

In Fig. **4-10**, both the desired and real trajectories for joints 2 and 3 (q_2 and q_3) are shown overlaid, stating its periodic feature for the case of a 1,5 kg payload. In Fig. **4-11**, the comparison of tracking errors for 1,5 kg and 1,7 kg shows that the error increases considerably at the most effort demanding points of the trajectories, this would be at the beginning of each period. Although the tracking errors for a load of 1,5 kg are relatively small, the system with adaptive control behaves better than the system with the UC, even at the most demanding points of the trajectories. The tracking errors for the load of 1,7 kg shows that the adaptive controller is not able to accomplish the control task due to an impractical growth in those errors, meaning that in simulation it can be

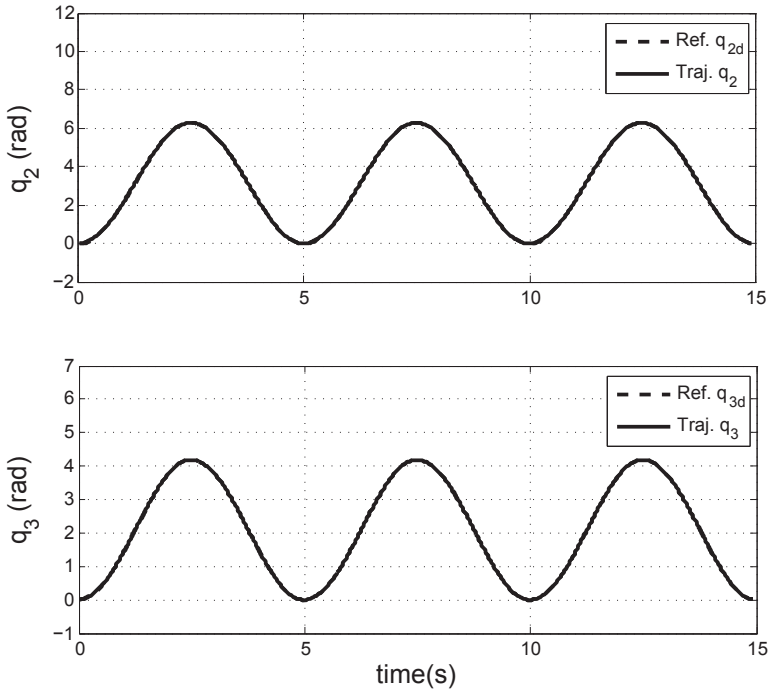

Figure 4-10.: Tracking trajectories and references for joints q_2 and q_3. Payload of 1,5 kg

observed several turns of the joints, which in reality it would represent saturation due to motion stops, with the corresponding effect in the errors. On the other hand, the system with UC continues with its adequate behavior.

A comparison of the ISE for q_2 and q_3 (shoulder and elbow joints of the manipulator) is shown in Fig. **4-12**, for both loads. The integration window for the period $T = 5$ s starts at $t - T$ s for the first computation, and moves along the 15 s simulation time. In the case of 1,5 kg load, the ISE stays steady after the first period for both controllers, with little changes at the most effort demanding points of the trajectories. For 1,7 kg the ISE for the UC stays small but the ISE for the adaptive controller increases along the trajectories as a consequence of its incapability to accomplish the control task with this load.

In Fig. **4-13** it is presented a comparison between control signals of both controllers for the two testing loads. It should be noticed for the 1,5 kg load that both controllers are able to recover from saturation in the entire trajectory. However, UC shows smoother control signals than the adaptive controller. For the 1,7 kg payload, the control signal for the adaptive controller turns unstable after 5 s, but the UC control signals remains bounded and smooth.

The Fig. **4-14** shows a comparison between CE for q_2 and q_3, in the cases of 1,5 kg and 1,7 kg, respectively. The integration window for the period $T = 5$ s starts at $t - T$ for the first computation,

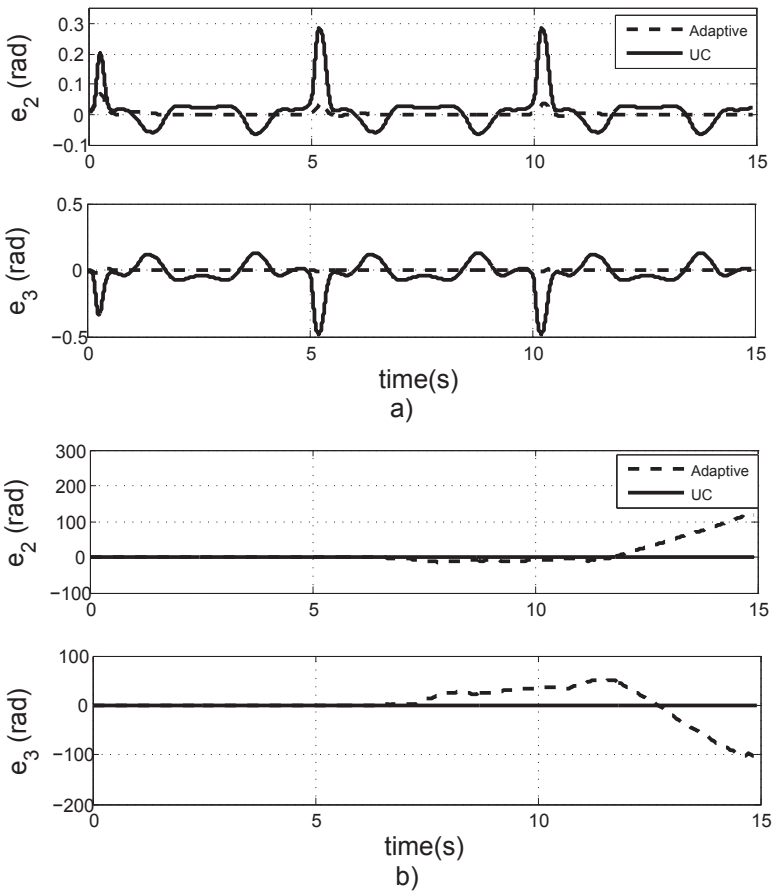

Figure 4-11.: Tracking errors for joints q_2 and q_3. a) Payload of 1,5 kg. b) Payload of 1,7 kg

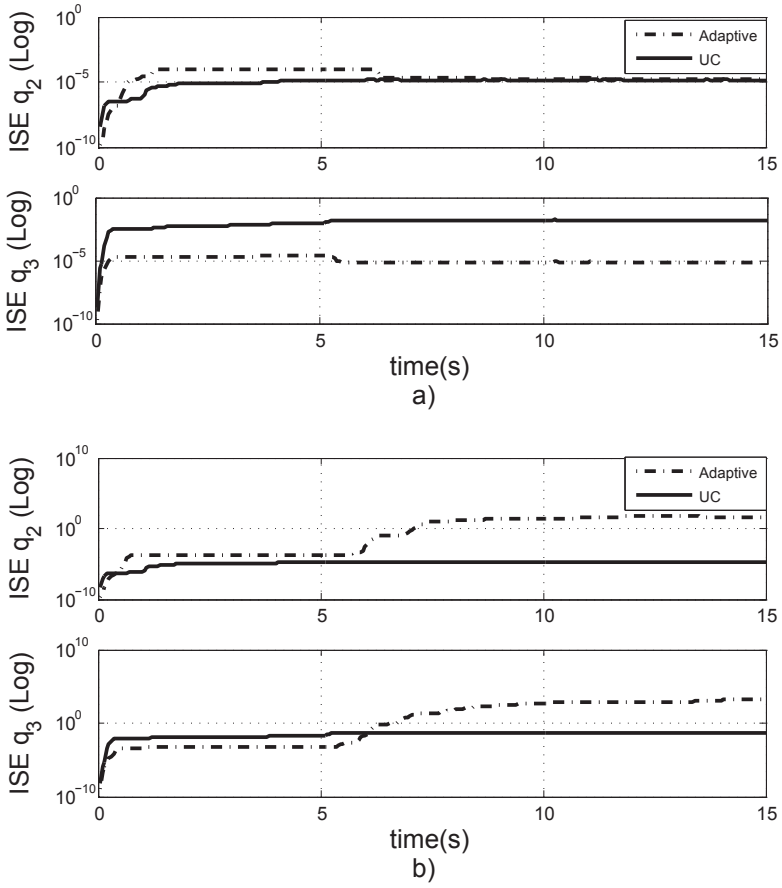

Figure 4-12.: Integral squared error (ISE) for joints q_2 and q_3. a) Payload of 1,5 kg. b) Payload of 1,7 kg

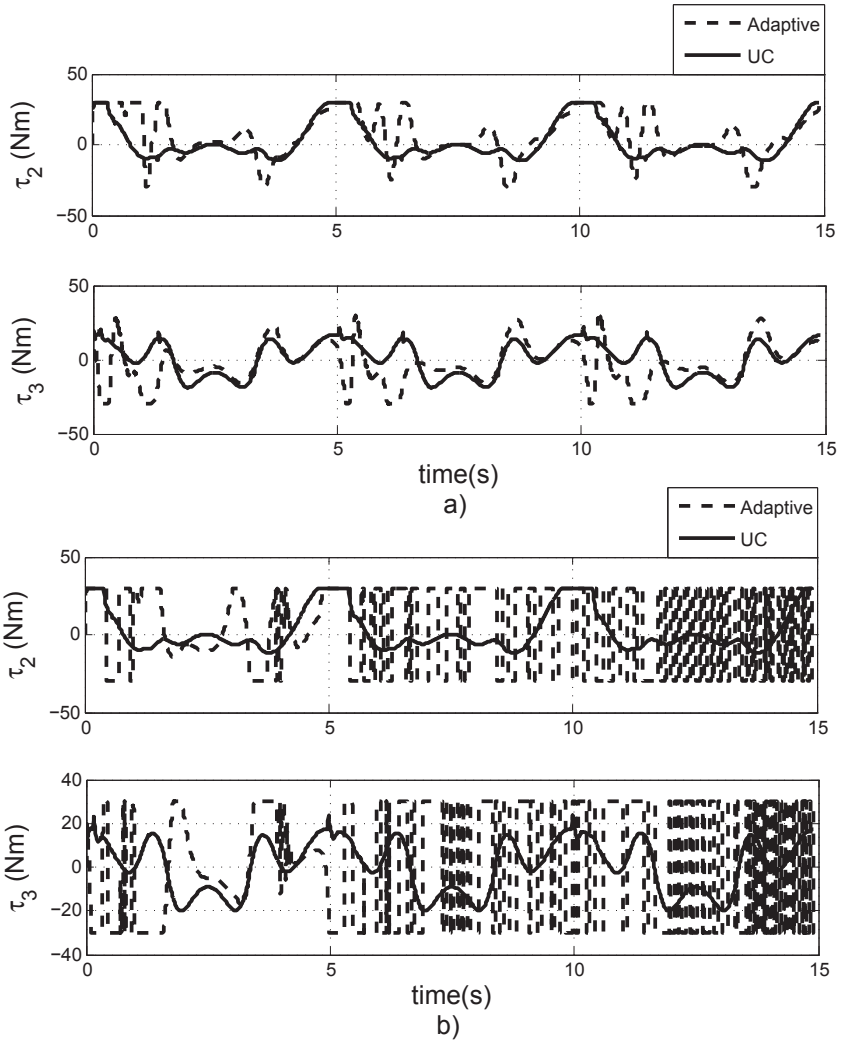

Figure 4-13.: Control torques for joints q_2 and q_3. a) Payload of 1,5 kg. b) Payload of 1,7 kg

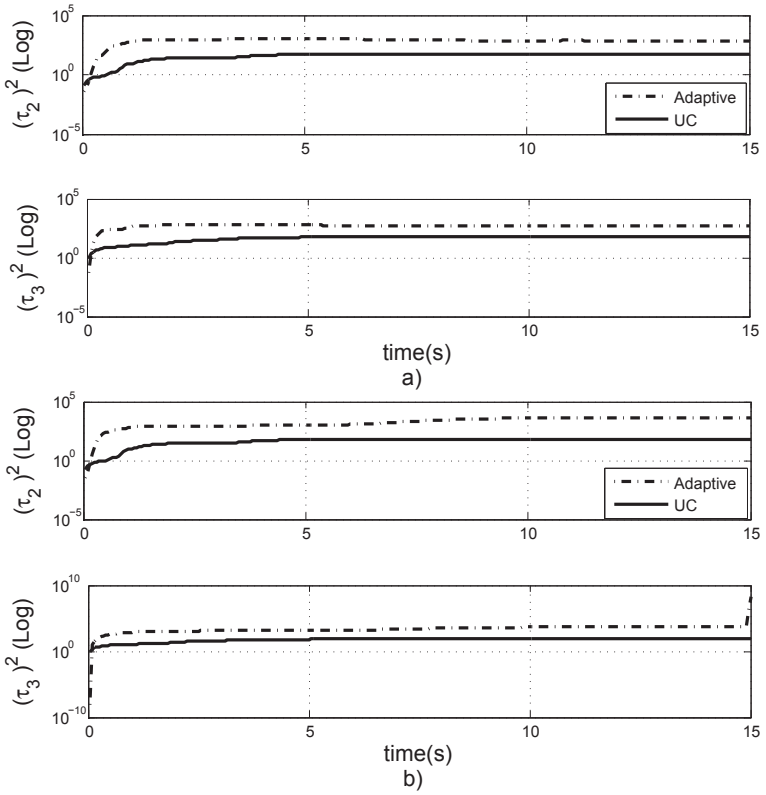

Figure 4-14.: Control effort (CE) for q_2 and q_3. a) Payload of 1,5 kg. b) Payload of 1,7 kg

and moves along the 15 s simulation time span. For the lighter loads, the CEs are similar, but for the 1,7 kg load, the control effort for the adaptive controller increases constantly after 5 s as a consequence of the unstable and saturated behavior presented in Fig. **4-13**.

The Fig. **4-15** shows for 1,5 kg load a complete trajectory period (between 5 and 10 s) of the cost functions in Eq. (3-17) and the changes of the controller parameter θ produced by the falsification algorithm: a change occurs each time the condition in Eq. (3-19) is satisfied. The algorithm searches for the minimum cost value to falsify and change the current controller parameter.

Table **4-1** shows a normalized performance comparison of controllers for joints 1 to 5, based on the ISE and CE for a time span of 15 s and an integration window of 5 s. Normalization is based on the NO LOAD case, presented at the same table. Note that the ISE stays bounded for the UC for both load values, but there is a significant increase in these performance indicator for the adaptive controller when the load passes from 1,5 kg to 1,7 kg, showing a performance loss (actually, the controller is not able to fulfill the control task for 1,7 kg. The mean value is shown in Table **4-1** by the light gray cells). This shows that for the present setting, the adaptive controller provokes a limited maximum load carrying capacity (DLCC) in the proposed load testing interval, as presented in [5]. It should be noted how the magnitudes of the CE increase for the adaptive controller when

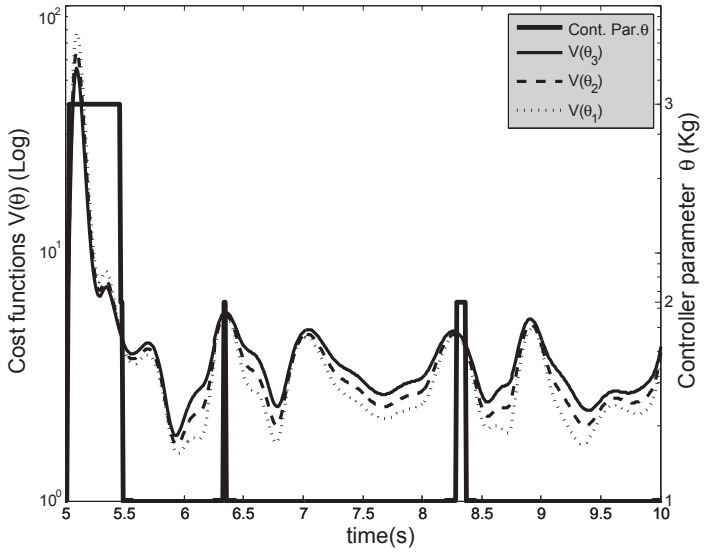

Figure 4-15.: UC Cost functions and controller parameter changes for a fixed load of 1,5 kg

the load changes from 1,5 kg to 1,7 kg, as expected, due to the unstable and saturated behavior of the control signals after the first period, confirming performance decay for the higher load (the mean value is shown in Table **4-1** by the dark gray cells. For q_5 the CE remains relatively small due to the orientation function of that joint). From Table **4-1**, the UC exhibits an acceptable ISE for the 1,7 kg load, showing how the manipulator is able to follow the desired trajectory with satisfactory behavior.

4.2.3. Controller performance analysis for periodic non-smooth load changes between two fixed values

This scenario evaluates the controllers performance when the load carried by the manipulator changes periodically (with period $T_l = 3$ s) between 0,5 kg and 1,5 kg and between 0,5 kg and 1,7 kg. Sudden (non-smooth) load changes can occur in real manipulator control tasks, as pick and place and palletizing (stacking cases of products onto a pallet), among others.

The cost functions and controller parameter changes for the UC are very similar to those presented in the Fig. **4-15**, despite of the load disturbance created by the changes between 0,5 kg and 1,5 kg and between 0,5 kg and 1,7 kg. There are no significant differences in this functions, related to the sudden change of load. Hence, the performance of UC did not change significantly with respect to the first scenario. In fact, in the scenarios to come and due to this consistency in results, they are summarized in tables focusing in the analysis of the topics of interest.

Table 4-1.: Controller performance comparison for joints q_1 to q_5 in a time span of 15 s. Normalization based on the NO LOAD case.

CONTROLLER		UC			ADAPTIVE		
PAYLOAD (kg)		NO LOAD	1.5	1.7	NO LOAD	1.5	1.7
ISE q_1	MAX	1,80E-05	1,80	2,23	3,40E-07	118,18	3,75E+09
	MEAN	1,66E-05	1,84	2,28	2,82E-07	99,26	2,12E+09
	STD.DEV.	3,08E-07	1,55	1,97	2,76E-08	566,69	1,82E+10
ISE q_2	MAX	1,40E-03	18,21	74,23	8,25E-07	1103,47	1,96E+10
	MEAN	1,29E-03	16,72	70,02	5,02E-07	86,66	2,98E+09
	STD.DEV.	2,21E-05	69,98	372,99	4,84E-08	2403,66	6,72E+10
ISE q_3	MAX	5,39E-03	13,91	47,55	4,43E-07	247,91	3,42E+10
	MEAN	5,02E-03	12,74	44,59	3,29E-07	248,83	9,54E+09
	STD.DEV.	7,78E-05	55,10	241,64	2,43E-08	607,31	1,46E+11
ISE q_4	MAX	2,00E-03	8,38	24,36	3,38E-08	648,56	6,11E+10
	MEAN	1,87E-03	7,82	22,96	3,14E-08	227,69	1,68E+10
	STD.DEV.	2,85E-05	29,80	117,16	1,33E-09	1990,52	4,12E+11
ISE q_5	MAX	8,94E-06	1,72	2,17	1,46E-07	712,70	4,10E+08
	MEAN	8,01E-06	1,78	2,25	1,26E-07	148,44	2,14E+08
	STD.DEV.	1,76E-07	1,37	1,80	1,29E-08	2073,68	1,53E+09
CE q_1	MAX	3,48E+01	4,10	4,68	1,18E+02	10,22	2,71E+07
	MEAN	3,35E+01	4,05	4,62	9,77E+01	9,80	1,64E+05
	STD.DEV.	3,80E-01	4,71	5,45	8,61E+00	9,74	2,62E+07
CE q_2	MAX	4,33E+02	2,16	2,30	4,85E+02	3,73	1,78E+10
	MEAN	4,16E+02	2,15	2,30	4,64E+02	3,14	9,33E+07
	STD.DEV.	6,25E+00	2,33	2,43	9,53E+00	10,37	6,40E+10
CE q_3	MAX	2,43E+02	2,85	3,13	2,95E+02	3,67	2,93E+10
	MEAN	2,40E+02	2,81	3,08	2,84E+02	3,47	1,53E+08
	STD.DEV.	1,85E+00	2,97	3,30	5,56E+00	6,88	1,10E+11
CE q_4	MAX	1,78E+01	3,38	3,80	2,28E+01	27,18	1,01E+07
	MEAN	1,76E+01	3,37	3,79	2,19E+01	24,27	5,28E+04
	STD.DEV.	1,19E-01	3,41	3,86	6,80E-01	31,71	2,38E+07
CE q_5	MAX	7,91E+00	6,31	7,38	4,59E+01	23,20	98,98
	MEAN	7,66E+00	6,31	7,38	3,92E+01	20,15	87,44
	STD.DEV.	9,29E-02	6,37	7,46	3,81E+00	27,64	353,20

Table 4-2.: Controller performance comparison for joints q_2/q_3 and non-smooth change of payload every 3 s. Normalization based on the NO LOAD case.

		ADAPTIVE CONTROLLER	
PAYLOAD CHANGE		0.5 - 1.5 kg	0.5 - 1.7 kg
ISE rad^2 (q_2 / q_3)	MAX	125,54 / 48,69	5,26E+10 / 7,25E+10
	MEAN	24,98 / 3,39	2,65E+10 / 3,33E+10
	STD.DEV.	654,67 / 159,63	3,34E+11 / 5,00E+11
CE Nm^2 (q_2 / q_3)	MAX	2,12 / 2,05	9,37 / 15,39
	MEAN	0,39 / 0,31	7,45 / 12,16
	STD.DEV.	27,04 / 22,64	136,45 / 247,64
		UNFALSIFIED CONTROLLER	
PAYLOAD CHANGE		0.5 - 1.5 kg	0.5 - 1.7 kg
ISE rad^2 (q_2 / q_3)	MAX	0,01 / 2,26	0,01 / 6,84
	MEAN	0,01 / 2,22	0,01 / 6,57
	STD.DEV.	0,09 / 17,69	0,12 / 53,54
CE Nm^2 (q_2 / q_3)	MAX	0,12 / 0,24	0,12 / 0,24
	MEAN	0,12 / 0,23	0,12 / 0,23
	STD.DEV.	0,10 / 1,21	0,10 / 1,51

As in Fig. **4-13**, a comparison between control signals applied to the robot by the UC and the adaptive controllers was done for the cases of sudden changes of the load at the end effector, finding similar results to those presented in Section 4.2.2. For the case of changes between 0,5 kg and 1,5 kg, smoother control signals for the UC were noted. For the case of changes between 0,5 kg and 1,7 kg, the control signal of the adaptive controller presented an unstable behavior, justifying a growing ISE and CE for this controller.

Table **4-2** shows a normalized performance comparison of both controllers for joints q_2 and q_3, based on the ISE and CE in a time span of 15 s, for sudden changes of load (every 3 s) between 0,5 kg and 1,5 kg and 0,5 kg and 1,7 kg, respectively. Normalization is based on the NO LOAD case presented in Table **4-1**. It also shows an increasing ISE for the adaptive controller in the case of non-smooth changes of payload between 0,5 kg and 1,7 kg, demonstrating that this controller is not able to fulfill the corresponding task (The mean value is shown in Table **4-2** by the light gray cell).

The growing CE for the adaptive controller, required to move q_2 and q_3 for sudden changes of payload between 0,5 kg and 1,7 kg, are related to the unstable and saturated control signal behaviors, similar to those presented in Fig. **4-13**.

Table 4-3.: Disturbed inertial parameter used for the worst case scenario.

PARAMETER	No-dist.	1σ dist.	2σ dist.
$m_i (i = 1 \dots 5)$ (kg)	1	1,32	1,45
l_1 (m)	0,35	0,46	0,51
$l_2 = l_3$ (m)	0,22	0,29	0,32
$l_4 = l_5$ (m)	0,14	0,18	0,2
$\mathbf{I_{xy}}$			
$x = 1-5$ and $y = 1,2,3$	0,1	0,13	0,15
$x = 1-5$ and $y = 4,5$	0	0	0

4.2.4. Performance analysis as a function of the payload: from the no-load condition to the maximum DLCC of the case of study

The precise identification of inertial parameters of real manipulators is not a trivial task, with categorizations as: uniquely identifiable, identifiable in linear combinations only, and unidentifiable [40]. Besides, there are several estimation methods, from robot disassembling and CAD/CAM databases, to on-line and off-line identification using simple least-squares (LS) methods [74]. Supposing a normal distribution, the deviations from the real values of parameters resulting of an identification procedure may be grouped in the 68 % and 90 % standard deviations around the actual parameters as presented in [90], corresponding to the 1σ and 2σ confidence intervals.

It is studied the robustness for both controllers, showing its model dependence on the application of disturbances (lack of precision in parameter estimation) to the inertial parameters of the model, based on the worst case scenario of possible parameter identification deviations of 1σ and 2σ confidence intervals, and presenting that the DLCC is affected by those disturbances. The values used for parameters from the no-disturbance case to the 2σ disturbance case are summarized in Table **4-3**.

The robustness was analyzed for the UC and the adaptive controller for the range between no-load and the maximum load proposed for the case of study (payload from 0 to 2 kg), with resolution of 0,1 kg, and considering the 1σ and 2σ confidence intervals of estimated inertial parameter as model disturbances, finding that the behavior from 0 kg to 1,4 kg is consistent and predictable from the previous scenarios analysis, even for the proposed disturbances. So, the following analysis is presented for payloads between 1,4 kg and 2 kg, with resolution of 0,1 kg.

Table **4-4** shows a normalized performance comparison of the controllers based on the ISE and CE just for joint 3 (q_3 as the elbow joint), because the consistency of results related to the other joints and its significance, as a function of the payload change from 1,4 kg to 2 kg, with 0,1 kg increments. Normalization is based on the No-disturbance case, shown in the same table. The table

presents three cases: the no-disturbance case (perfect identification of inertial parameters) and the cases of disturbances of 1σ and 2σ of the model inertial parameters.

From the Table **4-4** it can be concluded that, in the no-disturbance case, the ISE and the CE are lower for adaptive control until a load of 1,7 kg, where it looses its ability to fulfill the task (the ISE and CE values are shown in Table **4-4** by the light gray cells). The ISE and CE for the UC continue with a bounded tendency, showing how the UC is able to handle higher loads. In the case of 1σ model disturbance, the behavior is similar to the no-disturbance case, but for the 2σ disturbance, it is a reduction in the DLCC manageable by the adaptive controller, decreasing to 1,6 kg (the ISE and CE values are shown in Table **4-4** by the dark gray cells), but the performance of the UC stays consistent for the entire range, as expected.

Therefore, it shows that the robustness of model-based adaptive controller is related to the accuracy in the identification of the model parameters and the UC resulted to be more robust to this kind of disturbances. Besides, the DLCC of the adaptive controller would depend on the same condition. The UC shows to behave better for the higher loads of the testing interval.

4.2.5. Results

A UC strategy has been proposed for the control of a MDoF manipulator. The proposed scheme adapts the controller parameters to seek the best performance at different operating conditions based solely on the input-output data. This fact makes the control law less prone to modeling errors and changes in the operating conditions than other classical adaptive control schemes. The proposed UC strategy uses a cost function with a fading factor to achieve a better adaptation to highly changing operating conditions and the controller set was computed using feedback linearization. Simulation results under typical scenarios have revealed the advantages of the UC against classical adaptive control schemes for the higher loads of the testing interval. The UC is capable of a better behavior in a larger operating range. These results have also shown that the proposed control is more robust as can be concluded when the system parameters are perturbed. UC has also achieved a proper tracking with smoother control signals and lower control efforts in high loads. As future research remains the experimental validation of the UC in a Scorbot ER V Plus and more complex manipulators as the seven DoF Whole Arm Manipulator (WAM) manufactured by Barrett Thecnology Inc.

Table 4-4.: Controller robustness comparison using ISE and control effort, for joint q_3. Normalization based on the No-disturbance case.

No-disturbance to the model inertial parameters				
	ISE		CE	
PAYLOAD (kg)	UC	ADAPT.	UC	ADAPT.
1,4	1,41E-02	1,89E-06	6,31E+02	6,18E+02
1,5	6,36E-02	2,75E-05	6,64E+02	6,53E+02
1,6	1,34E-01	9,57E-04	7,00E+02	7,11E+02
1,7	2,23E-01	3,01E+03	7,36E+02	3,15E+29
1,8	3,25E-01	3,45E+03	7,73E+02	1,54E+30
1,9	4,34E-01	3,91E+04	8,12E+02	4,04E+33
2	5,49E-01	3,49E+03	8,53E+02	8,87E+31

Disturbance of 1σ to the model inertial parameters				
	ISE		CE	
PAYLOAD (kg)	UC	ADAPT.	UC	ADAPT.
1,4	0,2	1,29	0,99	1,00
1,5	0,4	2,20	0,99	1,00
1,6	0,6	2,91	0,99	1,02
1,7	0,8	6,16	0,98	302,20
1,8	0,8	8,94	0,98	116,17
1,9	0,9	0,31	0,98	0,00
2	0,9	31,49	0,98	578,41

Disturbance of 2σ to the model inertial parameters				
	ISE		CE	
PAYLOAD (kg)	UC	ADAPT.	UC	ADAPT.
1,4	0,04	1,54	0,98	1,00
1,5	0,11	3,23	0,98	1,00
1,6	0,54	1,70E+06	0,98	5,00E+25
1,7	0,67	2,15	0,98	123,87
1,8	0,75	4,63	0,98	12855,81
1,9	0,81	1,28	0,97	1,82
2	0,84	4,49	0,97	36,92

4.3. Unfalsified Adaptive Control (UAC) for the numerical model of the Whole Arm Manipulator (WAM)

As a consequence of the previous section, here it is developed and presented the application of the UAC to the WAM for the case of a fixed load attached at the end-effector and defined as $m_{load} = 1$ kg, with the purpose of verifying the adequate behavior of the controller and the system.

The load at the end of the manipulator is assumed attached to the end-effector of mass m_7 and unknown for the controller implementation.

For analysis purposes, the same kind of desired trajectories applied for the SCORBOT ER V PLUS and presented in the last section, were used:

$$q_{d_i} = \begin{cases} \frac{2\pi}{3}\left(1-\cos\left(\frac{2\pi}{5}t\right)\right), & \text{if } i = 1,3,5,7, \\ \pi\left(1-\cos\left(\frac{2\pi}{5}t\right)\right), & \text{if } i = 2,4,6. \end{cases}$$

The initial conditions for all simulations were $q_{d_i}(0) = 0$ and $\dot{q}_{d_i}(0) = 0$ ($i = 1,\ldots,7$). Note that trajectories are periodic, with period $T = 5$ s. The damping friction constant for all joints was defined as $\gamma = 0{,}1$. The parameter related to the controller Eq. (3-15) was set at $\lambda = 20$ as well. Although the actuator saturation torques are a function of the velocity, the upper and lower bounds of the control signal were assumed to be constant for simplicity, as ± 100 Nm, to avoid saturation and verify maximum computed torques for the desired trajectories.

The controller set $\mathbf{K}$ for the UC is defined by Eq. (3-14), where the parameter θ (load applied at the end of the manipulator, including the mass of the end effector) takes values $\hat{\theta}$ in a set Θ, for an interval similar to the one used in the previous section, *i.e.*:

$$\Theta = \{1,2,3\}. \tag{4-27}$$

In terms of the payload, and considering that $m_7 = 0{,}0755$ kg (actual mass of the last link without load), this means that the corresponding interval for the controller parameter (payload) is $[0{,}9245; 2{,}9245]$ kg.

The used cost function is defined in Eq. (3-17), with $\alpha = 0{,}001$ and $\eta = 0{,}9$ as the fading constant. The cost function is evaluated periodically with $T_s = 0{,}01$ s, based on the cost minimization hysteresis switching algorithm with fading memory presented in Section 3.3.2. The initial UC parameter used for the simulation was $\hat{\theta}(0) = 1$. The simulation was performed for a 15 s time interval, which includes three complete periods of the desired trajectories.

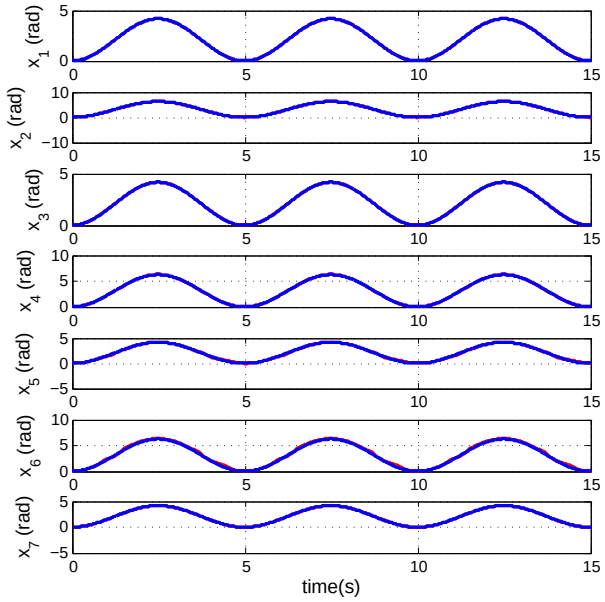

Figure 4-16.: Tracking trajectories of the WAM with UAC.

The results obtained by simulation are presented in the following figures. The Fig. **4-16** shows the desired trajectories for the seven (7) joints overlaid on the computed tracking trajectories.

The Fig. **4-17** presents bounded tracking errors on all joints, showing maximums on q_5 and q_6 (wrist joints) which may have effect in the orientation of the tool during the tracking process. Compared with the SCORBOT ER V PLUS, in general these errors shows to be in a similar range.

The Fig. **4-18** shows control torques without saturation of actuators. It should be noticed that he maximum torque is lower than ± 50 Nm for q_2 as the saturation bound parameter for the torques was defined on purpose as ± 100 Nm, for control signals characterization without saturation. Smooth control signals shows to be similar to those presented in the SCORBOT ER V PLUS analysis of the last section.

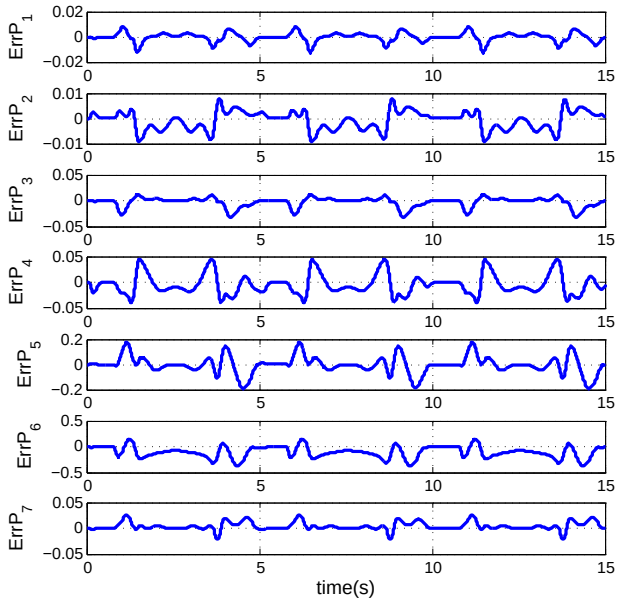

Figure 4-17.: Tracking errors of the WAM with UAC.

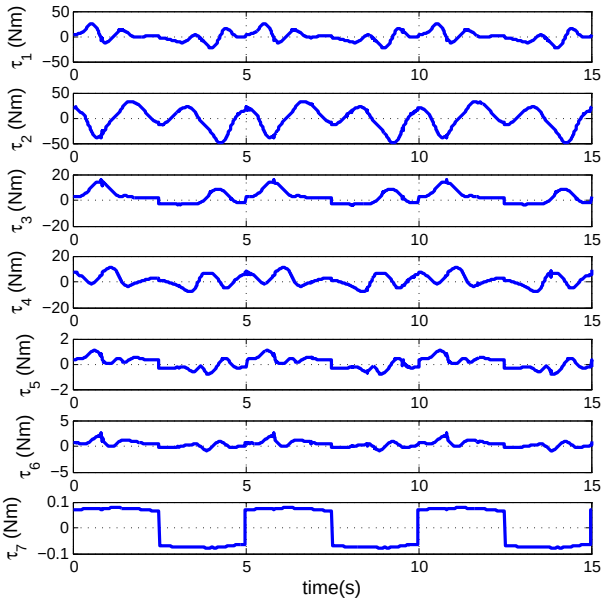

Figure 4-18.: Control torques of the WAM with UAC.

The Fig. **4-19** shows the UC switching parameter related with the cost functions change and comparison. The falsification of the controller occurs whenever it is a better performance related with the minimum cost function to any of the controllers from the candidate set, as stated by condition in Eq. (3-19).

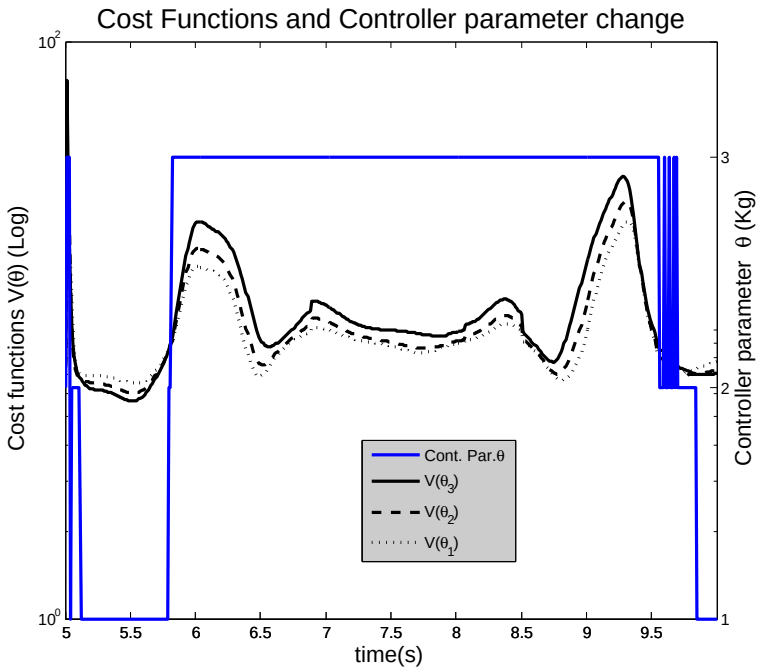

Figure 4-19.: UC parameter switching and costs functions. Payload of 1 kg.

4.3.1. Results

An UC strategy has been applied to the MDoF redundant WAM manipulator. As for the SCORBOT ER V PLUS, the proposed scheme adapts the controller parameters to seek the best performance at different operating conditions based only on the input-output data. It uses the same cost-detectable cost function with a fading factor to achieve a better adaptation using recent data. Simulation results under this typical scenario revealed the possibility of successful application of this controller for the case of study. For future work it is proposed an evaluation of other scenarios and the experimental application to the real manipulator in common human-robot interactive tasks like pick and place and lift and lower payloads.

5. Main Contributions and Future Work

5.1. Contributions

- The first chapter presents a chronological revision of three main current research topics: Human-Robot Interaction (HRI), the Unfalsified Adaptive Control (UAC) as an adaptive switching control strategy, and the payload computation for robot manipulators. After this, it is stated the research problem of this work, proposing to work in two aspects: a methodology for the computation of the maximum payload in the entire workspace, suggesting the use of cell to cell mapping to analyze the DLCC for MDoF manipulators; and then, it is proposed the application of Unfalsified Adaptive Control (UAD) in Multiple Degree of Freedom (MDoF) manipulators ($n > 2$ DoF), including the intrinsically safety, compliant and backdrivable Whole Arm Manipulator (WAM), suitable for HRI.

- The chapter 2 shows the procedure for dynamical modeling of multiple Degree of Freedom (MDoF) manipulators. This models are computed, numerically validated and used later for payload and control analysis and design. The compact inverse and direct dynamical models are analytically computed using the Newton-Euler recursion and applied to the SCORBOT ER V PLUS numerical model validation. Then, experimental validation of the numerical model obtained for the redundant Whole Arm Manipulator (WAM) is performed, finding challenging issues in the Coulomb friction modeling.

- In chapter 3, three nonlinear control strategies applied to robot manipulation and used in this work, are presented. The first two are traditional model-based control strategies known as Feedback Linearization and Adaptive Control, the third one is a current developing data-driven control strategy known as Unfalsified Adaptive Control (UAC) which, to the knowledge of the author, has not been applied for MDoF manipulators ($n > 2$ DoF) and required evaluation for usage in lightweight and low inertia manipulators like the WAM.

- In chapter 4, different traditional nonlinear control strategies for MDoF manipulators are applied for Dynamic Load Carrying Capacity (DLCC) computation. It is developed a methodology for DLCC computation of the entire workspace of MDoF manipulators using cell to cell mapping for the regulation task, showing a promising application to path planning. The DLCC computation considers the torque saturation of actuators as a common behavior in paths that reach the regulation objective. The performance of Feedback Linearization control, Adaptive control and PID with antiwindup for DLCC computation are compared,

showing a better performance of the Feedback Linearization control strategy, due to its ability to handle a higher payload in the entire workspace.

- In the same chapter, numerical experiments are used for the analysis of the data-driven Unfalsified Adaptive Controller with fading memory applied to MDoF manipulators. A comparison with the traditional model-based Adaptive controller was performed for three scenarios: performance of controllers for two fixed loads at the end of the manipulator, performance of controllers with periodic non-smooth load changes between two fixed values and performance of controllers applying the worst-case disturbances to the model inertial parameters. This control strategy is first applied to the 5 DoF SCORBOT ER V PLUS model, showing with the UAC a better performance for higher loads, higher DLLC handling abilities and more robust behavior. Then, the UAC is proved by simulation in the 7 DoF redundant WAM, showing adequate performance with relatively low tracking errors and smooth and bounded control signals.

5.2. Future Work

- It is required a careful identification or learning process of the friction model of the WAM, to improve the numerical model for simulation and control design. Then, it would be necessary to perform experimental validation of the dynamical model of the WAM, using the adequate friction model.
- Analysis of the Unfalsified Adaptive Control (UAC) for different base controllers and the application to practical settings of the WAM, related with payload handling in HRI configurations and considering saturation of the real actuators.
- Implementation of the maximum DLCC algorithm for the characterization of the entire workspace and evaluation of the potential path planning in different real WAM tasks, like lifting changing loads and picking different types of objects form shelfs at different heights.
- Evaluation of other conditions for maximum DLCC computation, like: the symmetry of the workspace, optimization of controller parameters and path, analysis of other nonlinear phenomena and the most effort demanding plane configuration.

A. Appendix: Whole Arm Manipulator (WAM) frame configuration

The variant form of the Denavit-Hartenberg (D-H) method presented in [85] is used to establish the coordinate frames in the zero position, presented in Fig. **A-1** for the 4 DoF configuration and in Fig. **A-2** for the 7 DoF configuration. A positive joint motion is based on the right hand rule for each axis.

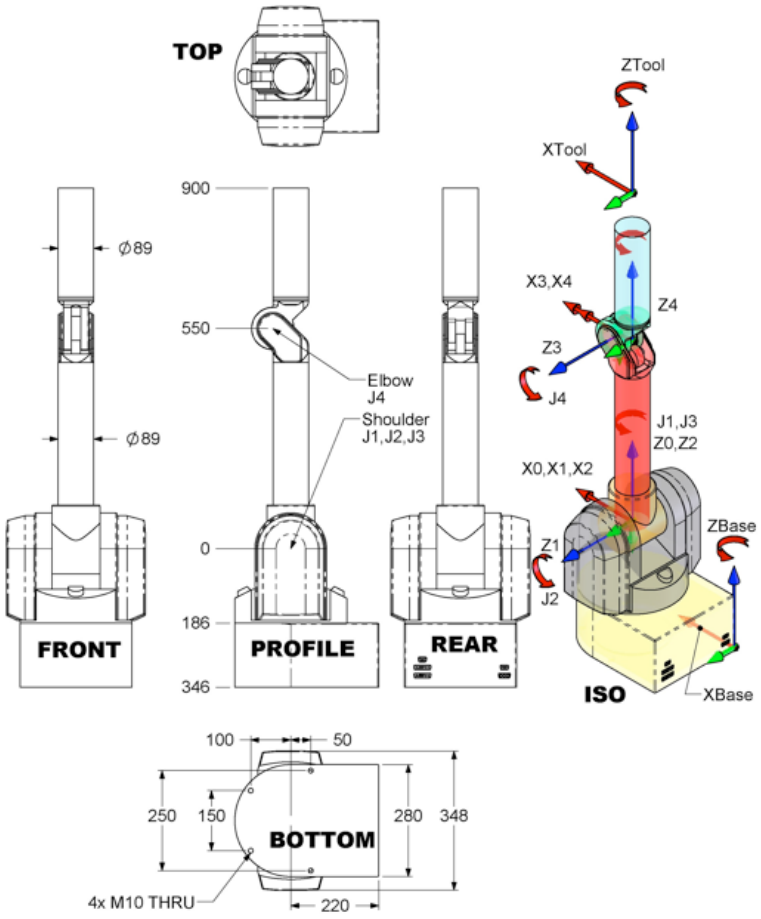

Figure A-1.: 4 DoF WAM dimensions and D-H frame configuration [2]

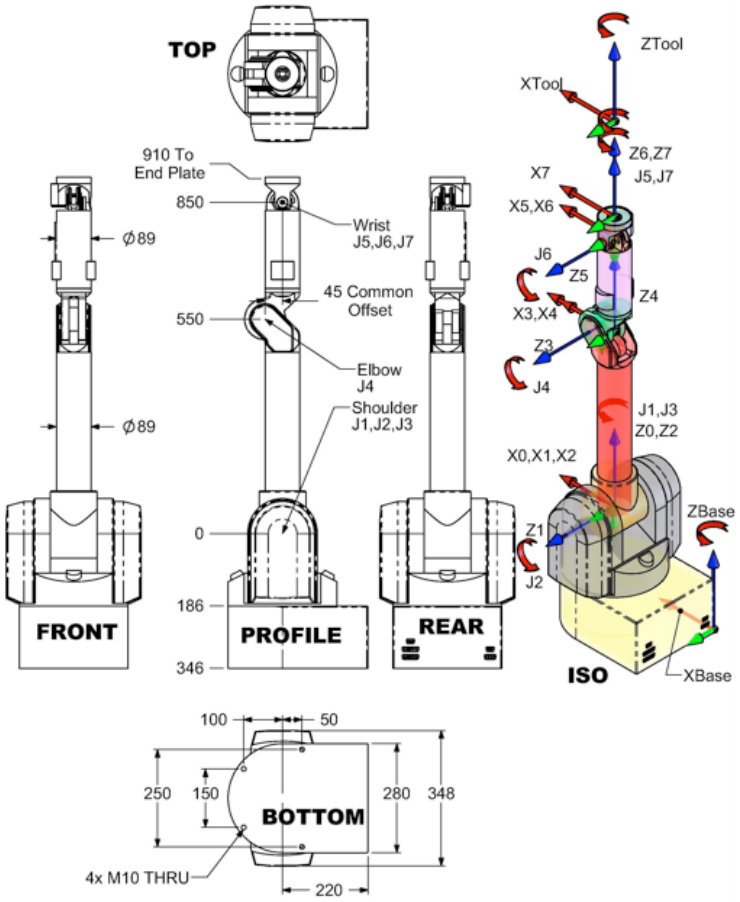

Figure A-2.: 7 DoF WAM dimensions and D-H frame configuration [2]

B. Appendix: UAC definitions and stability statement

The Fig. **B-1** shows the generic switching adaptive control system definition presented in [89]. Where u and y are the plant input and output vector signals. The adaptive controller switches the currently active controller $\hat{K}_t$ at times t_k, $k = 1, 2, ...$ with $t_k < t_k + 1$, $\forall k$. If finite, the total number of switches is denoted by N, so that the final switching time is t_N and the final controller is K_N.

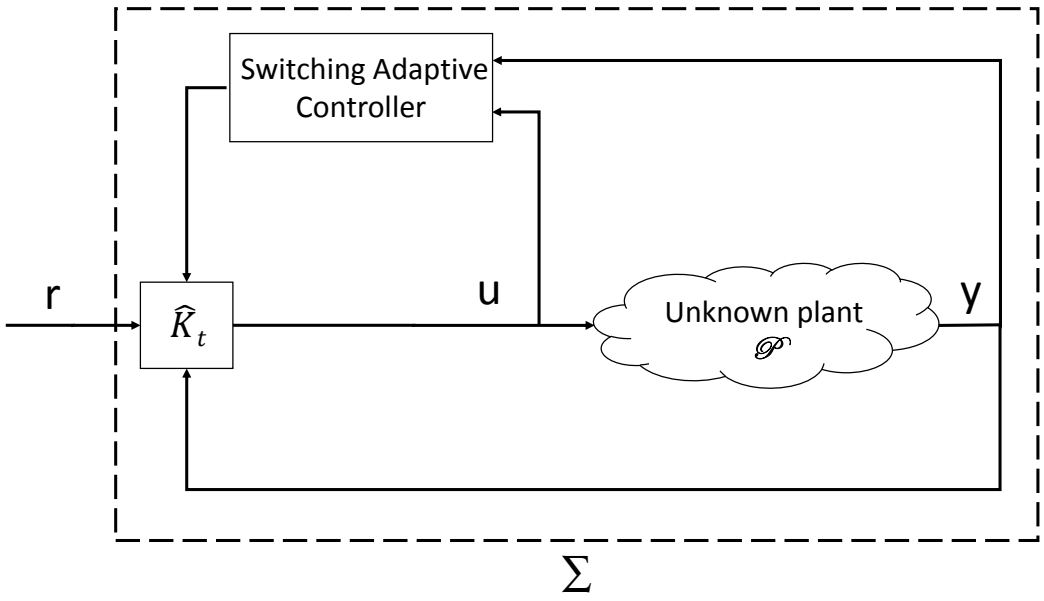

Figure B-1.: Switching adaptive control system definition presented in [89]

For stability in a multi-controller unfalsified setting, consider the system $\Sigma : \mathfrak{L}_{2e} \longrightarrow \mathfrak{L}_{2e}$. Stability of the system $\Sigma : \mathbf{w} \mapsto \mathbf{z}$ is said to be unfalsified by the data ($\mathbf{w}$, $\mathbf{z}$) if there exist β, $\alpha \geq 0$ such that the following holds:

$$\|\mathbf{z}\|_\tau < \beta \|\mathbf{w}\|_\tau + \alpha, \forall \tau > 0. \tag{B-1}$$

Otherwise, the stability of the system Σ is falsified by ($\mathbf{w}$, $\mathbf{z}$). In general, α may depend on the initial state. Furthermore, if (B-1) holds with a single pair β, $\alpha \geq 0$ for all $\mathbf{w} \in \mathfrak{L}_{2e}$, then the system is said to be finite-gain stable, in which case the gain of Σ is the least such β.

Lemma B.0.1. *([88]) Consider the switching feedback adaptive control system* Σ*, where uniformly bounded reference input r, as well as the output* $z = [u, y]$ *are given. Suppose there are finitely many switches. Let* t_N *and* K_N *denote the final switching instant and the final switched controller, respectively. Suppose that the final controller* K_N *is stably causally left invertible (SCLI) (i.e., the fictitious reference signal* $\tilde{r}$ *is unique and incrementally stable). Then*

$$\|\tilde{r}\|_t < \|r\|_\tau + \alpha < \infty, \forall t > 0. \tag{B-2}$$

The cost minimization ε-hysteresis switching algorithm [66] and the cost functional $\mathbf{J}(\mathbf{K}, \mathbf{z}, t)$ operate as a switching rule. This algorithm returns, at each t, a controller $\hat{K}_t$ which is the active controller in the loop:

$$K_t = \arg\min_{K \in \mathbf{K}} \{\mathbf{J}(\mathbf{K}, \mathbf{z}, t) - \varepsilon \delta_{K\hat{K}_{t^-}}\}, \tag{B-3}$$

where δ_{ij} is the Kronecker's δ, and t^- is the limit of τ from below as $t \to \tau$.

The switch occurs only when the current unfalsified cost related to the currently active controller exceeds the minimum (over the finite set of candidate controllers $\mathbf{K}$) of the current unfalsified cost by at least ε. The hysteresis step ε serves to limit the number of switches on any finite time interval to a finite number, and so prevents the possibility of the limit cycle type of instability. It also ensures a non-zero dwell time between switches [89].

Definition B.0.1. ([88]) Let r denote the input and $\mathbf{z}_d = \Sigma(\hat{K}_t, \mathscr{P})r$ denote the resulting plant data collected while $\hat{K}_t$ is in the loop. Consider the adaptive control system $\Sigma(\hat{K}_t, \mathscr{P})$ with input r and output z_d. The pair (**J**,**K**) is said to be cost detectable if, without any assumption on the plant $\mathscr{P}$ and for every $\hat{K}_t \in \mathbf{K}$ with finitely many switching times, the following statements are equivalent:

- $J(K_N, z_d, t)$ is bounded as t increases to infinity.
- Stability of the system $\Sigma(\hat{K}_t, \mathscr{P})$ is unfalsified by the input-output pair (r, z_d).

Theorem B.0.2. *([88]) Consider the feedback adaptive control system* Σ*, together with the* ε*-hysteresis switching algorithm [66]. Suppose the following holds: the adaptive control problem is feasible (there is at least one stabilizing controller in the candidate set, defined as the robust optimal controller* K_{RSP}*), the associated cost functional* $\boldsymbol{J}(\boldsymbol{K}, \boldsymbol{z}, t)$ *is monotone in time, the pair* $(\boldsymbol{J}, \boldsymbol{K})$ *is cost detectable, and the candidate controllers have stable causal left inverses. Then, the switched closed-loop system is stable. In addition, for each z, the system converges after finitely many switches to the controller* K_N *that satisfies the performance inequality*

$$J(K_N, \mathbf{z}, \mathbf{t}) \leq \mathbf{J}(\mathbf{K_{RSP}}) + \varepsilon, \textit{ for all } \tau. \tag{B-4}$$

The proof of the previous theorem is provided in [89].

Cost-detectable Cost Function with fading memory

In [38], the authors provide an example of the cost function and the conditions under which it ensures stability and finiteness of switches according to Theorem B-4. For the the output signal y and the controller signal u, let the fading memory functional be

$$F_\eta(y_t,t) = \sum_{\tau=0}^{t} y^2(\tau)\eta^{t-\tau}, \tag{B-5}$$

where $\eta < 1$ is the fading memory parameter. The cost function is defined as

$$J(K_N,z,\tau) = \frac{F_\eta((\tilde{r}-y)_t,t) + F_\eta(u_t,t)}{F_\eta((\tilde{r})_t,t) + c}, \tag{B-6}$$

where $\tilde{r}$ is a hypothetical signal that would have reproduced exactly the measured data z if the controller K had been in the loop for the time period over which the data z was collected, known as fictitious reference signal and c is a constant.

Bibliography

[1] *Barret Technology Inc.* http://www.barrett.com/robot/index.htm, . – Accessed: 2014-04-15

[2] *Barret Technology Inc. Support*. http://wiki.barrett.com/wiki/WAM/KinematicsJointRangesConversionFactors, . – Accessed: 2014-04-15

[3] *Barret Technology Inc. Support Dynamics*. http://web.barrett.com/support/WAM_Documentation/WAM_InertialSpecifications_AC-02.pdf, . – Accessed: 2014-04-15

[4] ANDERSON, Brian D. ; DEHGHANI, Arvin: Challenges of adaptive control-past, permanent and future. In: *Annu. Rev. Control* 32 (2008), Nr. 2, 123–135. http://dx.doi.org/10.1016/j.arcontrol.2008.06.001. – DOI 10.1016/j.arcontrol.2008.06.001. – ISSN 13675788

[5] ARANGO, J. ; ANGULO, F.: *Dynamical analysis and non linear control of a 5 DOF manipulator*, Universidad Nacional de Colombia, Diplomarbeit, 2008

[6] ÅSTRÖM, K.J. ; WITTENMARK, B.: *Adaptive Control: Second Edition*. Dover Publications, 2013 (Dover Books on Electrical Engineering). http://books.google.com.co/books?id=4CLCAgAAQBAJ. – ISBN 9780486319148

[7] BAEK, Seung-Min ; CHUNG, Tae-Hyok ; KIM, Dong-Hyeok ; KIM, Sung-Rak: Systems and algorithms for development of the robot safety function. In: *2012 9th Int. Conf. Ubiquitous Robot. Ambient Intell.* (2012), Nr. Urai, 471–475. http://dx.doi.org/10.1109/URAI.2012.6463044. – DOI 10.1109/URAI.2012.6463044. ISBN 978–1–4673–3112–8

[8] BALDI, Simone ; BATTISTELLI, Giorgio ; MOSCA, Edoardo ; TESI, Pietro: Multi-model unfalsified adaptive switching supervisory control. In: *Automatica* 46 (2010), Februar, Nr. 2, 249–259. http://dx.doi.org/10.1016/j.automatica.2009.10.034. – DOI 10.1016/j.automatica.2009.10.034. – ISSN 00051098

[9] BATTISTELLI, Giorgio ; HESPANHA, Joao ; MOSCA, Edoardo ; TESI, Pietro: Unfalsified adaptive switching supervisory control of time varying systems. In: *Proc. 48h IEEE Conf. Decis. Control held jointly with 2009 28th Chinese Control Conf.* 2 (2009), Dezember, 805–810. http://dx.doi.org/10.1109/CDC.2009.5399882. – DOI 10.1109/CDC.2009.5399882. ISBN 978–1–4244–3871–6

[10] BATTISTELLI, Giorgio ; MOSCA, Edoardo ; SAFONOV, MG ; TESI, P: Stability of unfalsified adaptive switching control. In: *IEEE Trans. Aut. Contr.* 55 (2010), Nr. 10, 2424–2429. http://scholar.google.com/scholar?hl=en&btnG=Search&q=intitle:Stability+of+Unfalsified+Adaptive+Switching#8

[11] BATURONE, A.O.: *Robótica: manipuladores y robots móviles*. Marcombo, 2001 (ACCESO RÁPIDO). http://books.google.com.co/books?id=TtMfuy6FNCcC. – ISBN 9788426713131

[12] BOHN, C. ; ATHERTON, D.: An analysis package comparing pid antiwindup strategies. In: *IEEE Systems Magazine* 15 (1995), Nr. 2, S. 34–40

[13] BREAZEAL, C ; BROOKS, A: Working collaboratively with humanoid robots. In: *Humanoid Robot. ...* (2004), 253–272. http://ieeexplore.ieee.org/xpls/abs_all.jsp?arnumber=1442126. ISBN 0780388631

[14] CETIN, a. E. ; ADLI, M. A.: Cooperative control of a human and a robot manipulator for positioning a cart on a frictionless plane. In: *Mechatronics* 16 (2006), Oktober, Nr. 8, 461–469. http://dx.doi.org/10.1016/j.mechatronics.2006.03.010. – DOI 10.1016/j.mechatronics.2006.03.010. – ISSN 09574158

[15] CHEN, Chun T. ; ZENG, Shi C.: Optimal configuration of a parallel kinematic manipulator for the maximum dynamic load-carrying capacity. In: *Proc. - 1st Int. Conf. Robot. Vis. Signal Process. RVSP 2011*, 2011, S. 122–125

[16] CHEN, Tiffany L. ; CIOCARLIE, Matei ; COUSINS, Steve ; GRICE, Phillip ; HAWKINS, Kelsey ; HSIAO, Kaijen ; KEMP, Charles C. ; KING, Chih-Hung ; LAZEWATSKY, Daniel a. ; LEEPER, Adam ; NGUYEN, Hai ; PAEPCKE, Andreas ; PANTOFARU, Caroline ; SMART, William D. ; TAKAYAMA, Leila: Robots for humanity: User-centered design for assistive mobile manipulation. In: *2012 IEEE/RSJ Int. Conf. Intell. Robot. Syst.* (2012), Oktober, 5434–5435. http://dx.doi.org/10.1109/IROS.2012.6386286. – DOI 10.1109/IROS.2012.6386286. ISBN 978–1–4673–1736–8

[17] CHEONG, Seunggyun: Unfalsified adaptive control: Finding the best controller among candidate controllers. In: *52nd IEEE Conf. Decis. Control* (2013), Dezember, 6910–6915. http://dx.doi.org/10.1109/CDC.2013.6760984. – DOI 10.1109/CDC.2013.6760984. ISBN 978–1–4673–5717–3

[18] COLLINS, E.G. J. ; FAN, C. ; MILLETT, R.: Automated PI tuning for a weigh belt feeder via unfalsified control. In: *Proc. 38th IEEE Conf. Decis. Control (Cat. No.99CH36304)* 1 (1999). http://dx.doi.org/10.1109/CDC.1999.832885. – DOI 10.1109/CDC.1999.832885. – ISBN 0–7803–5250–5

[19] CORKE, Peter I.: *Robotics, Vision & Control: Fundamental Algorithms in Matlab*. Springer, 2011

[20] CRAIG, J.J.: *Introduction to Robotics: Mechanics and Control*. Pearson/Prentice Hall, 2005 (Addison-Wesley series in electrical and computer engineering: control engineering). http://books.google.com.co/books?id=AsT5nQEACAAJ. – ISBN 9780201543612

[21] DE SANTIS, Agostino ; SICILIANO, Bruno ; DE LUCA, Alessandro ; BICCHI, Antonio: An atlas of physical human-robot interaction. In: *Mech. Mach. Theory* 43 (2008), Nr. 3, S. 253–270. http://dx.doi.org/10.1016/j.mechmachtheory.2007.03.003. – DOI 10.1016/j.mechmachtheory.2007.03.003. – ISSN 0094114X

[22] DUMORA, Julie ; GEFFARD, Franck ; BIDARD, Catherine ; ASPRAGATHOS, Nikos a. ; FRAISSE, Philippe: Robot Assistance Selection for Large Object Manipulation with a Human. In: *2013 IEEE Int. Conf. Syst. Man, Cybern.* (2013), Oktober, 1828–1833. http://dx.doi.org/10.1109/SMC.2013.315. – DOI 10.1109/SMC.2013.315. ISBN 978–1–4799–0652–9

[23] DURANGO, S. ; CALDERON, M.: *Kinematical, dynamical and manipulability model of the Scorbot ER V PLUS manipulator robot*, Universidad Tecnológica de Pereira, Diplomarbeit, 2006

[24] EDSINGER, Aaron ; KEMP, Charles C.: Human-Robot Interaction for Cooperative Manipulation: Handing Objects to One Another. In: *RO-MAN 2007 - 16th IEEE Int. Symp. Robot Hum. Interact. Commun.* (2007), 1167–1172. http://dx.doi.org/10.1109/ROMAN.2007.4415256. – DOI 10.1109/ROMAN.2007.4415256. ISBN 978–1–4244–1634–9

[25] FELICIO, P ; AZINHEIRA, J ; LOURTIE, Pedro: Experimental inverted pendulum unfalsified control. In: *Mediterr. Conf. Control Autom.* Barcelona, 2012. – ISBN 9781467325318, 1479–1484

[26] FELIU, V. ; RAMOS, F.: Strain gauge based control of single-link flexible very lightweight robots robust to payload changes. In: *Mechatronics* 15 (2005), Juni, Nr. 5, 547–571. http://dx.doi.org/10.1016/j.mechatronics.2004.11.001. – DOI 10.1016/j.mechatronics.2004.11.001. – ISSN 09574158

[27] FELIU, Vicente ; CASTILLO, Fernando J. ; RAMOS, Francisco ; SOMOLINOS, José a.: Robust tip trajectory tracking of a very lightweight single-link flexible arm in presence of large payload changes. In: *Mechatronics* 22 (2012), August, Nr. 5, 594–613. http://dx.doi.org/10.1016/j.mechatronics.2012.01.012. – DOI 10.1016/j.mechatronics.2012.01.012. – ISSN 09574158

[28] FRÉMY, J ; MICHAUD, F ; LAURIA, Michel: Pushing a robot along. A natural interface for human-robot interaction. In: *Robot. Autom. (ICRA ...* (2010), 3440–3445. http://ieeexplore.ieee.org/xpls/abs_all.jsp?arnumber=5509584. ISBN 9781424450404

[29] FU, K.S. ; GONZÁLEZ, R.C. ; LEE, C.S.G.: *Robotics: control, sensing, vision, and intelligence*. McGraw-Hill, 1987 (McGraw-Hill series in CAD/CAM robotics and computer vision). http://books.google.com.co/books?id=sAwoAQAAMAAJ. – ISBN 9780070226258

[30] GAN, Yahui ; DAI, Xianzhong: Human-like Manipulation Planning for Articulated Manipulator. In: *J. Bionic Eng.* 9 (2012), Nr. 4, 434–445. http://dx.doi.org/10.1016/S1672-6529(11)60136-4. – DOI 10.1016/S1672–6529(11)60136–4. – ISSN 16726529

[31] GHARIBLU, H. ; JAVANMARD, A.: Maximum allowable load of two cooperative manipulators. In: *2010 2nd Int. Conf. Comput. Eng. Appl. ICCEA 2010* Bd. 2, 2010, S. 566–570

[32] GOODRICH, Michael a. ; SCHULTZ, Alan C.: Human-Robot Interaction: A Survey. In: *Found. TrendsÂ® Human-Computer Interact.* 1 (2007), Nr. 3, 203–275. http://dx.doi.org/10.1561/1100000005. – DOI 10.1561/1100000005. – ISSN 1551–3955

[33] HELVOORT, Jeroen van ; JAGER, Bram de ; STEINBUCH, Maarten: Data-driven multivariable controller design using Ellipsoidal Unfalsified Control. In: *Syst. Control Lett.* 57 (2008), September, Nr. 9, 759–762. http://dx.doi.org/10.1016/j.sysconle.2008.03.001. – DOI 10.1016/j.sysconle.2008.03.001. – ISSN 01676911

[34] HOLLERBACH, J. ; KHALIL, W. ; GAUTIER, M.: Model identification. In: SICILIANO, B. (Hrsg.) ; KATHIB, O. (Hrsg.): *Springer Handbook of Robotics*. New York : Springer-Verlag, 2008

[35] HOU, Zhong-Sheng ; WANG, Zhuo: From model-based control to data-driven control: Survey, classification and perspective. In: *Inf. Sci. (Ny).* 235 (2013), Juni, 3–35. http://dx.doi.org/10.1016/j.ins.2012.07.014. – DOI 10.1016/j.ins.2012.07.014. – ISSN 00200255

[36] HUANG, A. ; CHIEN, M.: *Adaptive control of robot manipulators*. Singapore : World Scientific Publishing Co. Pte. Ltd., 2010

[37] INC., Intelitek: *Scorbot-ER 5Plus: User's Manual*. Intelitek Inc., 1996

[38] JIN, Huiyu ; CHANG, Michael W. ; SAFONOV, Michael G.: A fading memory data-driven algorithm for controller switching. In: *IEEE Conf. Decis. Control Eur. Control Conf.* Orlando, FL : IEEE, 2011. – ISBN 978–1–61284–801–3, 6097–6103

[39] KALAKRISHNAN, Mrinal ; RIGHETTI, Ludovic ; PASTOR, Peter ; SCHAAL, Stefan: Learning force control policies for compliant manipulation. In: *2011 IEEE/RSJ Int. Conf. Intell. Robot. Syst.* (2011), September, 4639–4644. http://dx.doi.org/10.1109/IROS.2011.6095096. – DOI 10.1109/IROS.2011.6095096. ISBN 978–1–61284–456–5

[40] KHOSLA, P.: Categorization of parameters in the Dynamic Robot Model. In: *IEEE Transactions on Robotics and Automation* 5 (1989), Nr. 3, S. 261–268

[41] KLINGBEIL, Ellen ; MENON, Samir ; GO, Keegan ; KHATIB, Oussama: Using haptics to probe human contact control strategies for six degree-of-freedom tasks. In: *2014 IEEE Haptics Symp.* (2014), Februar, 93–95. http://dx.doi.org/10.1109/HAPTICS.2014.6775438. – DOI 10.1109/HAPTICS.2014.6775438. ISBN 978–1–4799–3131–6

[42] KORAYEM, M. ; NIKOOBIN, A.: Maximum payload path planning for redundant manipulator using indirect solution of optimal control problem. In: *International Journal of Advanced Manufacturing Technology* 44 (2009), S. 725–736

[43] KORAYEM, M. H. ; AZIMIRAD, V. ; NIKOOBIN, a. ; BOROUJENI, Z.: Maximum load-carrying capacity of autonomous mobile manipulator in an environment with obstacle considering tip over stability. In: *Int. J. Adv. Manuf. Technol.* 46 (2009), Juni, Nr. 5-8, 811–829. http://dx.doi.org/10.1007/s00170-009-2146-0. – DOI 10.1007/s00170–009–2146–0. – ISSN 0268–3768

[44] KORAYEM, M. H. ; BAMDAD, M.: Dynamic load-carrying capacity of cable-suspended parallel manipulators. In: *Int. J. Adv. Manuf. Technol.* 44 (2009), Januar, Nr. 7-8, 829–840. http://dx.doi.org/10.1007/s00170-008-1890-x. – DOI 10.1007/s00170–008–1890–x. – ISSN 0268–3768

[45] KORAYEM, M. H. ; GHARIBLU, H.: The effect of base replacement on the dynamic load carrying capacity of robotic manipulators. In: *Int. J. Adv. Manuf. Technol.* 23 (2004), Nr. 1-2, 28–38. http://dx.doi.org/10.1007/s00170-002-1528-3. – DOI 10.1007/s00170–002–1528–3. – ISSN 0268–3768

[46] KORAYEM, M. H. ; HEIDARI, a. ; NIKOOBIN, a.: Maximum allowable dynamic load of flexible mobile manipulators using finite element approach. In: *Int. J. Adv. Manuf. Technol.* 36 (2007), Januar, Nr. 9-10, 1010–1021. http://dx.doi.org/10.1007/s00170-006-0893-8. – DOI 10.1007/s00170–006–0893–8. – ISBN 0017000608938

[47] KORAYEM, M. H. ; NIKOOBIN, a.: Maximum payload for flexible joint manipulators in point-to-point task using optimal control approach. In: *Int. J. Adv. Manuf. Technol.* 38 (2007), Juli, Nr. 9-10, 1045–1060. http://dx.doi.org/10.1007/s00170-007-1137-2. – DOI 10.1007/s00170–007–1137–2. – ISSN 0268–3768

[48] KORAYEM, M. H. ; NIKOOBIN, a.: Maximum payload path planning for redundant manipulator using indirect solution of optimal control problem. In: *Int. J. Adv. Manuf. Technol.* 44 (2008), Dezember, Nr. 7-8, 725–736. http://dx.doi.org/10.1007/s00170-008-1862-1. – DOI 10.1007/s00170–008–1862–1. – ISSN 0268–3768

[49] KORAYEM, M. H. ; SHOKRI, Mohsen: Maximum Dynamic Load Carrying Capacity of 6UPS-Stewart Platform flexible joint Manipulator. In: *2006 IEEE Int. Conf. Robot. Biomimetics* (2006), 727–732. http://dx.doi.org/10.1109/ROBIO.2006.340296. – DOI 10.1109/ROBIO.2006.340296. ISBN 1–4244–0570–X

[50] KORAYEM, MH ; BAMDAD, M: Analytical design of optimal trajectory with dynamic load-carrying capacity for cable-suspended manipulator. In: *Int. J. Adv. Manuf. Technol.* 60 (2012), 317–327. http://dx.doi.org/10.1007/s00170-011-3579-9. – DOI 10.1007/s00170–011–3579–9

[51] KORAYEM, M.H. ; BASU, A.: Dynamic load carrying capacity of robotic manipulators with joint elasticity imposing accuracy constraints. In: *Rob. Auton. Syst.* 13 (1994), Oktober, Nr. 3, 219–229. http://dx.doi.org/10.1016/0921-8890(94)90037-X. – DOI 10.1016/0921–8890(94)90037–X. – ISSN 09218890

[52] KORAYEM, MH ; DAVARPANAH, F ; FARAHMANDPOUR, SE: Dynamic Load Carrying Capacity of Flexible Joint Robot. In: *Proc. Int. Manuf. Leaders Forum Glob. Compet. Manuf.* Adelaide, 2005, 1–8

[53] KORAYEM, M.H. ; DAVARPANAH, F. ; GHARIBLU, H.: Load carrying capacity of flexible joint manipulators with feedback linearization. In: *Int. J. Adv. Manuf. Technol.* 29 (2006), März, Nr. 3-4, 389–397. http://dx.doi.org/10.1007/s00170-005-2525-0. – DOI 10.1007/s00170–005–2525–0. – ISSN 0268–3768

[54] KORAYEM, M.H. ; GHARIBLU, H.: Maximum allowable load on wheeled mobile manipulators imposing redundancy constraints. In: *Rob. Auton. Syst.* 44 (2003), Nr. 2, 151–159. http://dx.doi.org/10.1016/S0921-8890(03)00043-5. – DOI 10.1016/S0921–8890(03)00043–5. – ISSN 09218890

[55] KORAYEM, M.H. ; GHARIBLU, H.: Analysis of wheeled mobile flexible manipulator dynamic motions with maximum load carrying capacities. In: *Rob. Auton. Syst.* 48 (2004), September, Nr. 2-3, 63–76. http://dx.doi.org/10.1016/j.robot.2004.07.010. – DOI 10.1016/j.robot.2004.07.010. – ISSN 09218890

[56] KORAYEM, M.H. ; GHARIBLU, H. ; BASU, A.: Maximum allowable load of mobile manipulators for two given end points of end effector. In: *Int. J. Adv. Manuf. Technol.* 24 (2004), Nr. 9-10, 743–751. http://dx.doi.org/10.1007/s00170-003-1748-1. – DOI 10.1007/s00170–003–1748–1. – ISSN 0268–3768

[57] KORAYEM, Moharam H. ; BAMDAD, M. ; TOURAJIZADEH, H. ; KORAYEM, a. H. ; BAYAT, S.: Analytical design of optimal trajectory with dynamic load-carrying capacity for cable-suspended manipulator. In: *Int. J. Adv. Manuf. Technol.* 60 (2011), August, Nr. 1-4, 317–327. http://dx.doi.org/10.1007/s00170-011-3579-9. – DOI 10.1007/s00170–011–3579–9. – ISSN 0268–3768

[58] KORAYEM, Moharam H. ; TOURAJIZADEH, H. ; BAMDAD, M.: Dynamic Load Carrying Capacity of Flexible Cable Suspended Robot: Robust Feedback Linearization Control Approach. In: *J. Intell. Robot. Syst.* 60 (2010), Mai, Nr. 3-4, 341–363. http://dx.doi.org/10.1007/s10846-010-9423-x. – DOI 10.1007/s10846–010–9423–x. – ISSN 0921–0296

[59] KRONANDER, Klas ; BILLARD, Aude: Learning Compliant Manipulation through Kinesthetic and Tactile Human-Robot Interaction. In: *IEEE Trans. Haptics* (2013), 1–14. http://dx.doi.org/10.1109/TOH.2013.54. – DOI 10.1109/TOH.2013.54. – ISSN 1939–1412

[60] KRÜGER, J. ; LIEN, T.K. ; VERL, a.: Cooperation of human and machines in assembly lines. In: *CIRP Ann. - Manuf. Technol.* 58 (2009), Januar, Nr. 2, 628–646. http://dx.doi.org/10.1016/j.cirp.2009.09.009. – DOI 10.1016/j.cirp.2009.09.009. – ISSN 00078506

[61] LEE, Heedon ; YU, Seungnam ; LEE, Seunghoon ; HAN, Jungsoo ; HAN, Changsoo: Development of human-robot interfacing method for assistive wearable robot of the human upper extremities. In: *2008 SICE Annu. Conf.* (2008), August, 1755–1760. http://dx.doi.org/10.1109/SICE.2008.4654948. – DOI 10.1109/SICE.2008.4654948. ISBN 978–4–907764–30–2

[62] LUH, J. ; M., Walker ; R., Paul: On-Line Computational Scheme for Mechanical Manipulators. In: *ASME J. Dyn. Sys., Meas., Control* 102 (1980), Nr. 2, S. 69–76

[63] MATSUO, Kazuya ; MURAKAMI, Kouji ; HASEGAWA, Tsutomu ; TAHARA, Kenji ; KURAZUME, Ryo: Segmentation method of human manipulation task based on measurement of force imposed by a human hand on a grasped object. In: *2009 IEEE/RSJ Int. Conf. Intell. Robot. Syst.* (2009), 1767–1772. http://dx.doi.org/10.1109/IROS.2009.5354069. – DOI 10.1109/IROS.2009.5354069. ISBN 978–1–4244–3803–7

[64] MITROVIC, Djordje ; NAGASHIMA, Sho ; KLANKE, Stefan ; MATSUBARA, Takamitsu ; VIJAYAKUMAR, Sethu: Optimal Feedback Control for Anthropomorphic Manipulators. In: *2010 IEEE Int. Conf. Robot. Autom.* Anchorage : IEEE, 2010. – ISBN 9781424450404, S. 4143–4150

[65] MORSE, A. ; MAYNE, D. ; GOODWIN, G.C.: Applications of hysteresis switching in parameter adaptive control. In: *IEEE Trans. on Autom. and Control* 37 (1992), S. 1343–1354

[66] MORSE, A. S. ; MAYNE, David Q. ; GOODWIN, Graham C.: Applications of hysteresis switching in parameter adaptive control. In: *IEEE Trans. Automat. Contr.* 37 (1992), Nr. 9, S. 1343–1354

[67] MUKAI, T. ; HIRANO, S. ; YOSHIDA, M. ; NAKASHIMA, H. ; HAYAKAWA, Yoshikazu: Whole-body contact manipulation using tactile information for the nursing-care assistant robot RIBA. In: *2011 IEEE/RSJ Int. Conf. Intell. Robot. Syst.* (2011), September, 2445–2451. http://dx.doi.org/10.1109/IROS.2011.6094403. – DOI 10.1109/IROS.2011.6094403. ISBN 978–1–61284–456–5

[68] PAIK, Jamie K. ; SHIN, Bu H. ; BANG, Young-bong ; SHIM, Young-Bo: Development of an Anthropomorphic Robotic Arm and Hand for Interactive Humanoids. In: *J. Bionic Eng.* 9 (2012), Nr. 2, 133–142. http://dx.doi.org/10.1016/S1672-6529(11)60107-8. – DOI 10.1016/S1672–6529(11)60107–8. – ISSN 16726529

[69] PANDEY, Amit K. ; SAUT, Jean-Philippe ; SIDOBRE, Daniel ; ALAMI, Rachid: Towards planning Human-Robot Interactive manipulation tasks: Task dependent and human oriented autonomous selection of grasp and placement. In: *2012 4th IEEE RAS EMBS Int. Conf. Biomed. Robot. Biomechatronics* (2012), Juni, 1371–1376. http://dx.doi.org/10.1109/BioRob.2012.6290776. – DOI 10.1109/BioRob.2012.6290776. ISBN 978–1–4577–1200–5

[70] PAUL, Ayanendu ; AKAR, Mehmet ; SAFONOV, Michael G. ; MITRA, Urbashi: Adaptive power control for wireless networks using multiple controllers and switching. In: *IEEE Trans. Neural Netw.* 16 (2005), Nr. 5, 1212–8. http://dx.doi.org/10.1109/TNN.2005.853420. – DOI 10.1109/TNN.2005.853420. – ISSN 1045–9227

[71] PAWLUK, M. ; ARENT, K.: Unfalsified control of manipulators: simulation analysis. In: *Bulletin of Polish academy of Sciences: Technical Sciences* 53 (2005), Nr. 1, S. 19–29

[72] POPPER, K. R.: *Conjectures and Refutations: The Growth of Scientific Knowledge.* London : Routhledge, 1963

[73] QUINTERO, Camilo P. ; FOMENA, Romeo T. ; SHADEMAN, Azad ; RAMIREZ, Oscar ; JAGERSAND, Martin: Interactive Teleoperation Interface for Semi-autonomous Control of Robot Arms. In: *2014 Can. Conf. Comput. Robot Vis.* (2014), 357–363. http://dx.doi.org/10.1109/CRV.2014.55. – DOI 10.1109/CRV.2014.55. ISBN 978–1–4799–4337–1

[74] RADKHAH, K. ; KULIC, D. ; CROFT, E.: Dynamic Parameter Identification for the CRS A460 Robot. In: *Proc. on the IEEE/RSJ International Conference on Intelligent Robots and Systems*. San Diego (USA), Oktober 2007, S. 3842–3847

[75] RAHMAN, S. M. M. ; IKEURA, Ryojun ; YU, Haoyong: Lifting and lowering objects manually and with a power assist robot: Analysis of human features to develop biomimetic

control. In: *2011 IEEE Int. Conf. Robot. Biomimetics* (2011), Dezember, 2175–2180. http://dx.doi.org/10.1109/ROBIO.2011.6181614. – DOI 10.1109/ROBIO.2011.6181614. ISBN 978–1–4577–2138–0

[76] RAHMAN, SM: Novel human-centric force control methods of power assist robots for object manipulation. In: *Robot. Biomimetics ...* (2013), Nr. December, 340–345. http://ieeexplore.ieee.org/xpls/abs_all.jsp?arnumber=6739482. ISBN 9781479927449

[77] ROOKS, B.: The harmonious robot. In: *Industrial Robot: An International Journal* 33 (2006), Nr. 1, S. 125–130

[78] SAFONOV, M.: Data-driven robust control design: Unfalsified Control. In: *Achieving Successful Robust Integrated Control System Designs for 21st Century Military Applications. Part II*. NATO, Dezember 2006, S. 4–1–4–18

[79] SAFONOV, M.G.: The unfalsified control concept and learning. In: *IEEE Trans. Automat. Contr.* 42 (1997), Juni, Nr. 6, 843–847. http://dx.doi.org/10.1109/9.587340. – DOI 10.1109/9.587340. – ISSN 00189286

[80] SAFONOV, MG: Unfalsified control: A behavioral approach to learning and adaptation. In: *Proc. 40th IEEE Conf. Decis. Control.* (2001), Nr. December, 2682–2685. http://ieeexplore.ieee.org/xpls/abs_all.jsp?arnumber=980675

[81] SHIBATA, Satoshi ; MURAKAMI, T: Human interactive motion of redundant manipulator by virtual nonholonomic constraint. In: *Adv. Motion Control. 2004. AMC' ...* (2004), 375–379. http://ieeexplore.ieee.org/xpls/abs_all.jsp?arnumber=1297898

[82] SICILIANO, B. ; SCIAVICCO, L. ; VILLANI, L. ; ORIOLO, G.: *Robotics: Modelling, Planning and Control*. London : Springer Verlag, 2009

[83] SLOTINE, J. ; LI, W.: *Applied Nonlinear Control*. New Jersey : Prentice Hall, 1991

[84] SLOTINE, J.J. ; LI, W.: Adaptive Manipulator Control: A Case Study. In: *IEEE Transactions on Automatic Control* 3 (1988), Nr. 11, S. 995–1003

[85] SPONG, M.W. ; HUTCHINSON, S. ; VIDYASAGAR, M.: *Robot Modeling and Control*. ProQuest Information and Learning Company, 2005 (Wiley select coursepack). http://books.google.com.co/books?id=muCMAAAACAAJ. – ISBN 9780471765790

[86] STANGER, C.a. ; ANGLIN, C. ; HARWIN, W.S. ; ROMILLY, D.P.: Devices for assisting manipulation: a summary of user task priorities. In: *IEEE Trans. Rehabil. Eng.* 2 (1994), Nr. 4, 256–265. http://dx.doi.org/10.1109/86.340872. – DOI 10.1109/86.340872. – ISSN 10636528

[87] STEFANOVIC, M. ; WANG, R. ; SAFONOV, M.G.: Stability and convergence in adaptive systems. In: *Proc. 2004 Am. Control Conf.* Bd. 2. Massachusetts, 2004. – ISBN 0–7803–8335–4, S. 1923–1928

[88] STEFANOVIC, Margareta ; SAFONOV, Michael G.: Safe Adaptive Switching Control: Stability and Convergence. In: *IEEE Trans. Automat. Contr.* 53 (2008), Oktober, Nr. 9, 2012–2021. http://dx.doi.org/10.1109/TAC.2008.929395. – DOI 10.1109/TAC.2008.929395. – ISSN 0018–9286

[89] STEFANOVIC, Margareta ; SAFONOV, Michael G. ; THOMA, M. (Hrsg.) ; ALLGÖWER, F. (Hrsg.) ; MORARI, M. (Hrsg.): *Lecture Notes in Control and Information Sciences 405: Safe Adaptive Control*. Longon : Springer-Verlag, 2011. – 145 S. http://dx.doi.org/10.1007/978-1-84996-453-1. http://dx.doi.org/10.1007/978-1-84996-453-1. – ISBN 9781849964524

[90] SWEVERS, J. ; GANSEMAN, C. ; BILGIN, D. ; DE SCHUTTER, J. ; VAN BRUSSEL, H.: Optimal Robot Excitation and Identification. In: *IEEE Transactions on Robotics and Automation* 13 (1997), S. 730–740

[91] SWEVERS, J. ; VERDONCK, W. ; SCHUTTER, J. D.: Dynamic model identification for industrial robots Integrated experiment design and parameter estimation. In: *IEEE Control Systems Magazine,* 27 (2007), S. 58–71

[92] THOMAS, M. ; YUAN-CHOU, H. ; TESAR, D.: Optimal actuator stiffness distribution for robotic manipulators based on local dynamic criteria. In: *Proceedings. 1985 IEEE Int. Conf. Robot. Autom.* 2 (1985). http://dx.doi.org/10.1109/ROBOT.1985.1087268. – DOI 10.1109/ROBOT.1985.1087268. – ISSN 07380666

[93] TOWNSEND, W.T. ; GUERTIN, J.A.: Teleoperator slave-WAM design methodology. In: *Industrial Robot* 26 (1999), Nr. 3, S. 167–177

[94] TSAO, T. ; SAFONOV, M.G.: Unfalsified Direct Adaptive Control of a Two Link Robot Arm. In: *Proc. on the IEEE Conference on Control Applications*. Hawai (USA), August 1999, S. 680–686

[95] VISIOLI, A.: Modified anti-windup scheme for pid controllers. In: *IEEE Control Theory and Applications* 150 (2003), Nr. 1, S. 49–54

[96] WALTERS, M ; DAUTENHAHN, Kerstin: Robotic etiquette: results from user studies involving a fetch and carry task. In: *...-Robot Interact. (HRI ...* (2007), 317–324. http://ieeexplore.ieee.org/xpls/abs_all.jsp?arnumber=6251706. ISBN 9781595936172

[97] WANG, L.T. ; RAVANI, B.: Dynamic load carrying capacity of mechanical manipulators Part I: Problem formulation. In: *ASME, Journal of Dynamic Systems and Control* 110 (1988)

[98] WANG, R ; PAUL, A: Cost detectability and stability of adaptive control systems. In: *Int. J. robust Nonlinear Control* 17 (2007), Nr. October 2006, 549–561. http://dx.doi.org/10.1002/rnc. – DOI 10.1002/rnc

[99] WANG, R. ; SAFONOV, M.G.: Stability of unfalsified adaptive control using multiple controllers. In: *Proc. 2005, Am. Control Conf. 2005.* (2005), 3162–3167. http://dx.doi.org/10.1109/ACC.2005.1470458. – DOI 10.1109/ACC.2005.1470458. ISBN 0–7803–9098–9

[100] WILLEMS, J.C.: Paradigms and puzzles in the theory of dynamical systems. In: *IEEE Trans. Automat. Contr.* 36 (1991), März, Nr. 3, 259–294. http://dx.doi.org/10.1109/9.73561. – DOI 10.1109/9.73561. – ISSN 00189286

[101] WONGHONG, Tanet ; ENGELL, Sebastian: Automatic controller tuning via unfalsified control. In: *J. Process Control* 22 (2012), Dezember, Nr. 10, 2008–2025. http://dx.doi.org/10.1016/j.jprocont.2012.08.002. – DOI 10.1016/j.jprocont.2012.08.002. – ISSN 09591524

[102] WU, J. ; WANG, J. ; ; YOU, Z.: An overview of dynamic parameter identification of robots. In: *Robotics and Computer-Integrated Manufacturing* 26 (2010), S. 414–419

[103] YAO, Y.L. ; KORAYEM, M.H. ; BASU, A.: Maximum allowable load of flexible manipulators for given dynamic trajectory. In: *Robot. Comput. Integr. Manuf.* 10 (1993), Nr. 4, S. 301–309. http://dx.doi.org/10.1016/0736-5845(93)90043-J. – DOI 10.1016/0736–5845(93)90043–J. – ISSN 07365845

[104] YUE, S. ; TSO, S. ; XU, W.: The unfalsified control concept and learning. In: *Elsevier, Mechanism and Machine Theory* 36 (2001), S. 785–800

[105] ZHAO, Yanan ; COLLINS, Emmanuel G.: Comparison of two approaches to automated PI controller tuning for an industrial weigh belt feeder. In: *ISA Trans.* 43 (2004), Oktober, Nr. 4, 611–21. http://www.ncbi.nlm.nih.gov/pubmed/15535398. – ISSN 0019–0578